Lehigh University
Lehigh Preserve

Theses and Dissertations

2011

Modeling and Optimization of Condensing Heat Exchangers for Cooling Boiler Flue Gas

Daniel David Hazell
Lehigh University

Follow this and additional works at: http://preserve.lehigh.edu/etd

Recommended Citation
Hazell, Daniel David, "Modeling and Optimization of Condensing Heat Exchangers for Cooling Boiler Flue Gas" (2011). *Theses and Dissertations.* Paper 1252.

This Thesis is brought to you for free and open access by Lehigh Preserve. It has been accepted for inclusion in Theses and Dissertations by an authorized administrator of Lehigh Preserve. For more information, please contact preserve@lehigh.edu.

Modeling and Optimization of Condensing Heat Exchangers for Cooling Boiler Flue Gas

by

Daniel Hazell

A Thesis

Presented to the Graduate and Research Committee

of Lehigh University

in Candidacy for the Degree of

Master of Science

in

Mechanical Engineering

Lehigh University

April 2011

Copyright

Daniel D. Hazell

II

Thesis is accepted and approved in partial fulfillment of the requirements for the Master of Science in Mechanical Engineering.

Modeling and Optimization of Condensing Heat Exchangers for Cooling Boiler Flue Gas

Daniel D. Hazell

_____

Date Approved

_____

Dr. Edward K. Levy

Thesis Advisor

_____

Dr. Gary Harlow

Department Chair Person

Acknowledgments

I'd like to thank the following people for their help in this work:

Dr. Edward Levy

Dr. Harun Bilirgen

Michael Kessen

Steve Dunbar

Jason Thompson

Ursla Levy

Jodie Johnson

Michael Lavigne

Kwangkook Jeong

Contents

Tables

Figures

Abstract

A large amount of water is present in vapor form in the flue gas of a coal power plant. Reduction of total water usage in power plants is the goal of this investigation. A secondary goal is to recover the heat that exists in the flue gas and transfer it to the feed water for usage elsewhere. To accomplish both of these goals a heat exchanger is used with bundles of in-line circular tubes. Cooling water is pumped through these tubes and flue gas is forced around these tubes resulting in convective heat transfer. Eventually the flue gas temperature drops below the water vapor dew point and water is condensed out of the flue gas. In addition, heat is transferred from the hot flue gas (135^{o}F – 300^{o}F) to the cooling water (90^{o}F – 105^{o}F) that is being pumped through the tubes.

A previously developed computer simulation code was modified to predict heat transfer, condensation and pressure drop through a full scale heat exchanger. The heat exchanger was designed to carry the load of a 550 MW power plant producing 6 million lb/hr of flue gas. Tube spacing optimization was carried out and it was determined that relatively small transverse spacings and large longitudinal spacings resulted in the best heat transfer to cost ratio.

Heat exchanger cost consisted of capital cost and operating cost. Capital cost was considered as a function of tube material. Stainless steel 304 was the most cost effective material in regions of water condensation. Nickel Alloy 22 was the most effective material in regions before water condensation where there was sulfuric acid condensation.

Two different operating locations for the heat exchanger were considered: downstream of an ESP unit and downstream of an FGD unit. Use of the heat exchanger downstream of the FGD unit gave better water condensation per cost and a better heat transfer rate per cost. Operating conditions and different flow rate ratios were considered and predicted condensation efficiencies of up to 59% were attained with some configurations.

Nomenclature

A	stress area (in^2)
A_1	Pipe area before expansion (in)
A_2	Pipe area after expansion (in)
A_i	inner tube wall area (ft^2)
A_o	outer surface area of tube (ft^2)
AFC	annual fixed cost ($)
C_D	coefficient of drag
$C_{p,cw}$	specific heat of cooling water (BTU/lbm*^oF)
$C_{p,fg}$	specific heat of flue gas (BTU/lbm*^oF)
d	tube diameter (in)
d_i	inner tube diameter (in)
d_o	outer tube diameter (in)
dA	incremental area (ft^2)
dT	incremental temperature (^oF)
dT_{cw}	incremental cooling water temperature (^oF)
E	modulus of elasticity (ksi)
F	force (lbf)
f	friction factor
G	mass flux (lb/hr*ft^2)
h_{cw}	cooling water convective heat transfer coefficient (BTU/hr*^oF*ft^2)
h_g	latent heat of water vapor (BTU/lb)
h_l	head loss through length of pipe (psi)
h_{l1}	head loss across tubing inlet manifold (psi)
h_{l2}	expansion head loss (psi)
h_{l3}	head loss across exit manifold (psi)
h_{l4}	contraction head loss (psi)
Hd	adiabatic head of gas column (ft)
ID	inner pipe diameter (in)
K	compressibility factor
K_1	minor pressure loss coefficient
k	specific heat ratio
k_{fg}	thermal conductivity of flue gas (BTU/hr*^oF*ft)
k_m	mass transfer coefficient (lb/hr*ft^2*mol)
k_{wall}	thermal conductivity (BTU/hr*^oF*ft)
L	duct length (ft)
l	length between tube supports (in)
I	moment of inertia (in^4)
L_{tube}	length of tube (in)
M	bending moment (lbf*in)
$\dot{m}_{cw}$	mass flow rate of cooling water (lbm/hr)
$\dot{m}_{fg}$	mass flow rate of flue gas (lbm/hr)
N_b	empirical bend loss factor
N_L	number of tube rows
Nu_{fg}	flue gas Nusselt number
OD	outer pipe diameter (in)

p	internal cooling water pressure (psi)
P_{atm}	atmospheric pressure (psi)
P_{tot}	pressure of the flue gas (psi)
Pr	Prandtl number of flue gas
Pr_s	Prandtl number based on wall temperature
Q	volumetric flow rate (ft^3/sec)
q	heat transfer rate (BTU/hr)
r_1	inner tube radius (in)
r_2	outer tube radius (in)
Re	Reynolds number
$R_{cooling\ water}$	thermal resistance of cooling water (hr*^oF/BTU)
$R_{flue\ gas}$	thermal resistance of flue gas (hr*^oF/BTU)
R_{total}	thermal resistance of tube wal, flue gas and cooling water (hr*^oF/BTU)
R_{wall}	thermal resistance of tube wall (hr*^oF/BTU)
$Re_{fg,max}$	maximum Reynolds number of flue gas
S_1	transverse tube spacing (in)
S_2	longitudinal tube spacing (in)
S_l	longitudinal tube spacing (in)
S_t	transverse tube spacing (in)
T_{fg}	bulk mean flue gas temperature (^oF)
$T_{fg,avg}$	average flue gas temperature (^oF)
T_i	liquid-vapor interfacial temperature (^oF)
T_{in}	initial flue gas temperature (^oF)
T_{iw}	temperature at the inner wall of tube (^oF)
T_{ow}	temperature at the outer wall of tube (^oF)
T_w	average tube wall temperature (^oF)
$T_{H20\ DP}$	dew point temperature of water vapor (^oF)
T_{cw}	bulk mean cooling water temperature (^oF)
t	tube wall thickness (in)
SA	total heat exchanger tube surface area (ft^2)
U_o	heat transfer coefficient between the cooling water and wall interface (BTU/hr*^oF*ft^2)
V	flue gas velocity (ft/sec)
V_{exit}	velocity of water at pipe exit (ft/sec)
$V_{fw,exit}$	velocity of water after pipe contraction (ft/sec)
V_{inlet}	velocity of water at pipe inlet (ft/sec)
V_{max}	maximum velocity of flue gas (ft/sec)
v	specific volume (ft^3/lb)
w	distributed load (lbf/in)
$\dot{W}_{pump}$	pumping power for water pump (hp)
x_{tube}	distance from end of tube (in)
x	correction factor
y	distance from center of gravity (in)
y_{H2O}	mole fraction of water vapor in the flue gas (vol%wet)
y_i	mole fraction of water vapor at the wall interface (vol%wet)

Greek Symbols

Δ_{max}	maximum deflection (in)
ΔP	pressure drop (psi)
ΔP_{bends}	pressure drop across tube bends (psi)
ζ	pressure drop coefficient
η_{fan}	fan efficiency (%)
η_{pump}	pump efficiency (%)
ρ	density (lbm/ft^3)
ρ_{exit}	density of cooling water at pipe exit (lbm/ft^3)
ρ_{inlet}	density of cooling water at pipe inlet (lbm/ft^3)
σ	normal stress (psi)
σ_1, σ_2	principle stresses (psi)
σ_{hoop}	hoop stress (psi)
σ_m	maximum stress (psi)

1. Introduction

Coal fired power plants use large quantities of cooling water to operate. There has been a considerable amount of effort to reduce the total amount of fresh water that power plants consume. This particular investigation deals with recovering water that is in the flue gas. If the power plant could retain part of this water vapor, total water intake could be reduced, saving the plant money and reducing harmful environmental effects.

A conventional plant producing 550 MW of net power produces 6 million lb/hr of flue gas. The mole fraction of moisture in this flue gas can vary depending on the type of coal burned. For example, a 550 MW power plant burning lignite coal has a moisture flow rate of 0.6 million lb/hr, or about 10 weight % of the flue gas flow rate. A large portion of the moisture contained in the flue gas is released into the atmosphere. A full scale water cooled condensing heat exchanger has been modeled in MATLAB and optimized to capture part of this moisture.

Two applications of the condensing heat exchanger were investigated: 1) condensing flue gas downstream of the electrostatic precipitator (ESP) and 2) condensing flue gas downstream of a flue gas desulfurization (FGD) unit. The heat exchanger considered is a counter current cross flow bare tube exchanger. Cooling water would run through the banks of bare tubes and flue gas would circulate around the outside of these tubes. Flue gas would be cooled down below the water vapor dew point such that water condensation would occur. This water condensation could then be treated for use in the plant. A co-benefit of the heat exchanger system is the condensation and recovery of sulfuric acid vapor and the efficiency benefits of heat recovery. Heat recovery to the cooling water could be used in the turbine cycle of the plant, thereby lowering boiler requirements.

Total cost of the system was estimated by considering contributions from the capital cost and the operating cost. Capital cost as functions of the type and amount of tubing material were calculated

using current tubing prices and published correlations. Operating costs were based off of the power requirements for pumping the flue gas and cooling water through the heat exchanger.

The effects of tube arrangements and geometry on performance and cost were investigated. Tube spacings have a large effect on both the heat transfer and the pressure drop through the heat exchanger. Pressure drop through the heat exchanger governs the fan power required on the flue gas side and therefore is part of the operating cost. For this reason, the tube spacings were investigated to find the optimal ratio of thermal performance to total cost required. The effect of cooling water flow rates and temperatures were also considered for thermal performance and pressure drop. Cooling water pumping power requirements were investigated to determine the contribution to the operating cost of the heat exchanger.

Since the heat exchanger would be installed in a very acidic environment, the application of different materials was considered. Basic strength analysis was done in order to estimate proper tube wall thickness for each material being considered. The thermal performance of each material was then investigated and recommendations were made on what materials to use based on cost and effectiveness. In addition, inlet conditions of both the cooling water and flue gas were considered for their effect on performance and cost. Lastly, the thermal performance and cost effects of using streamlined tubes was considered.

2. Theory

2.1 Heat Transfer

Modeling the full scale heat exchanger was done in MATLAB. The original version of the MATLAB code described in this thesis was developed by Kwangkook Jeong (1). Jeong's version of the code predicts condensation and heat transfer out of a water cooled, bare tube, cross flow heat exchanger. Hot flue gas is on the external side of the tubes and cooling water runs through the internal side of the tubes. Sections of the heat exchanger are discretized by dividing up the total tube area into cells and calculations from governing equations are performed on each individual cell. The majority of the following heat transfer theory was written into the code by Jeong. Modifications, which focus on use of the code to model full scale heat exchangers, were developed by the author as part of the present investigation.

The main governing equation for heat and mass transfer, when in the presence of condensation, is the Colburn-Hougen equation (2). When the wall temperature of the heat exchanger tubing is below the flue gas dew point temperature water condensation occurs. Therefore heat transfer to the tubes and to the water side becomes both sensible and latent. The following Colburn-Hougen equation takes that into account:

$$h_{fg}(T_{fg} - T_i) + k_m * h_g(y_{h_2o} - y_i) = U_0(T_i - T_{cw})$$

In this equation, h_{fg} is the convective heat transfer coefficient on the flue gas side, T_i is the liquid-vapor interfacial temperature, h_g is the latent heat of water vapor, k_m is the mass transfer coefficient, y_{H2O} and y_i are the mole fraction of water vapor in the flue gas and at the interface respectively and U_o is the heat transfer coefficient between the cooling water and interface. U_o is defined as:

$$U_o = \frac{1}{\frac{r_2}{r_1}\frac{1}{h_{cw}} + \frac{r_2}{k_{wall}}\ln\frac{r_2}{r_1}}$$

This equation takes into account the thermal resistance between the cooling water and the tube inner diameter and the thermal resistance of the wall. The calculations done by Jeong for temperature at the tube wall neglected the effect of the wall conductivity. However, since this investigation looks into the effect of relatively low thermal conductivity materials, it was necessary to account for the thermal resistance of the wall. The outer wall radius and inner wall radius are r_2 and r_1 respectively, h_{cw} is the convection coefficient of the cooling water and k_{wall} is the thermal conductivity of the wall material.

When there is no water condensation, the energy balance and Colburn-Hougen equation are greatly simplified to:

$$q = \frac{T_{fg} - T_{cw}}{R_{total}}$$

$$R_{total} = R_{wall} + R_{flue\ gas} + R_{cooling\ water}$$

The thermal resistance of a radial wall is:

$$R_{wall} = \frac{\ln {}^{r_2}/_{r_1}}{2\pi k L_{tube}}$$

where r_2 and r_1 are the outer and inner radius, respectively, k is the thermal conductivity of the wall material and L_{tube} is the length of tube. The thermal resistance of the wall can be used in conjunction with the resistance contribution from the flue gas and cooling water which are:

$$R_{flue\ gas} = \frac{1}{2\pi r_2 L h_{fg}}$$

$$R_{cooling\ water} = \frac{1}{2\pi r_1 L h_{cw}}$$

The convective heat transfer coefficients of the flue gas and cooling water are h_{fg} and h_{cw}, respectively. These resistances are used to determine the overall heat transfer.

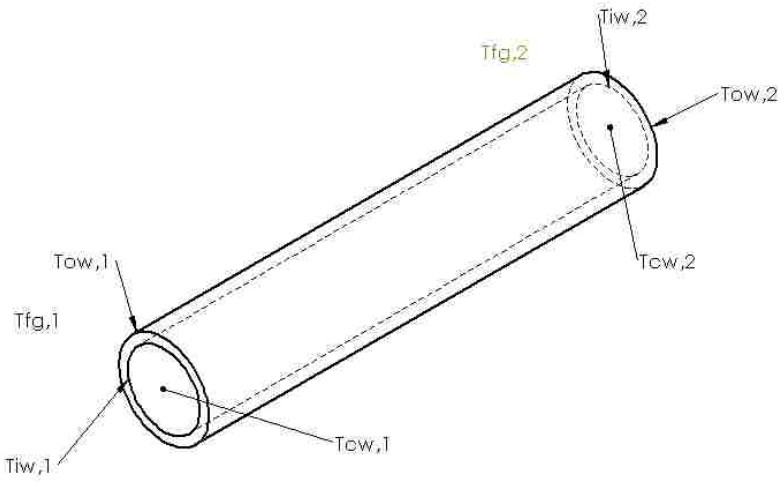

Figure 1 - Discretized tube cell in heat exchanger

When discretizing the heat exchanger, the inlet conditions at the first iteration of the flue gas and cooling water are known along with the total thermal resistance. Tube wall outer temperature is not known. Assuming no condensation at the beginning of the heat exchanger, initial tube wall temperature is calculated by using the total heat balance across the flue gas and cooling water.

$$q = \frac{T_{fg} - T_{cw}}{R_{total}}$$

This heat is initially transferred to the wall.

$$q = h_{fg} A_o \left(T_{fg} - T_{wo}\right)$$

Rearranging yields:

$$T_{wo} = T_{fg} - \frac{q}{h_{fg} A_o}$$

Tube outer wall temperature is T_{wo} and A_o is the discretized outer surface area along the tube.

When not at the beginning of the heat exchanger, cell inlet conditions, $T_{cw,1}$, $T_{fg,1}$, $T_{iw,1}$, and $T_{ow,1}$, are known from the previous iteration. A governing equation provides the energy balance in the flue gas, equating the change in enthalpy of the flue gas to the convective heat transfer to the tube wall.

$$\dot{m}_{fg} C_{p,fg} dT = h_{fg} \left(T_{fg} - T_w\right) dA$$

Applying the equation over a discretized cell and applying it to calculate the flue gas temperature at the end of the cell gives:

$$T_{fg,2} = \frac{\left(\dot{m}_{fg} C_{p,fg} - \frac{h_{fg}}{2} A_o\right) T_{fg,1} + h_{fg} A_o T_{ow,1}}{\dot{m}_{fg} C_{p,fg} + \frac{h_{fg}}{2} A_o}$$

When condensation begins, the same equation is used except that the wall temperature term $T_{ow,1}$ is replaced by the gas-liquid interface temperature, $T_{i,1}$:

$$T_{fg,2} = \frac{\left(\dot{m}_{fg} C_{p,fg} - \frac{h_{fg}}{2} A_o\right) T_{fg,1} + h_{fg} A_o T_{i,1}}{\dot{m}_{fg} C_{p,fg} + \frac{h_{fg}}{2} A_o}$$

Without condensation, the governing equation for calculating the cooling water temperature at the end of the iterated cell is based on convection heat transfer from the flue gas to the outside of the wall. The equation is given as:

$$h_{fg} \left(T_{fg,avg} - T_{ow,1}\right) A = \dot{m}_{cw} C_{p,cw} dT_{cw}$$

Applying over a discretized cell gives:

$$T_{cw,2} = T_{cw,1} - \frac{h_{fg}\left(T_{fg,avg} - T_{ow,1}\right)A_o}{\dot{m}_{cw}C_{p,cw}}$$

When accounting for water condensation, the heat transfer equation has to be combined with the Colburn-Hougen equation to obtain the following:

$$T_{cw,2} = T_{cw,1} - \frac{\left[h_{fg}\left(T_{fg} - T_i\right) + h_{fg}k_m\left(y_{h_2o} - y_i\right)\right]A_i}{\dot{m}_{cw}C_{p,cw}}$$

The interfacial mole fraction of water vapor at the flue gas – condensate interface, y_i, is determined at the beginning of each cell through the Antoine equation, given as (3):

$$y_i = \frac{e^{\left(a - \frac{b}{T_i + c}\right)}}{P_{tot}}$$

where a = 16.262, b = 3799.89 and c = 226.35. P_{tot} is the pressure of the flue gas.

After knowing the cooling water energy change, a governing equation is used to determine the inner tube wall temperature. The equation takes into account the convective heat transfer of the cooling water along with the energy gained from an increase in temperature. The equation reads:

$$h_{cw}dA\left(T_{iw,2} - T_{cw,2}\right) = \dot{m}_{cw}C_{p,cw}dT$$

Applying over a discretized cell gives:

$$T_{iw,2} = T_{cw,2} + \frac{\dot{m}_{cw}C_{p,cw}(T_{cw,1} - T_{cw,2})}{h_{cw}A_i}$$

The version of the code by Jeong assumed that the outer wall temperature was the same as the cooling water temperature. However, the following equations were added to take into account the

thermal resistance of the wall. To obtain the outer wall temperature for the next iteration, the heat balance equation is used between the inner and outer wall and the cooling water:

$$q = \dot{m}_{cw} C_{p,cw}\left(T_{cw,1} - T_{cw,2}\right) = \frac{T_{ow,2} - T_{iw,2}}{R_{wall}} = \frac{T_{ow,2} - T_{iw,2}}{\frac{\ln {}^{r_2}/_{r_1}}{2\pi k L_{tube}}}$$

Rearranging gives:

$$T_{ow,2} = T_{iw,2} + \frac{\dot{m}_{cw} C_{p,cw} (T_{cw,1} - T_{cw,2}) \ln {}^{r_2}/_{r_1}}{2\pi k L_{tube}}$$

Both of the equations that were used to calculate tube outer wall and tube inner wall temperature can be used if water condensation is occurring because they rely on the temperature change on the inside of the tube.

Since various tube arrangements will be used, the Nusselt number calculations for the flue gas side in the full-scale simulation code had to be refined to account for these. The average Nusselt number over a tube bank is characterized by the equation (4):

$$Nu_{fg} = C Re_{fg,max}^{m} Pr^{0.36} \left(\frac{Pr}{Pr_s}\right)^{1/4}$$

Prandtl number is represented by Pr. Reynolds number is represented by Re. Both C and m are functions of tube configuration and alignment. In regions where $10^3 < Re_{fg,max} < 2x10^5$, C is typically 0.27 for in-line tube configurations (4). The variable 'm' depends on transverse and longitudinal spacing. In previous versions of the code by Jeong the exponent 'm' was assumed to be 0.63. This was recommended for general use in tube banks. However, since more complex tube spacings and arrangements will be considered, 'm' has been interpolated in the code based on experimental data. It is evaluated graphically from experimental data from Zukauskas (5). Linear interpolation is used in the

code to evaluate a suitable value for 'm'. This is especially important since the exponent 'm' has a large effect on the Nusselt number and therefore flue gas side convection coefficient represented in the equation below.

$$h_{fg} = \frac{Nu_{fg} k_{fg}}{d_o}$$

2.2 Pressure Drop

The previous version of the code did not calculate pressure drop across the flue gas side or the cooling water side. The updated version includes these calculations. Pumping power requirements on the gas side and water side of a gas-liquid bare tube heat exchanger depend heavily on the pressure drop across the circuits. There are two options for tube arrangements for the external (flue gas side) pressure drop: staggered arrangement and in-line arrangements. In the figure S_1 (S_t) is the transverse spacing between tubes and S_2 (S_l) is the longitudinal spacing.

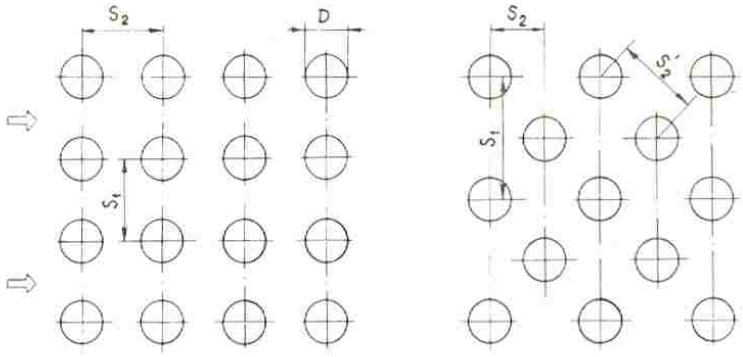

Figure 2 - in-inline (left) vs. staggered (right) (5)

2.2.1 Flue Gas Side Pressure Drop

Since both in-line and staggered arrangements were considered for their effect on heat transfer, their effects on the pressure drop were also considered. Experiments carried out by Zukauskas determine a friction coefficient that depends on transverse pitch, longitudinal pitch, and the maximum

Reynolds numbers of the flue gas flow (5). Correction factors were found for different ratios of transverse pitch and longitudinal pitch. The friction coefficient and correction factor were used in the following overall pressure drop equation:

$$\Delta p = N_L x \left(\frac{\rho V_{max}^2}{2}\right) f$$

where N_L is the total number of rows, x is the correction factor, ρ is the flue gas density, V_{max} is the maximum velocity (velocity between tubes) and f is the friction factor. Maximum velocity, density and friction coefficient are calculated at each cell of the heat exchanger. At the end of the program, these values are averaged and then used in the above pressure drop equation to find the flue gas pressure drop over the entire heat exchanger.

For purposes of verification and a second correlation, pressure drop calculations were also determined from Idelchik's experimental work (6). Idelchik performed experiments for a number of geometric configurations and Reynolds numbers ranging from 3 X 10^3 to 10^5. For the following correlations $S_2^{'}$ is defined below and N_L is the total number of rows of tubes.

$$S_2' = \sqrt{\frac{1}{4}S_1^2 + S_2^2}$$

For staggered configurations (6):

- $S_1/_d < 1.44$ & $0.1 \leq \frac{(S_1-d)}{(S_2'-d)} < 1.7$:
  - $\zeta = \left\{3.2 + 0.66\left(1.7 - \frac{S_1-d}{S_2'-d}\right)^{1.5} + \left(13.1 - \frac{9.1S_1}{d}\right)\left[0.8 + 0.2\left(1.7 - \frac{S_1-d}{S_2'-d}\right)^{1.5}\right]\right\} Re^{-0.27}(N_L + 1)$

- ${S_1}/{d} \geq 1.44$ & $0.1 \leq \frac{(S_1-d)}{(S_2'-d)} < 1.7$:
    - $\zeta = \left\{3.2 + 0.66\left(1.7 - \frac{S_1-d}{S_2'-d}\right)^{1.5}\right\} Re^{-0.27}(N_L + 1)$
- ${S_1}/{d} < 1.44$ & $1.7 \leq \frac{(S_1-d)}{(S_2'-d)} \leq 6.5$:
    - $\zeta = \left\{\left(1.88 - {S_1}/{d}\right)\left(\frac{S_1-d}{S_2'-d} + 1\right)^2 Re^{-0.27}(N_L + 1)\right\}$
- $1.44 \leq {S_1}/{d} < 3.0$ & $1.7 \leq \frac{(S_1-d)}{(S_2'-d)} \leq 6.5$:
    - $\zeta = 0.44\left(\frac{S_1-d}{S_2'-d} + 1\right)^2 Re^{-0.27}(N_L + 1)$
- $3 \leq {S_1}/{d} < 10$ & $\frac{(S_1-d)}{(S_2'-d)} > 1.7$:
    - $\zeta = 1.83\left(\frac{S_1}{d}\right)^{-1.46} Re^{-0.27}(N_L + 1)$

For in-line configurations (6):

- ${S_1}/{d} \leq {S_2}/{d}$ & $\frac{(S_1-d)}{(S_2'-d)} \leq 1.0$
    - $\zeta = 2\left(\frac{S_1}{d} - 1\right)^{-0.5} Re^{-0.5}(N_L)$
- ${S_1}/{d} > {S_2}/{d}$:
    - $1.0 < \frac{(S_1-d)}{(S_2'-d)} \leq 8.0$
        - $\zeta = 0.38\left(\frac{S_1-d}{S_2-d} - 0.94\right)^{-0.59}\left(\frac{S_1}{d} - 1\right)^{-0.5} Re^{{-0.2}/{\left(\frac{S_1-d}{S_2-d}\right)^2}}(N_L)$
    - $8.0 < \frac{(S_1-d)}{(S_2'-d)} \leq 15.0$
        - $\zeta = 0.118\left(\frac{S_1}{d} - 1\right)^{-0.5}(N_L)$

ζ is defined as the pressure drop coefficient and is used in the following equation to calculate external pressure drop:

$$\Delta p = \zeta \left(\frac{\rho V_{max}^2}{2} \right)$$

The values of Reynolds numbers for each individual cell are averaged and that value is used in the above equations with the total number of rows to determine a value for ζ. Density and maximum velocity values from each cell are also averaged and these individual values are used along with the ζ value in the above equation to determine the overall flue gas pressure drop across the tube bank.

The calculations for both the Zakauskas method and the Idelchik method were performed independently and then the results were compared and agreement was checked. In most cases as will be seen in the results, they differ by at most 10%. These pressure drop calculations were transformed to practical fan power requirements for the flue gas through thermodynamic equations for isentropic compressors (7).

$$Power = \frac{\dot{m} C_{p,fg} T_{in} \left[\left(\frac{P_{out}}{P_{in}} \right)^{\frac{k-1}{k}} - 1 \right]}{\eta_{fan}}$$

The mass flow rate of flue gas is $\dot{m}$, $C_{p,fg}$ is the specific heat of the gas, T_{in} is the initial flue gas temperature, P_{out} would be P_{atm} plus the calculated ΔP, P_{in} is only P_{atm}, k is the ratio of the specific heats and η_{fan} is the proposed fan efficiency. In this investigation 80% was used for the fan efficiency.

For verification purposes fan power calculations were also made using the concept of adiabatic head (8).

$$Hd = \frac{k \Delta P C_1}{\rho}$$

$$Power = \frac{\dot{m}_{fg} (Hd) C_2}{\eta_{fan}}$$

Hd is the developed adiabatic head of gas column (ft), k is a compressibility factor, ΔP is the total pressure increase required (in. wg), ρ is density (lb/ft^3), C_1 is a constant of 5.20, $\dot{m}_{fg}$ is flue gas flow rate (lb/hr) and C_2 is a constant 0.505×10^{-6}. This gives power in horsepower.

2.2.2 Water Side Pressure Drop

A great amount of cooling water is required for the heat exchanger. This cooling water was assumed to enter at the temperature of the boiler feedwater. This typically ranges from approximately 90^o to 105^o F. As the water circulated through the heat exchanger, the temperature was raised. The pressure drop across all components of the heat exchanger was calculated to provide power requirement estimations. The large majority of resistance came from the major head loss through the length of the pipe. Since water flow would be turbulent, head loss came from the following relation (9):

$$h_l = \rho f \frac{L_{tube}}{d_i} \frac{V_{avg}{}^2}{2}$$

The friction factor is f, L_{tube} is total length of pipe, d_i is internal diameter and V_{avg} is the average water velocity. The friction factor was determined from the Moody equation combined with Reynolds numbers, inner tube diameters and tube roughness. Since the tube would most likely be manufactured through a drawing process, the roughness was equal to 5 X 10^{-6} feet (9).

Pressure drop across the inlets of the tubing from the manifold reservoir were also considered. This was considered a part of the minor head losses and a minor loss coefficient, K_1, was tabulated based on the radius of curvature of the the inlet port and the tube diameter. A larger radius of curvature gave low pressure losses and a sharp cornered inlet increased the minor loss coefficient. The following equation was used:

$$h_{l1} = K_1 \, {}^1\!/_2 \, \rho_{inlet} V_{inlet}^2$$

Sudden expansion created pressure losses at the exit of the tubes into the exit manifold reservoir. Area ratios were calculated and the following equation from Babcock and Wilcox was used (8):

$$h_{l2} = \left(1 - \frac{A_1}{A_2}\right)^2 {}^1\!/_2 \, \rho_{exit} V_{exit}^2$$

Pressure losses from the 180^o bending of tubes through the length of the heat exchanger were calculated from Babcock and Wilcox using empirical bend loss factors, N_b. These were calculated as a function of bend radius and internal diameter of the pipe. N_b was then used in the following equation to determine the pressure loss contribution from bends:

$$\Delta P_{bends} = \frac{N_b v (G \times 10^{-5})^2}{12}$$

The specific volume is v (ft^3/lb), G is the mass flux (lb/hr*ft^2) and ΔP is pressure drop (psi).

Sudden expansion and sudden contraction resulted in pressure losses for the feed water pipe to the inlet manifold reservoir and the exit manifold reservoir to the exit feed water pipe, respectively. For the expansion case, the method used by Babcock and Wilcox was used again with the following equation (8):

$$h_{l3} = \left(1 - \frac{A_1}{A_2}\right)^2 {}^1\!/_2 \, \rho_{inlet} V_{inlet}^2$$

Contraction coefficients, K_c, were tabulated based on the area ratios and were used with the following head loss equations (9):

$$h_{l4} = K_c \, {}^1\!/_2 \, \rho_{exit} V_{fw,exit}^2$$

The addition of the major head loss and all of the minor head losses provide a good estimation for the internal pressure drop through a full-scale heat exchanger. This kind of manifold was the primary

one considered. After pressure losses throughout the water circuit are added up they are used in the pumping power equation below where Q is volumetric flow rate, ΔP is total pressure drop and η_{pump} is the efficiency of the pump. In this investigation 80% was used for the pump efficiency.

$$\dot{W}_{pump} = \frac{Q\Delta P}{\eta_{pump}}$$

3. Verification

3.1 Verification with Kwangkook Jeong Results

After many changes to the simulation code, it was necessary to make certain that the code still yields correct results. For this reason, verification was performed by comparing heat and mass transfer results with those of previous simulations. Kwangkook Jeong was the creator of the code that was modified in this investigation. He modeled the first version of a full-scale counter-current flow heat exchanger for use in a coal fired power plant (1). His heat exchanger consisted of the geometry and conditions shown in Table 1:

Table 1 - Jeong Conditions and Geometry

Inlet Conditions				
Mfg (lbm/hr)	Mcw (lbm/hr)	Tcw (F)	yH2O (%)	Tfg (F)
6.00E+06	3.00E+06	90	0.16	300

HX Geometry (in-line arrangement)						
OD (in)	Tube thick (in)	St (in)	Sl (in)	Duct Depth (ft)	Duct Height (ft)	Duct Length (ft)
2	0.14	2.8	4	40	20	20

With this sort of geometry and conditions, Jeong's simulations yielded a condensation efficiency of 12.6%, an average flue gas outlet temperature of 163°F and a cooling water outlet temperature of 196°F. Using the modifications presented earlier, the current code, using the same geometry and inlet

conditions yields a condensation efficiency of 12.45%, an average flue gas outlet temperature of 179.51^{o} and a cooling water outlet temperature of 184.64^{o}F. The current code predicts a lower flue gas side heat transfer coefficient and therefore less heat transfer. This is mainly due to the refinements for calculating Nusselt number based on more specific tube geometry. However, these numbers still do not vary significantly with the highest percent difference being between the predicted flue gas outlet temperatures at 10.13%.

Jeong also looked at the effect of increasing surface area on the condensation efficiency. Simulations were run with the revised code to verify that the same trends resulted. Heat exchanger geometry and inlet conditions that were used are shown in Table 2.

Table 2 - Conditions and geometry for verification with Jeong

Inlet Conditions						
Mfg (lbm/hr)	Mcw (lbm/hr)	Tcw (F)	yH2O (%)	Tfg (F)		
6.00E+06	6.00E+06	90	0.16	300		
HX Geometry (in-line arrangement)						
OD (in)	Tube thick (in)	St (in)	Sl (in)	Duct Depth (ft)	Duct Height (ft)	Duct Length (ft)
2	0.14	2.8	4	40	20	varies

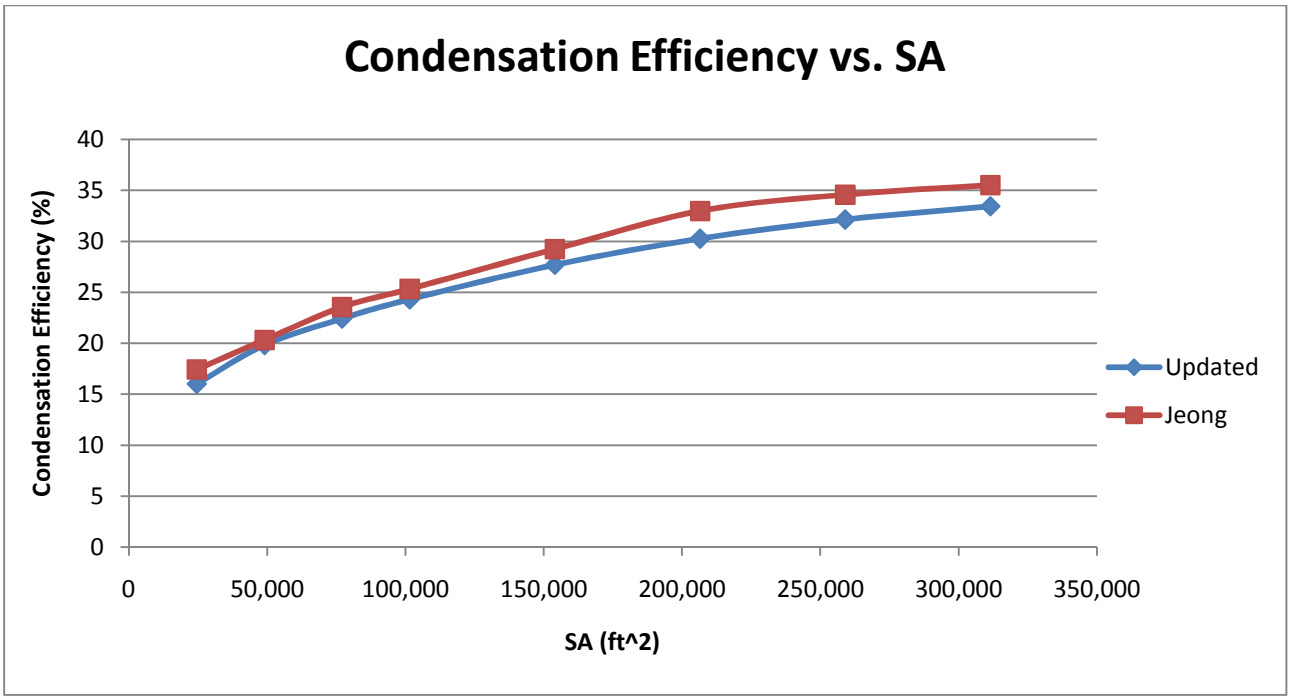

Figure 3 – Agreement between condensation results of updated code and Jeong

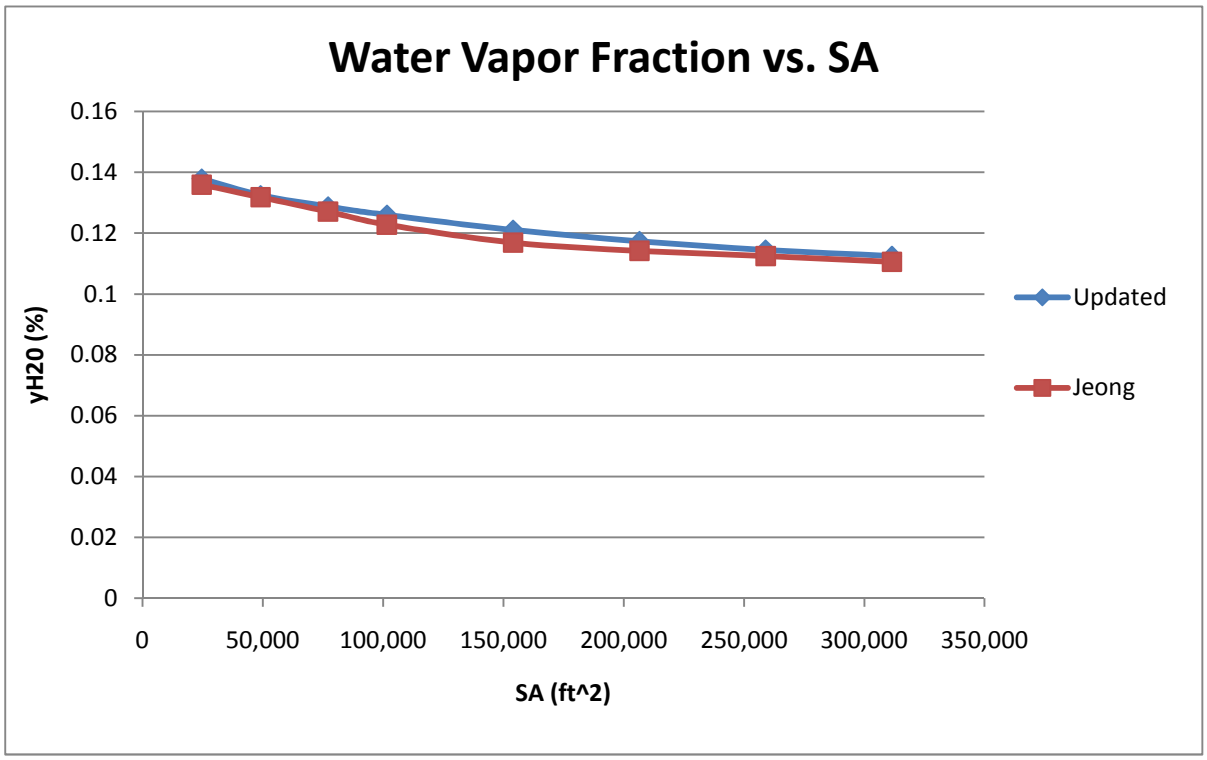

Figure 4 - Fraction of water vapor in flue gas at exit of heat exchanger

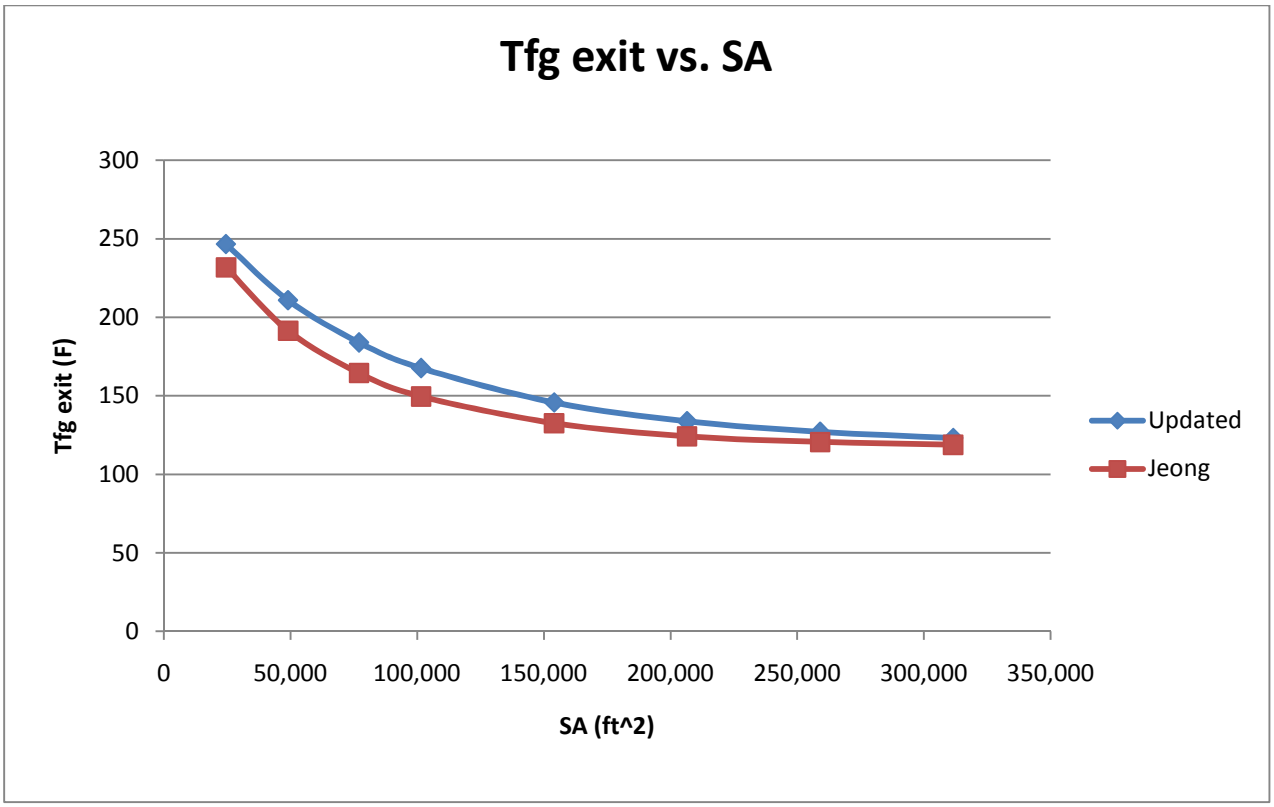

Figure 5 – Agreement between exit flue gas temperature of updated code and Jeong

The resulting graphs in Figure 3 and Figure 4 show that as you increase the surface area or length of a heat exchanger you increase the condensation rate and therefore decrease the water vapor percentage at the exit of the heat exchanger. This in turn decreases the flue gas exit temperature as shown in Figure 5. However, this effect eventually asymptotes due to the limits imposed on the flue gas exit temperature by the cooling water inlet temperature. The same trends were found by Jeong as can be seen. Again, the reason for slightly lower condensation efficiency and higher flue gas exit temperature is because of the refinements done for calculating the flue gas side Nusselt number, and therefore the flue gas side heat transfer coefficient.

3.2 Verification with Michael Lavigne Results

Verification was also done against the work of Michael Lavigne (10). Lavigne edited the MATLAB code that was initially written by Jeong. While most of his simulations dealt with oxyfuel there were some simulations which dealt with regular coal fired flue gas. The geometries and conditions used are shown in Table 3.

Table 3 - Conditions and geometry used by Lavigne

Inlet Conditions						
Mfg (lbm/hr)	Mcw (lbm/hr)	Tcw (F)	yH2O (%)	Tfg (F)		
2.00E+06	1.00E+06	70	0.125	300		
HX Geometry (in-line arrangement)						
OD (in)	Tube thick (in)	St (in)	Sl (in)	Duct Depth (ft)	Duct Height (ft)	Duct Length (ft)
2	0.14	4	4	40	40	20

Figure 6 and Figure 7 are temperature profiles from the simulation. These profiles closely agree with the ones from Lavigne's work. In addition, Table 4 shows the difference in a few key results between Lavigne's calculations and the updated calculations. These agree well, with the percent difference being less than 1%.

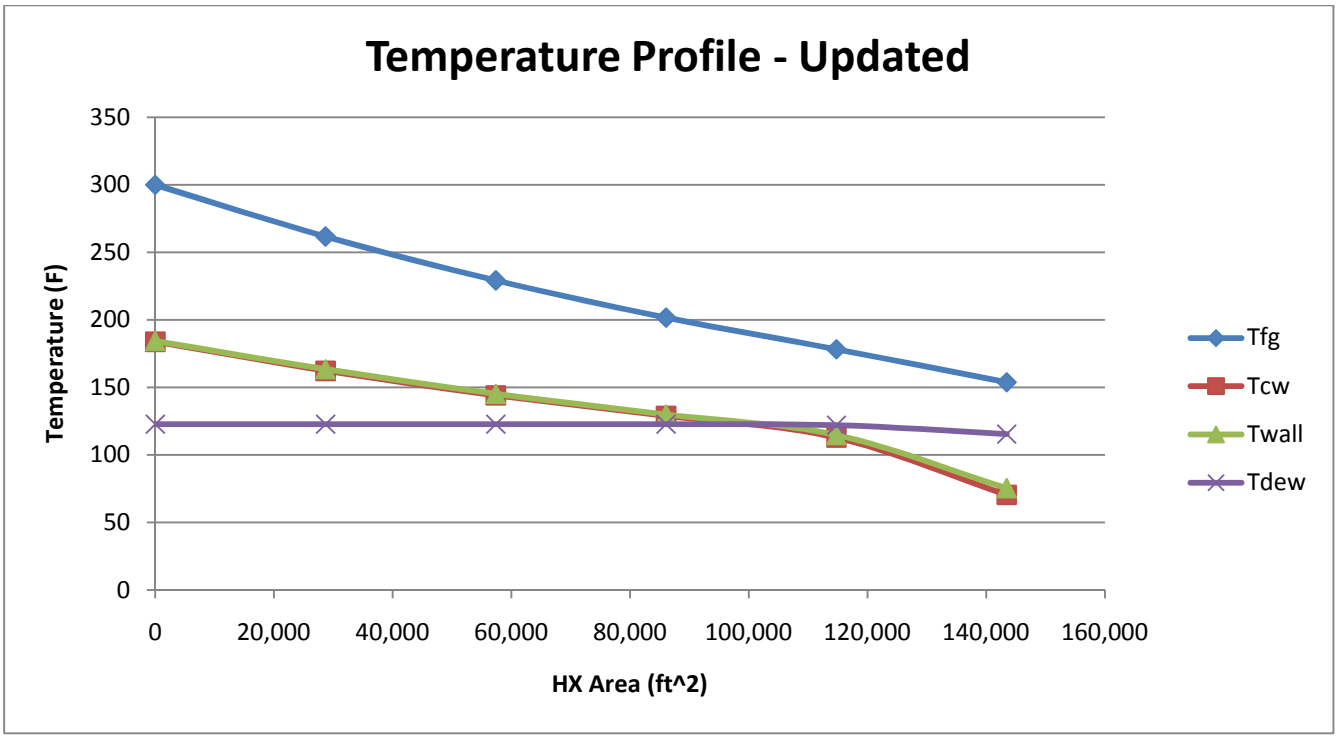

Figure 6 – Temperature profile of results from updated code

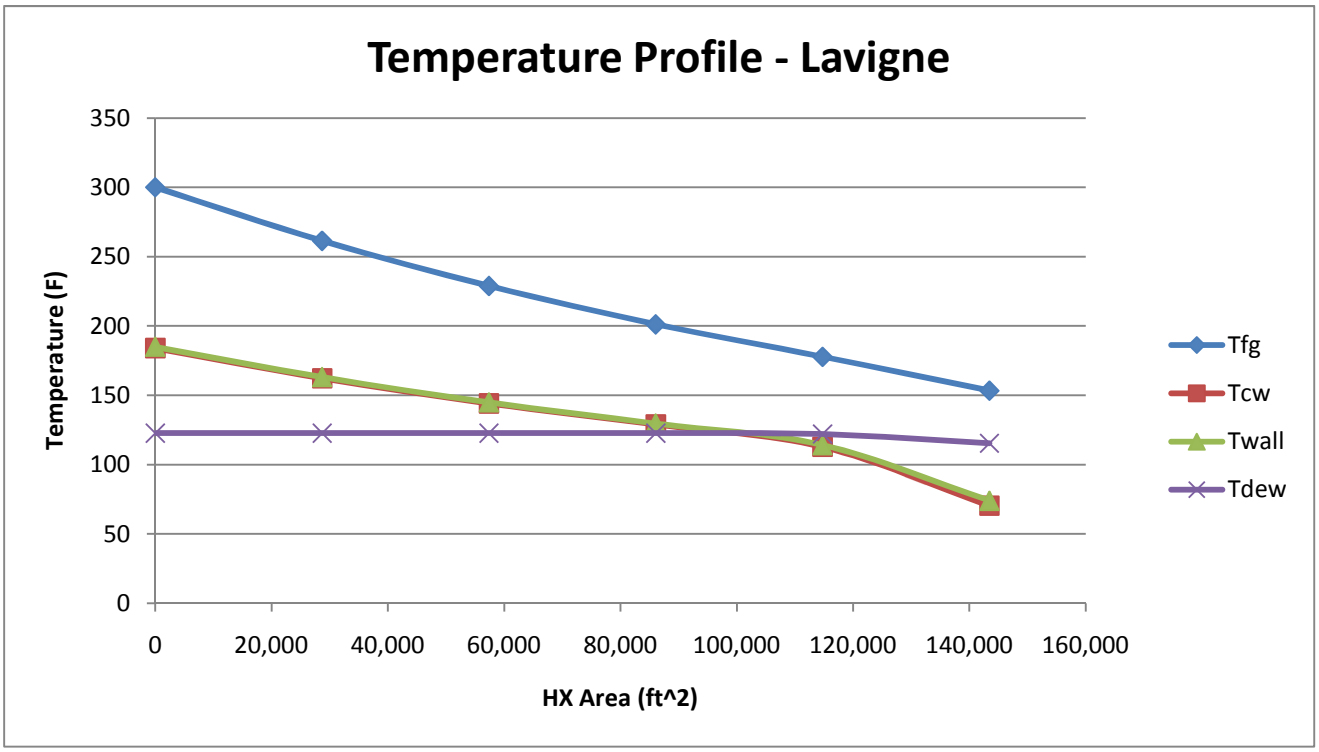

Figure 7 – Temperature profile of results from Lavigne's code

Table 4 - Results agreement between Lavigne code and updated code

	Lavigne	Updated
Condensation Efficiency (%)	20.58	20.53
Total Heat Transfer (BTU/hr)	1.140E+08	1.137E+08
Tfg exit (F)	153.40	153.79
Tcw exit (F)	184.03	183.74

Additional simulations were run with Lavigne's conditions to look at the effects of cooling water to flue gas flow rate ratios on condensation rate and overall heat transfer. The same heat exchanger geometry was used as shown above in Table 4.

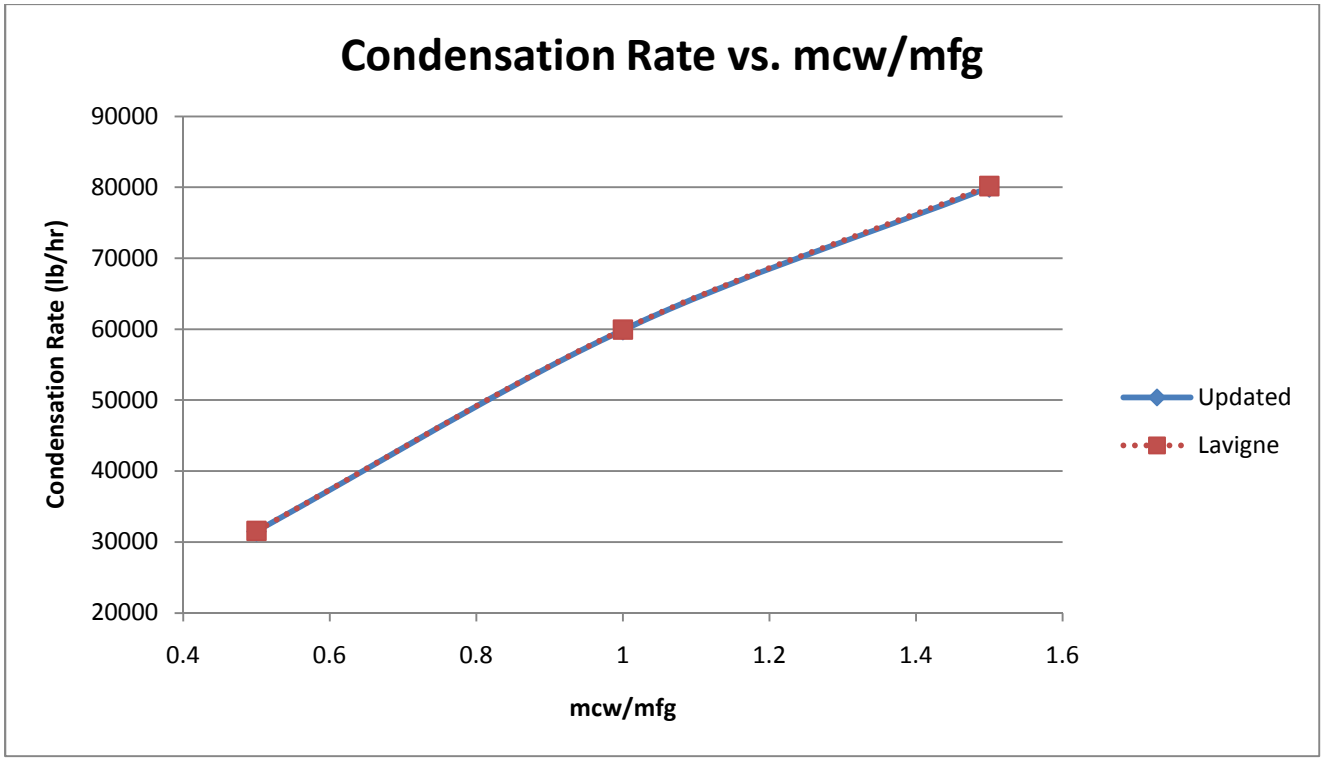

Figure 8 - Agreement for condensation rate for different cw/fg ratios between Lavigne and updated code

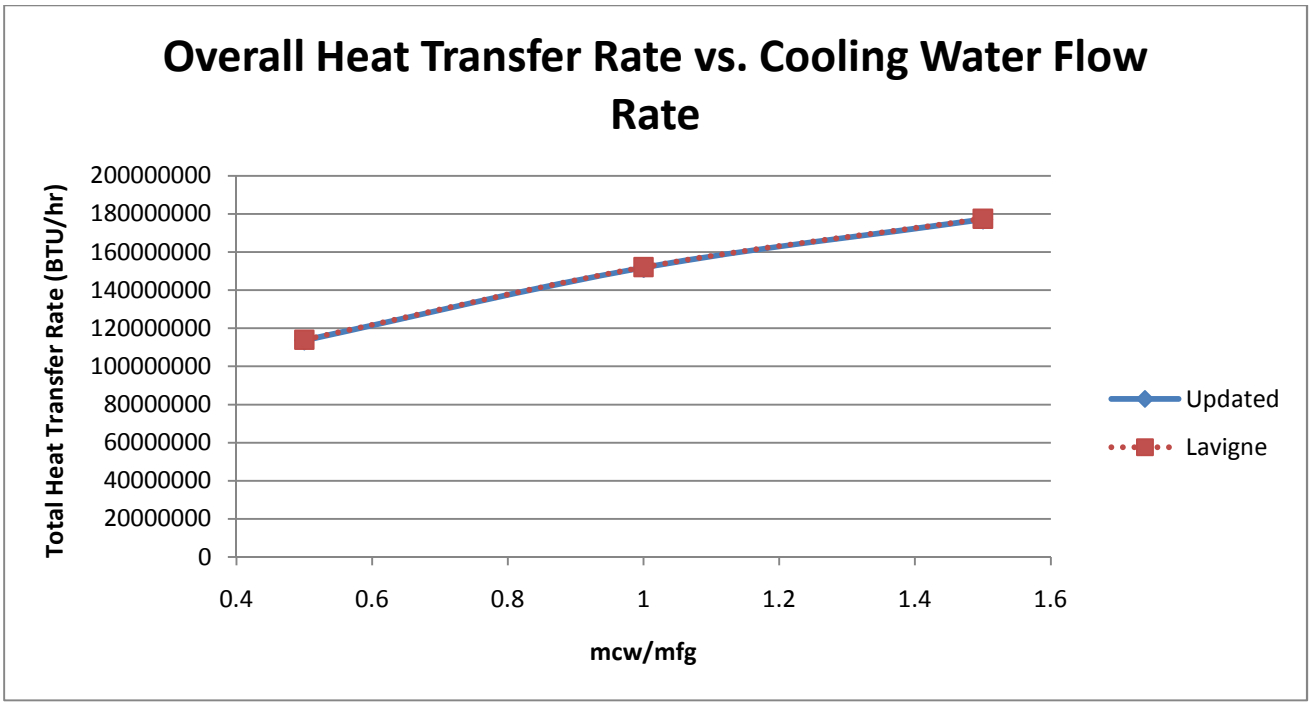

Figure 9 – Agreement for heat transfer for different cw/fg ratios between Lavigne and updated code

As can be seen from Figure 8 and Figure 9, the trends between condensation and heat transfer and cw/fg flow ratios agree well with the simulations and results from Lavigne's work. In addition to showing agreement, the simulations also show the large improvements which can be gained from increasing the water supply rate or decreasing the amount of flue gas through an individual heat exchanger.

4. Heat Exchanger Cost Estimation

4.1 Capital Costs

The costs associated with the heat exchanger are capital costs and operating costs. Capital costs consist of the material cost and fabrication and installation costs. Operating costs are assumed to be mainly a function of the power required for the heat exchanger.

The type of tube material used will have a major influence on what percentage of the total cost is tube material cost alone. The heat exchange surfaces, the tubes themselves, will be the main contributor to the material cost due to the very large surface area (>100,000 ft^2). Information in the published literature on heat exchanger costs led to basing the fabrication and installation costs off of a factor of the raw tube material cost. Fabrication and material costs from the literature were identified as percentages of total capital heat exchanger cost for shell and tube heat exchangers. It was found that as the heat exchanger size increases, the ratio of material cost to total cost rises and the ratio of fabrication cost to total cost decreases (11). For a standard carbon steel heat exchanger, the ratios eventually plateau to where labor cost is roughly three times the cost of the tubing material. This trend is seen in Figure 10. As more expensive materials such as stainless steel and nickel alloys are used, the cost of the heat exchanger is dominated by the tube material cost. For example, with the use of high Nickel Alloy C-276 tubing, the percentage of the total heat exchanger cost that consists of tube material cost is 88%. For estimation purposes, the labor cost involved in assembling a heat exchanger from a relatively expensive tube material was assumed to be the same as the labor cost for fabricating a carbon steel heat exchanger of the same size.

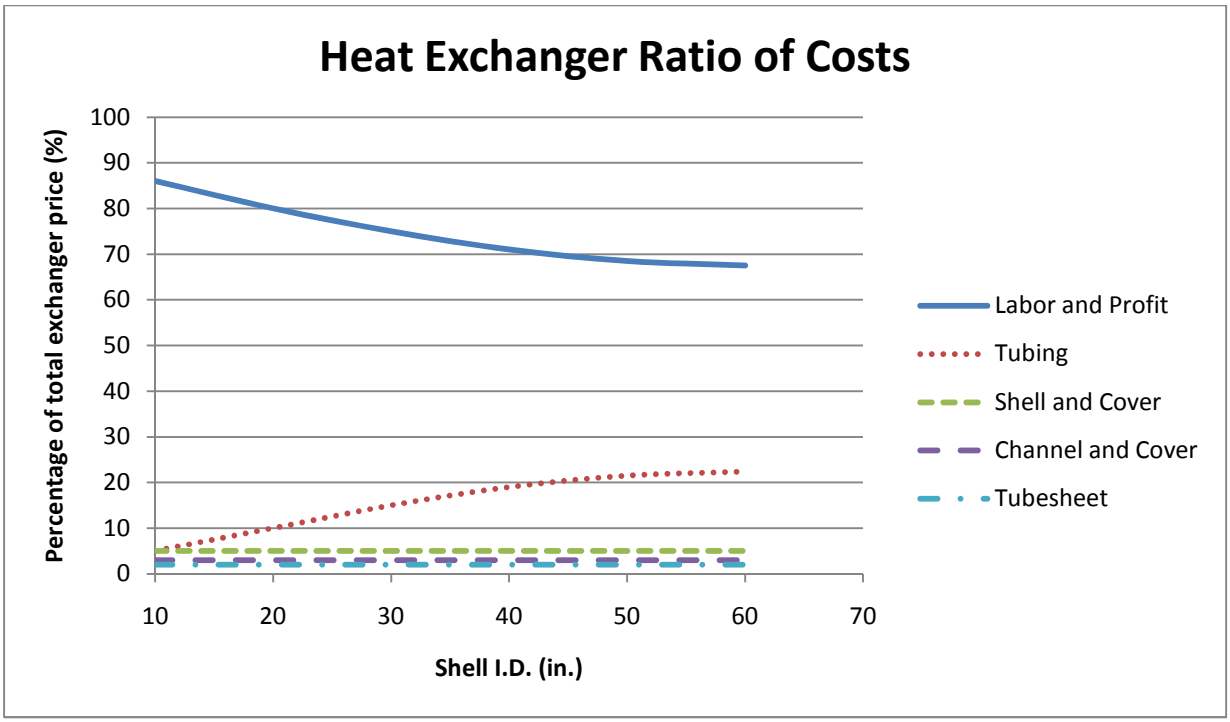

Figure 10 - Ratio of costs (11)

The principal difference between shell and tube heat exchangers that were investigated for costing purposes and the tube bundle heat exchangers investigated in this study is that the shell and tube heat exchangers are manufactured and assembled at the factory and then shipped as a complete unit, whereas with the heat exchangers investigated here, the tubes would be assembled into bundles, shipped to the plant and then installed into a duct at the plant. For this reason, it was assumed that the cost factor used in the literature for manufacture and assembly for shell and tube heat exchangers was going to be much the same as the factor used for manufacture and plant installation of the tube bundle heat exchangers investigated here. As was shown in Figure 10, as heat exchanger surface area increases, the ratio of material cost to total cost rises and the ratio of fabrication cost to total cost decreases. To determine the appropriate factors between fabrication and assembly cost and tube material cost, four cases in the available literature with large heat exchanger surface areas were studied. The calculations showed that the average factor for manufacture and assembly for carbon steel tube heat exchangers is

3.00 times the cost of the material as seen in Table 5 (11). An extra 30% was added to this factor for any unaccounted costs, making the total factor for manufacture and installation of a tube bundle heat exchanger to be 3.90 times the carbon steel tube material cost.

Table 5 - Heat exchanger cost factors (11)

	(Tube Material) / Total	(Manufacture and Assembly)/Total	Ratio
Case 1	20.58	59.42	2.89
Case 2	20.42	59.58	2.92
Case 3	18.90	61.10	3.23
Case 4	20.10	59.90	2.98
Average	**20.00**	**60.00**	**3.00**

Cost of stainless steel tubing was found by getting quotes from manufacturers. Stainless Steel 304 tubing in the 2" OD range was quoted at $2.34/lb (Rolled Alloys). For tubes with an OD of 2.375" and 0.195" thick walls, the translated cost is $10.69/ft. A ratio that is generally used when comparing the cost of stainless steel 304 tubing to carbon steel tubing is 2.80 (11) (12). This would indicate that carbon steel tubing with the same dimensions of the stainless steel 304 tubing mentioned above would cost approximately $3.82/ft. Using the factor mentioned above of 3.90, the manufacture and installation cost would be $14.89/ft. This manufacture and installation cost applies for any tube material. For example, for stainless steel 304 tubing which costs $10.69/ft, the relative manufacture and installation factor is 1.393 making the cost to be the same as carbon steel manufacture and installation at $14.89/ft.

An investigation into the cost of Nickel Alloy 22 tubing led to a cost of $22.00/lb. For a 2.375" OD and 0.195" thick walls, this translates to $110.71/ft. A manufacture and installation cost of $14.89/ft leads to a relative factor of 0.135. The material cost dominates the total capital cost of the heat exchanger for expensive materials. Table 6 shows the relative cost factors and total cost for each type of tube material that was considered.

Table 6 - Cost factors

Carbon Steel		
Type	**Relative Cost Factor**	**Cost/ft ($/ft)**
Tube Material Cost	1.00	$ 3.82
Manufacture and Installation Cost	3.90	$ 14.89
Total	**4.90**	$ 18.71

SS 304		
Type	**Relative Cost Factor**	**Cost/ft ($/ft)**
Tube Material Cost	1.00	$ 10.69
Manufacture and Installation Cost	1.39	$ 14.89
Total	**2.39**	$ 25.58

PTFE (Teflon)		
Type	**Relative Cost Factor**	**Cost/ft ($/ft)**
Tube Material Cost	1.00	$ 40.48
Manufacture and Installation Cost	0.37	$ 14.89
Final Factor	**1.37**	$ 55.37

Ni Alloy 22		
Type	**Relative Cost Factor**	**Cost/ft ($/ft)**
Tube Material Cost	1.00	$ 110.71
Manufacture and Installation Cost	0.13	$ 14.89
Total	**1.13**	$ 125.60

The total installed cost based on the factors above was converted into an annual fixed cost that takes into consideration capital amortization and tax and insurance costs. A monthly payment was derived using the following equation (13):

$$PF = \frac{i(1+i)^n}{(1+i)^n - 1}$$

where PF stands for the monthly payment factor, n is the period of the loan in months and i is the interest rate per month. The period of loan for this research was 20 years and the annual interest rate

was taken to be 5%. This gives a monthly payment factor of 0.0066. This monthly payment factor was used to calculate the annual fixed cost using the following equation:

$$AFC = (12 * PF + 0.015) * (Total\ Installed\ Cost)$$

where AFC stands for annual fixed cost, PF is the monthly payment factor, 0.015 is a factor to take into account taxes and insurance and the total installed cost was explained before. This annual fixed cost does not take into account the power requirements for the full scale heat exchanger.

4.2 Operating Costs

Operating costs come from the power requirements to pump the flue gas through the heat exchanger and the pumping requirements for the cooling water. Fan power for the flue gas was calculated using the method based on pressure drop explained in the section on pressure drop. That section also explained how pumping requirements for the cooling water circuit were calculated. The total operating cost is based on these two power requirements. A 20 year lifetime of the heat exchanger was assumed. There is an assumption that the heat exchanger would be used 7000 hours per year. Finally, a power cost of $0.05/kWhr was assumed, resulting in the final equation:

$$20\ Year\ Operating\ Cost = Power(kW) * \frac{7000\ hrs}{year} * {}^{\$0.05}/_{kWhr} * 20\ years$$

5. Optimization

5.1 Inlet Conditions and HX Geometries

Optimizing the counter-current cross flow heat exchanger consisted of maximizing benefits and minimizing costs. The benefits that needed to be maximized were the rate of water condensation out of the heat exchanger and the total heat transfer to the cooling water from the flue gas.

Operating conditions for the heat exchanger were based on a conventional coal-fired power plant producing about 550 MW of net power. The flue gas flow rate is about 6 million lb/hr. For the base case analysis, the cooling water flow rate was one half that of the flue gas (3 million lb/hr). Flue gas would typically come into the heat exchanger at 300^{o}F and cooling water would typically be available in ranges of 90^{o}F to 105^{o}F. The cross sectional area of the heat exchanger is constrained by available power plant space. The length of the heat exchangers was one of the variables that needed to be optimized and will be discussed later.

Economizers in steam power plants were studied because of their similarities to the heat exchangers being investigated here. Economizers preheat boiler feed water through a series of usually bare tube, in-line, cross-flow heat exchangers. Economizer tubes typically range between OD 1.75" and 2.50" (8). Tubes smaller than 1.75" cause too much water side resistance and therefore high pumping power requirements. In this research, tubes at the upper end of this range were investigated due to their increased surface area for heat transfer, the higher flue gas velocity and therefore higher convective coefficient and the lower water side resistance offered. The investigation into economizers also provided some insight into in-line vs. staggered arrangements. In general, bare tubes arranged in-line have the lowest gas side resistance per unit of heat transfer (8). In addition, in-line arrangements are less likely to plug on the gas side and are easier to clean.

Approximately 70 tube spacing configurations were evaluated. After determining a tube diameter, tube spacings in the transverse and longitudinal directions were considered for both their heat transfer capabilities and the effect they would have on pumping power. A range of suitable spacings was considered. Zaukauskas published experimental results for heat transfer correlations for banks of tubes based on their tube spacing to tube diameter ratio (5). These were defined as:

$$a = {S_t}/{d_o} \quad \& \quad b = {S_l}/{d_o}$$

Recommendations from existing economizer design suggest that the longitudinal spacing, S_l, should be no less than 1.25 times the tube outside diameter. The possible ranges for practical use and for which there are empirical correlations are the following:

$$1.30 \leq a \leq 2.60 \quad \& \quad 1.25 \leq b \leq 2.60$$

This means that for a standard schedule 40 or 80 size 2" pipe with an outside diameter of 2.375", the center to center transverse spacing can range from 3.09" to 6.17" and the center to center longitudinal spacing can range from 2.97" to 6.17". The length of the overall heat exchanger has a great effect on costs because both heat transfer surface area and flue gas side resistance are directly proportional to it. With a given cross-section of 40' by 40' for the heat exchanger, a practical range of lengths was chosen to be from 20' to 50'. Based on preliminary calculations, lengths shorter than 20' would hinder the heat transfer capabilities while lengths longer than 50' would most likely increase the gas side pressure drop too much.

The best way to optimize a particular heat exchanger is to set as many constraints as possible. Flue gas and cooling water inlet conditions were set constant. The duct cross section was kept constant at 40' by 40'. A common schedule pipe size was kept constant at schedule 80 2" pipe. The variables that would then be optimized would then be the tube transverse and longitudinal spacings, S_t and S_l, and the duct length, L. As mentioned before, a suitable range of values for those three variables was chosen. Table 7 shows inlet conditions and heat exchanger geometry that were used for the initial optimization calculations.

Table 7 - Conditions and geometry used for initial optimization

Inlet Conditions				
Mfg (lbm/hr)	Mcw (lbm/hr)	Tcw (F)	yH2O (%)	Tfg (F)
6.00E+06	3.00E+06	100	0.12	300

HX Geometry (in-line arrangement)						
OD (in)	Tube thick (in)	St (in)	Sl (in)	Duct Depth (ft)	Duct Height (ft)	Duct Length (ft)
2.375	0.218	variable	variable	40	40	variable

5.2 Geometric Effects on Cost and Performance

To analyze the individual influence of each of these three variables, S_t, S_l and L, a Taguchi optimization technique was used. In the Taguchi process orthogonal arrays of experiments are used to investigate how different parameters affect the mean and variance of the end goal (14). For this investigation, the two end goals are to maximize condensation or heat transfer and minimize power requirements. To get appropriate size increments without over complicating the process, the parameters and levels which were used are shown in Table 8.

Table 8 - Parameters and levels used for Taguchi optimization

Parameters and Levels				
Parameter	**Level 1**	**Level 2**	**Level 3**	**Level 4**
A: Duct Length (L)(ft)	20	30	40	50
B: Transverse Tube Spacing (S_t)(in)	3.09	4.12	5.14	6.17
C: Longitudinal Tube Spacing (S_l)(in)	2.97	4.04	5.11	6.17

Using the Taguchi process, a setup with three parameters and four levels dictated a L16 orthogonal array as shown in Table 9. Sixteen simulations were run in the heat exchanger code with the parameters and levels shown in Table 9. The numbers 1, 2, 3 and 4 in Table 9 represent the levels of each parameter for that respective column.

Table 9 - L16 array (14)

L16 Orthogonal Array			
Simulation	**L**	**S_t**	**S_l**
1	1	1	1
2	1	2	2
3	1	3	3
4	1	4	4
5	2	1	2
6	2	2	1
7	2	3	4
8	2	4	3
9	3	1	3
10	3	2	4
11	3	3	1
12	3	4	2
13	4	1	4
14	4	2	3
15	4	3	2
16	4	4	1

To obtain the effect of each parameter on the condensation efficiency, we need to take the average of the condensation efficiency of each experiment whenever one level of one parameter is used. For this setup, since there are four levels for three parameters, there will be a total of four of these values for each parameter. For example in Table 10, to find the value for $S_{t,2}$ you would average the condensation efficiencies from simulations 2, 6, 10 and 14. Table 10 shows full scale heat exchanger simulation results of condensation efficiency whenever one level of each parameter, L, S_t, or S_l, is used. For example, the average condensation efficiency you can expect to get when using the L_1 (parameter L with level 1) length of 20' is 5.90%.

Table 10 - Average condensation efficiency for each level of each parameter

L_1	$S_{t,1}$	$S_{l,1}$
5.90	8.50	8.92
L_2	$S_{t,2}$	$S_{l,2}$
6.87	7.25	7.33
L_3	$S_{t,3}$	$S_{l,3}$
7.50	6.61	6.47
L_4	$S_{t,4}$	$S_{l,4}$
8.19	6.09	5.73

Graphically this is shown in Figure 11. As would be expected, increasing the length (level) of the heat exchanger generally increases surface area and therefore increases the condensation. Also, decreasing the spacing between tubes, in both the transverse and longitudinal direction, generally increases surface area and causes the gas side convective coefficient to rise, therefore increasing condensation efficiency. Another thing that can be learned from this graph is the relative effect of one parameter compared to the others. For example, within the range of possible spacing and length, longitudinal spacing has the greatest effect, closely followed by transverse spacing and length of heat exchanger.

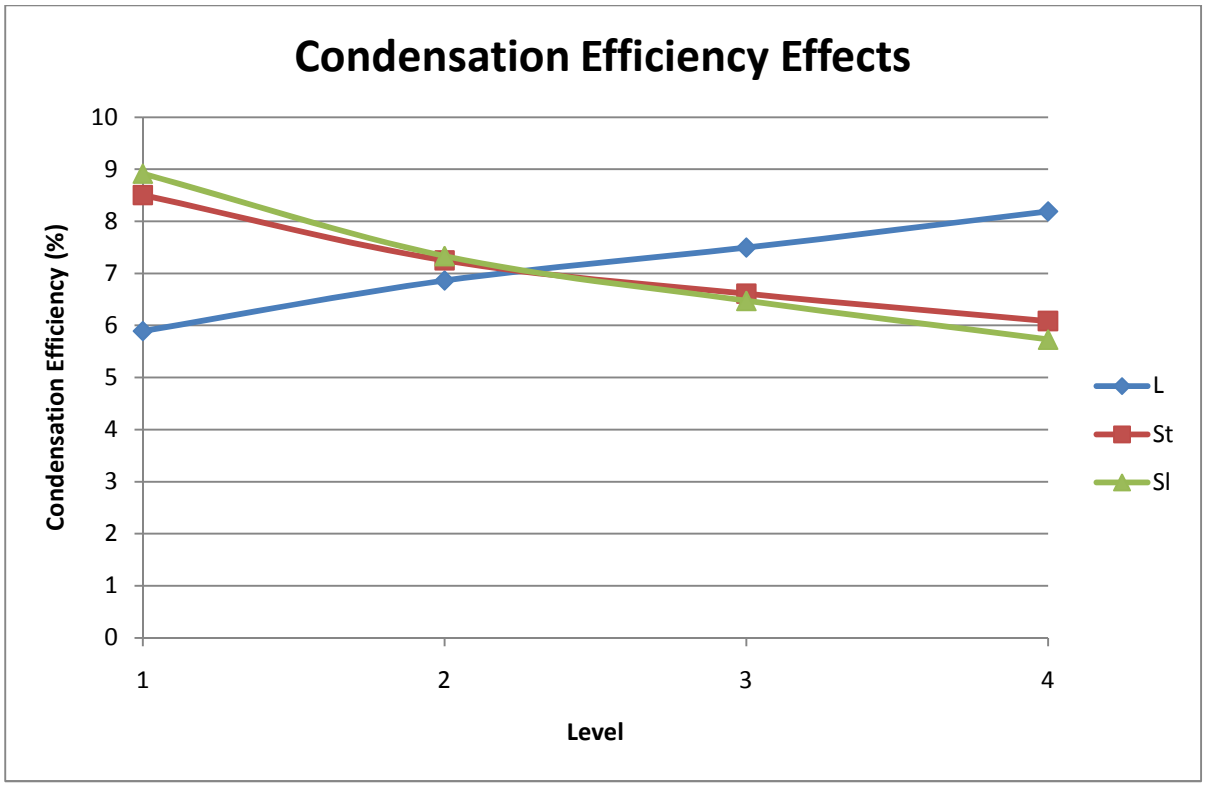

Figure 11 – Plot showing effect of each parameter on condensation efficiency

Table 11 - Levels of parameters that give highest condensation efficiency

L_4 (ft)	$S_{t,1}$ (in)	$S_{l,1}$ (in)
50.00	3.09	2.97

As shown in Table 11, to get the highest condensation rate possible, the length would have to be maximized to 50 ft and the transverse and longitudinal spacing would have to be minimized to 3.09" and 2.97" respectively. However, using these levels will increase the overall cost of the heat exchanger dramatically. Shown in Table 12 is the average capital cost, annual fixed cost times 20 years, operating cost and total 20 year cost for each level of each parameter. The 20 year cost is based on the pumping power requirements of the flue gas fan and cooling water pump combined with the annual fixed cost over the 20 year span. The tubing consists of stainless steel 304 downstream of the onset of water vapor condensation, and Nickel Alloy 22 upstream of the onset of water condensation. Table 13 shows that

the capital cost rise is proportional to increase in tube surface area. This is because the cost of Nickel Alloy 22 tubes is the main contributor to the total capital cost as mentioned before in section 3.1.

Table 12 - Average capital cost and operating cost for each parameter and level

Parameter & Level	Capital Cost	20 Years x Annual Fixed Cost	20 Year Operating Cost	Total 20 Year Cost
L1	$ 26,563,814.81	$ 50,043,405.34	$ 13,280,080.81	*$ 63,323,486.16*
L2	$ 39,379,803.08	$ 74,187,365.85	$ 18,838,962.45	*$ 93,026,328.30*
L3	$ 49,928,344.59	$ 94,059,697.53	$ 22,175,385.67	*$ 116,235,083.20*
L4	$ 61,594,186.99	$ 116,036,905.39	$ 26,524,032.87	*$ 142,560,938.26*
St,1	$ 59,119,617.84	$ 111,375,079.97	$ 48,767,291.70	*$ 160,142,371.67*
St,2	$ 45,425,776.26	$ 85,577,337.09	$ 13,013,557.76	*$ 98,590,894.84*
St,3	$ 39,704,466.80	$ 74,798,997.81	$ 9,660,790.34	*$ 84,459,788.15*
St,4	$ 33,216,288.58	$ 62,575,959.25	$ 9,376,822.00	*$ 71,952,781.25*
Sl,1	$ 60,549,893.31	$ 114,069,567.02	$ 19,353,878.70	*$ 133,423,445.72*
Sl,2	$ 45,248,331.39	$ 85,243,049.79	$ 20,790,863.71	*$ 106,033,913.50*
Sl,3	$ 39,045,732.16	$ 73,558,011.72	$ 20,226,194.03	*$ 93,784,205.74*
Sl,4	$ 32,622,192.63	$ 61,456,745.59	$ 20,447,525.36	*$ 81,904,270.95*

Table 13 - Average capital cost and tube surface area

Parameter & Level	Capital Cost	20 Years x Annual Fixed Cost	Tube Surface Area (ft^2)
L1	$ 26,563,814.81	$ 50,043,405.34	1.59E+05
L2	$ 39,379,803.08	$ 74,187,365.85	2.29E+05
L3	$ 49,928,344.59	$ 94,059,697.53	2.86E+05
L4	$ 61,594,186.99	$ 116,036,905.39	3.50E+05
St,1	$ 59,119,617.84	$ 111,375,079.97	3.35E+05
St,2	$ 45,425,776.26	$ 85,577,337.09	2.61E+05
St,3	$ 39,704,466.80	$ 74,798,997.81	2.31E+05
St,4	$ 33,216,288.58	$ 62,575,959.25	1.97E+05
Sl,1	$ 60,549,893.31	$ 114,069,567.02	3.41E+05
Sl,2	$ 45,248,331.39	$ 85,243,049.79	2.60E+05
Sl,3	$ 39,045,732.16	$ 73,558,011.72	2.28E+05
Sl,4	$ 32,622,192.63	$ 61,456,745.59	1.95E+05

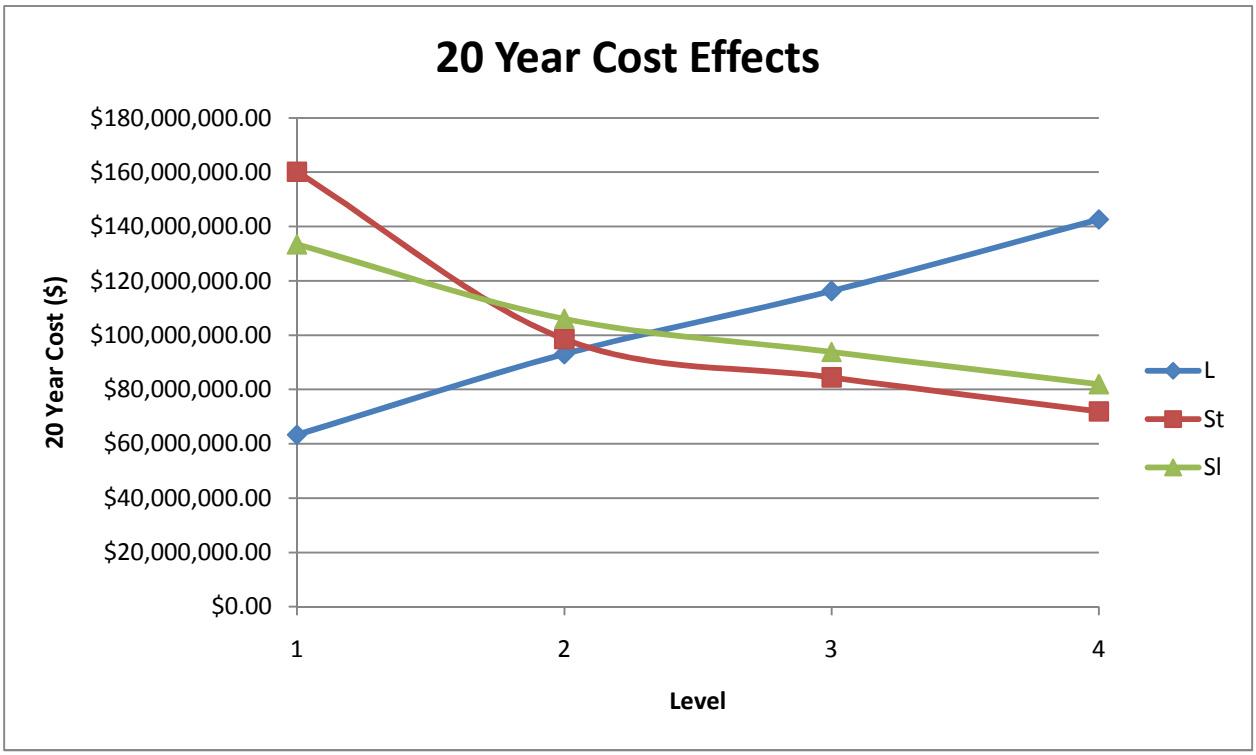

Figure 12 – Plot showing effect of each parameter on total cost

There are many things to be learned from the trends illustrated in Figure 12. Transverse spacing, S_t, dramatically affects the overall cost because it is directly related to the velocity of the flue gas through the heat exchanger and therefore related to the flue gas pressure drop. As S_t increases, there is more free stream area, allowing lower velocities and decreasing pressure drop. Longitudinal spacing, S_l, affects the overall cost because as it increases, less turbulence is caused in the heat exchanger meaning a smaller overall pressure drop. Increasing the length of the heat exchanger adds more tubing, adding cost. Also, flue gas pressure drop is linearly proportion to the number of rows in the heat exchanger which is directly proportional to the length. The optimal levels of each parameter to achieve minimum overall cost are given in Table 14.

Table 14 - Levels of each parameter for lowest total cost

L_1 (ft)	$S_{t,4}$ (in)	$S_{l,4}$ (in)
20	6.17	6.17

These levels are the opposite of the levels needed for the best condensation efficiencies and heat transfer. However, they give confidence to the calculations and simulations. They also give valuable information about which parameters have the most effect.

For a more robust optimization technique, condensation efficiencies and rates of heat transfer must be directly compared against overall cost. The program code is written in MATLAB. This makes computing time relatively short. For this reason it is possible to run several simulations in one session. Referencing the parameters and levels table from above gives three parameters and four levels. This would equate to $4^3 = 64$ possible combinations of length, transverse spacing and longitudinal spacing. Doing this many simulations would take time but would ensure the best and worst combinations are

looked at. The same inlet conditions as the ones above were used. The results of these combinations, plotted as condensation efficiency vs. overall cost are shown in Figure 13. (Note: Some points are omitted because the exit cooling water temperature would have to be above boiling.) As would be expected the graph shows that as condensation efficiency increases so does the overall cost of the heat exchanger.

Figure 14 shows the influence of longitudinal spacing, S_l, on the condensation efficiency. This graph used the same data as the figure before it. However, the series were separated according to constant S_l. It is seen that in most cases the smaller longitudinal spacing of 2.97" gives better condensation efficiency per overall heat exchanger cost. This is due to the fact that the extra tubes in that direction raise the surface area value without causing too much flue gas side pressure drop. Figure 15, showing the influence of transverse spacing, S_t, exhibits less of an impact from changing S_t. Transverse spacings ranging from 4.12" to 6.17" show similar condensation efficiency per total cost while a spacing of 3.09" shows lower condensation per cost than the other levels. However, when looking at the best fit lines, the transverse spacing of 6.17" shows slightly better condensation performance in that it gives slightly better condensation efficiencies per overall cost than the smaller spacings.

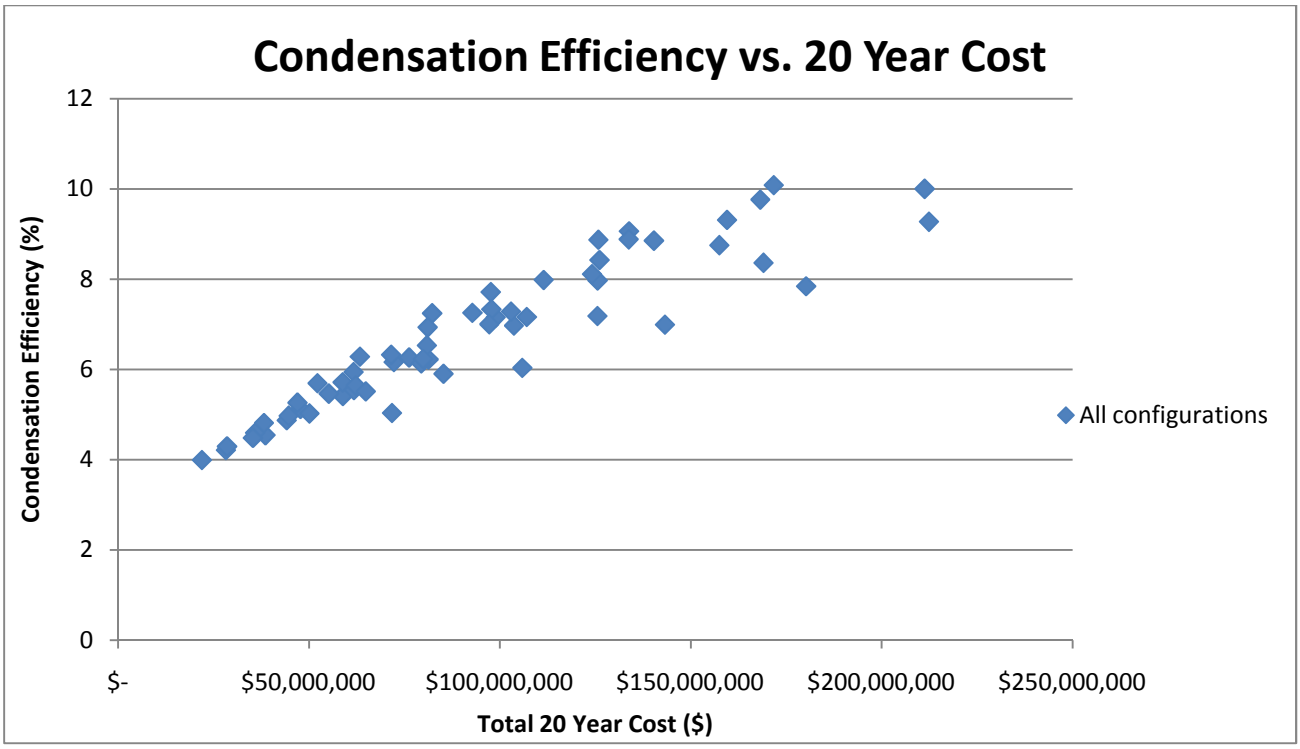

Figure 13 – Condensation efficiency for all cases

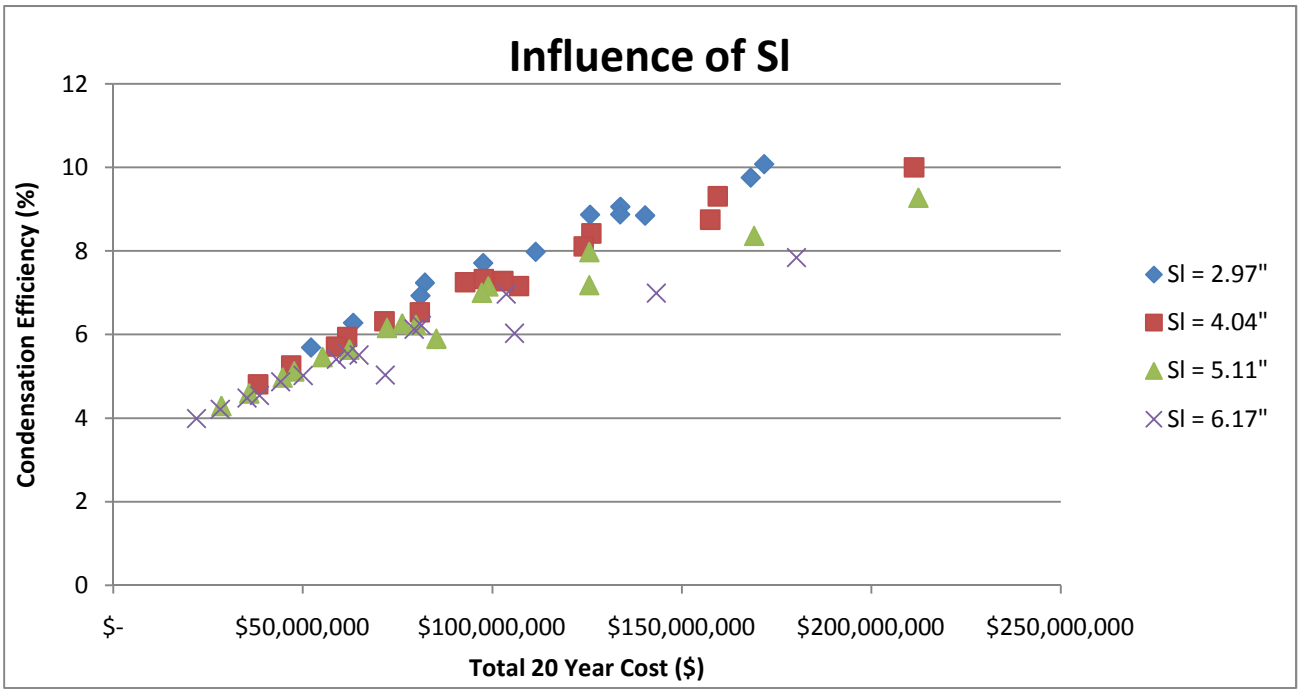

Figure 14 – Longitudinal spacing effect on condensation

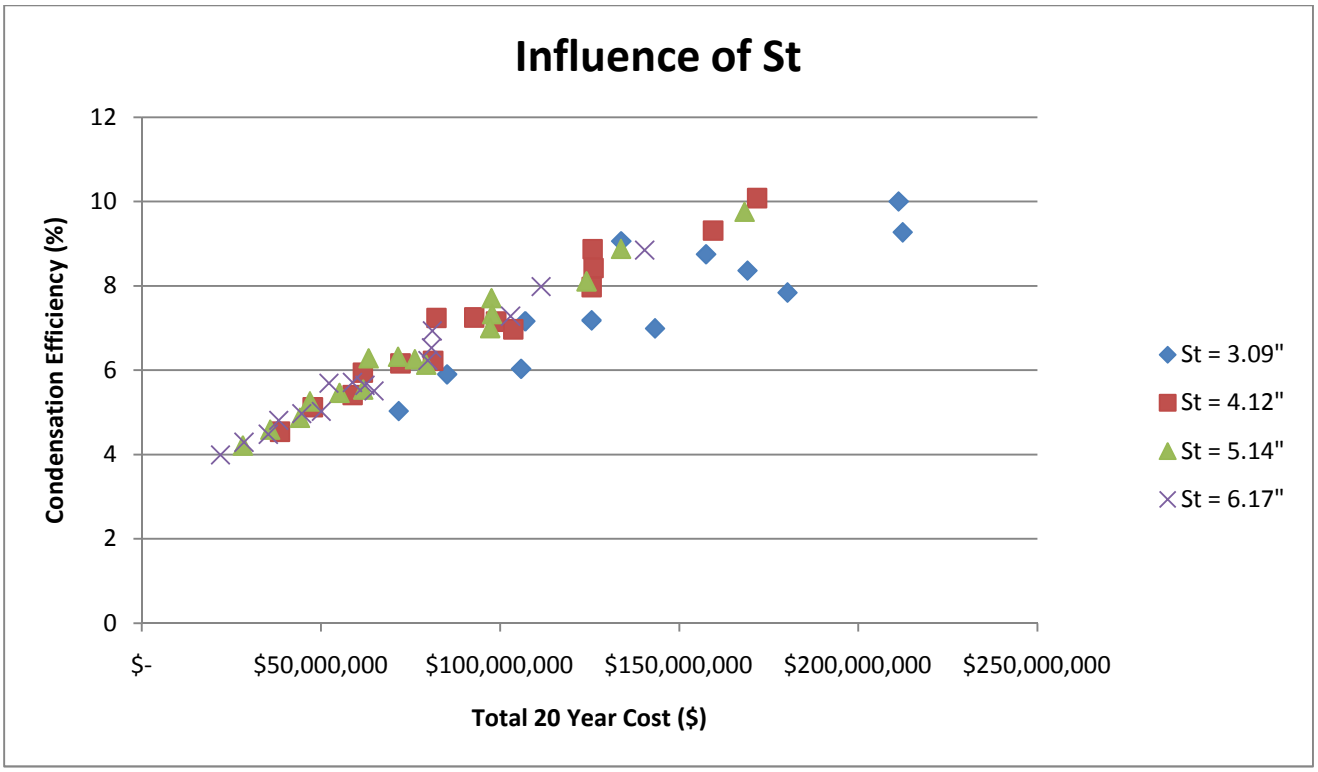

Figure 15 – Transverse spacing effect on condensation

Figure 16 shows that total heat transfer vs. 20 year overall cost. The overall heat transfer to the cooling water from the flue gas is an added benefit to the system. Figure 17, which illustrates the influence of S_l, shows that the smaller spacings of 2.97" provide slightly better heat transfer than the larger spacings. The graph that shows the influence of S_t, Figure 18, is more mixed but generally shows that a transverse spacing between 4.12" and 6.17" gives better heat transfer performance. Both the condensation optimization and heat transfer optimization therefore show that the smaller size of 2.97" for S_l provides the best condensation and heat transfer per total cost of the system. While the results for the other parameter, S_t, were a bit more mixed, generally the larger spacings between 4.12" and 6.17" gave better condensation and heat transfer performance. This is expected because a larger longitudinal spacing will provide more surface area for heat transfer while not increasing the flue gas side pressure drop significantly. In contrast, decreasing the transverse spacing increases the flow resistance in the tube bank considerably.

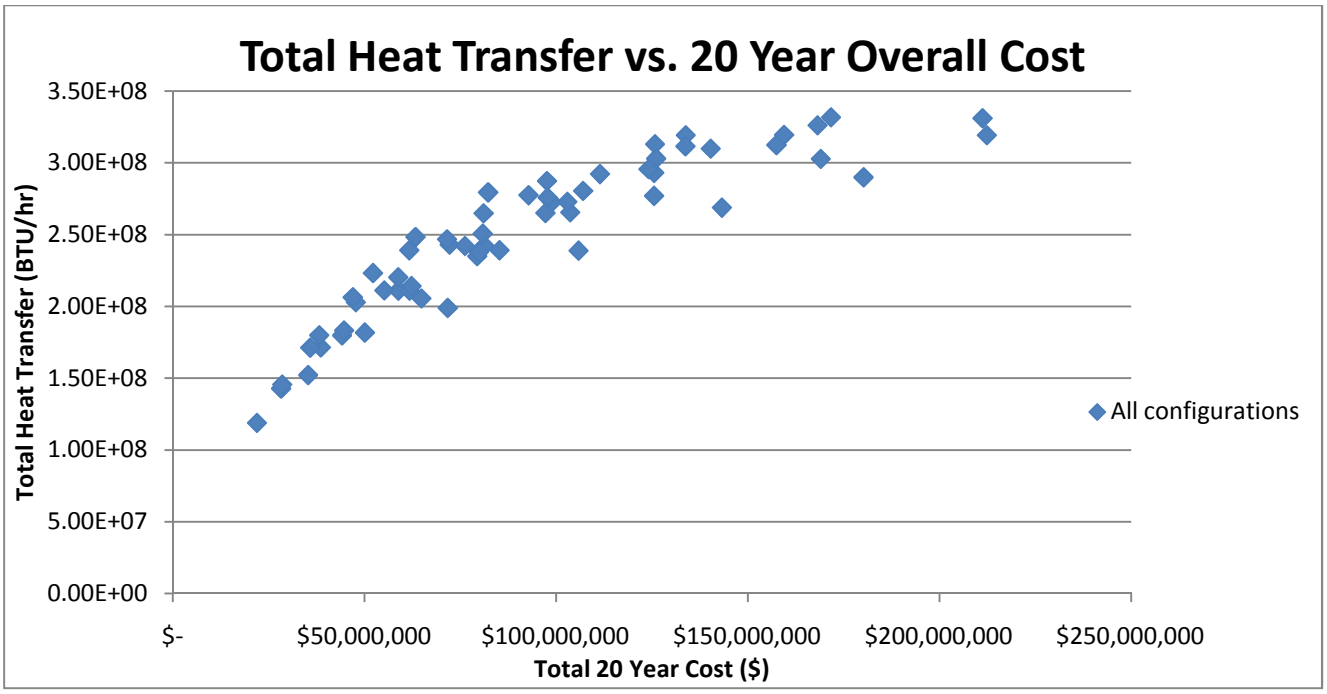

Figure 16 – Heat transfer for all cases

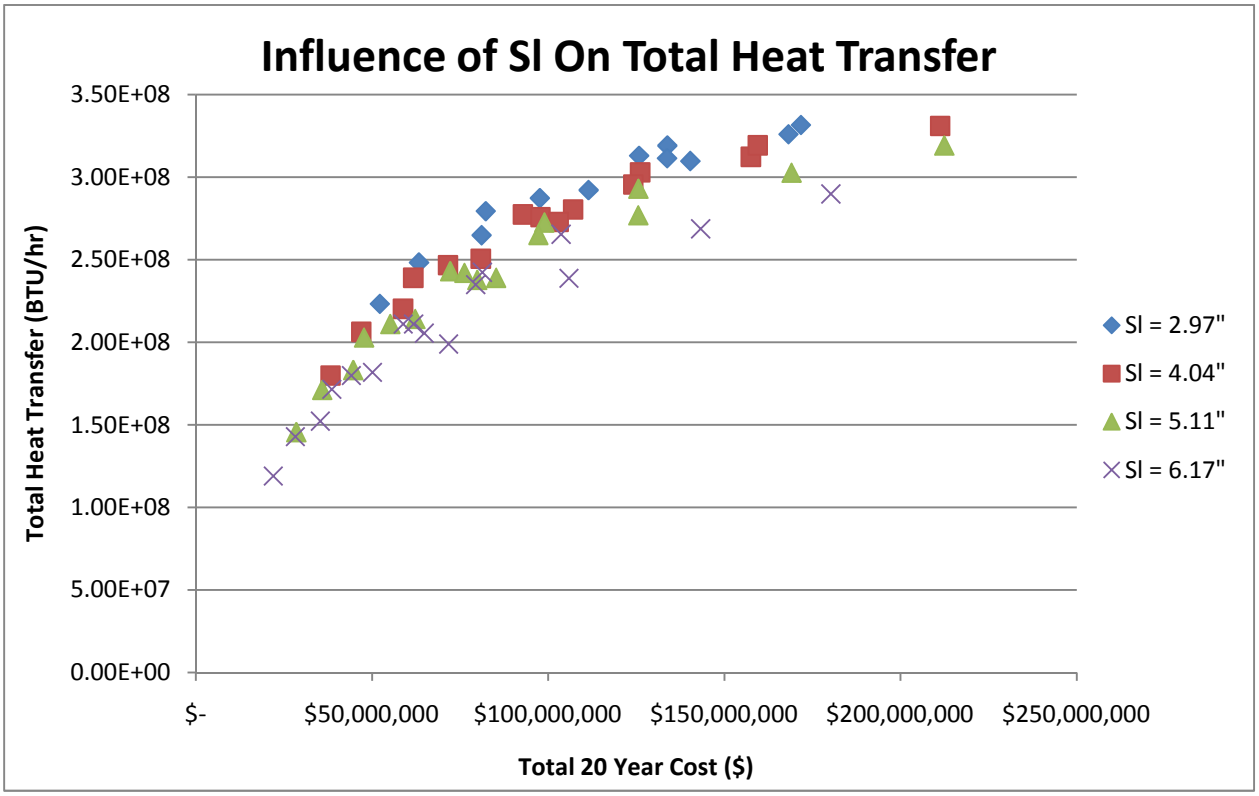

Figure 17 – Longitudinal spacing effect on heat transfer

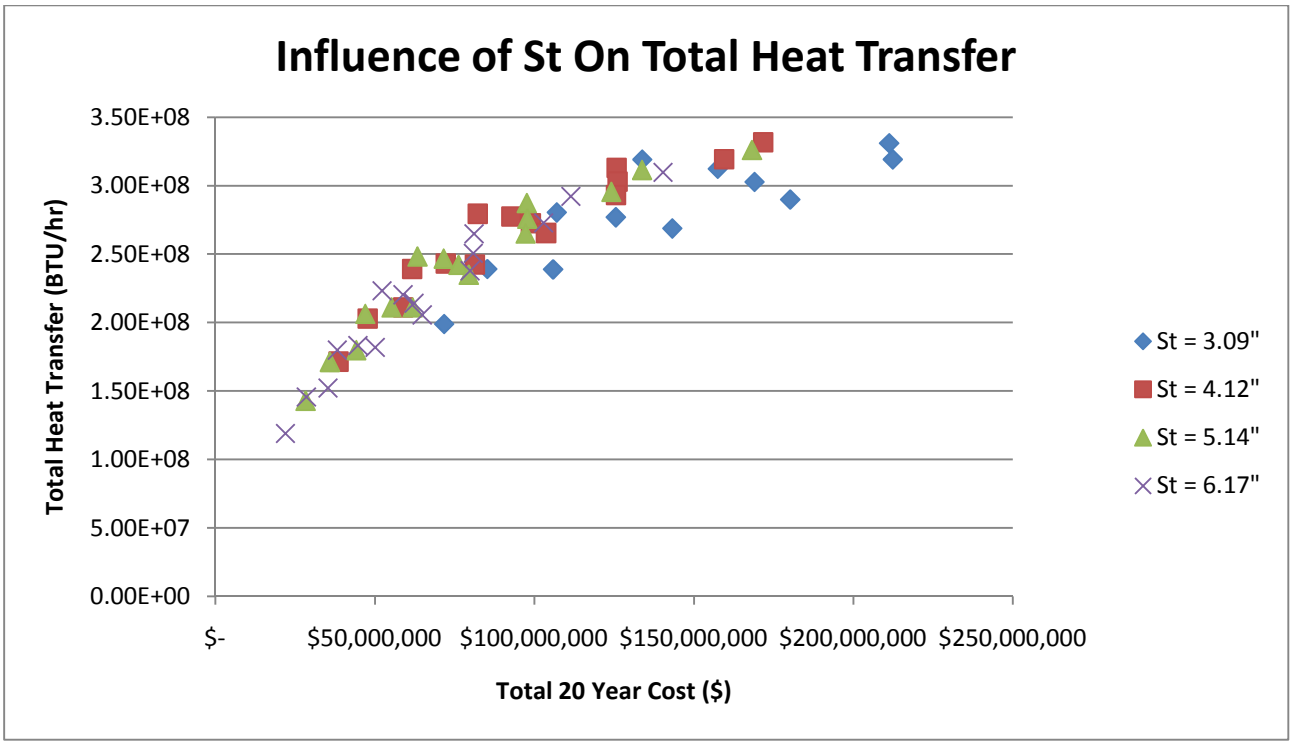

Figure 18 – Transverse spacing effect on heat transfer

6. Materials

6.1 Possible Tube Materials

The choice of tubing material to be used in the full scale condensing heat exchanger is a critical issue. The outside of the heat exchanger tubing is constantly being subjected to sulfuric acid condensation. Figure 19 shows the dew point temperature of sulfuric acid vs. acid and water vapor volumetric concentrations. The standard inlet conditions considered in this research were flue gas at 300^{o}F with a water vapor concentration of 12% and an acid concentration of 15 ppm. This corresponds to a sulfuric acid dew point temperature of 290^{o}F. For these conditions, sulfuric acid would condense on the surface of the tubes throughout the entire heat exchanger. The dew point temperature of water vapor in the presence of non-condensable gases with a mole wet fraction of water vapor of 12% is 121^{o}F. Water vapor dew point temperature vs. volumetric concentration is shown below in Figure 20.

For the length of heat exchanger in which there is both water and sulfuric acid condensation ($T_{wall} < T_{H2O\ DP}$), the liquid mixture of water and sulfuric acid which forms on tube surfaces is approximately two orders of magnitude more dilute in sulfuric acid than the highly concentrated acid solutions which form at temperatures above the water vapor dew point temperature, but below the sulfuric acid dew point temperature.

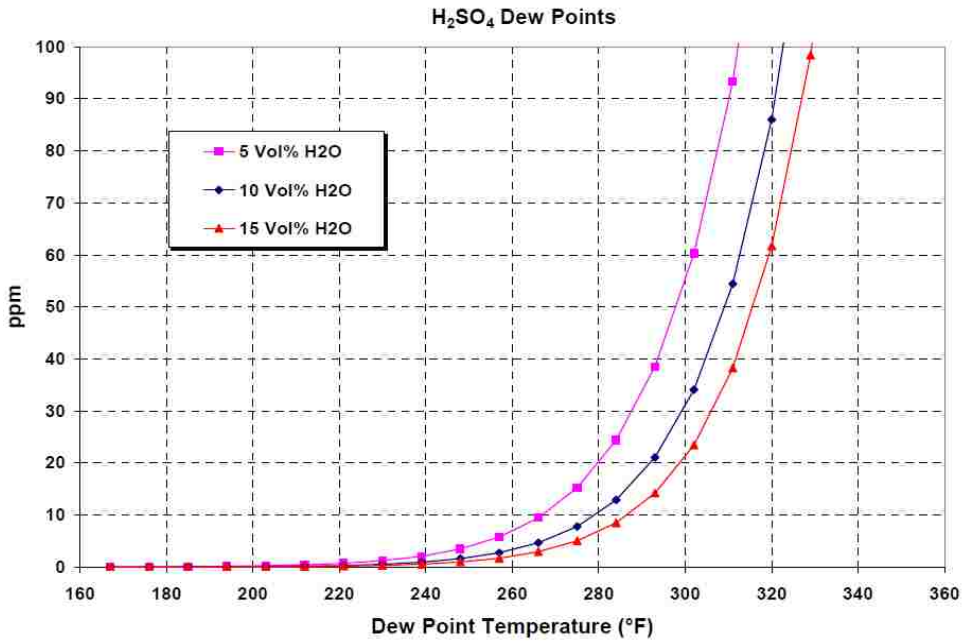

Figure 19 (15) – Sulfuric acid dewpoint

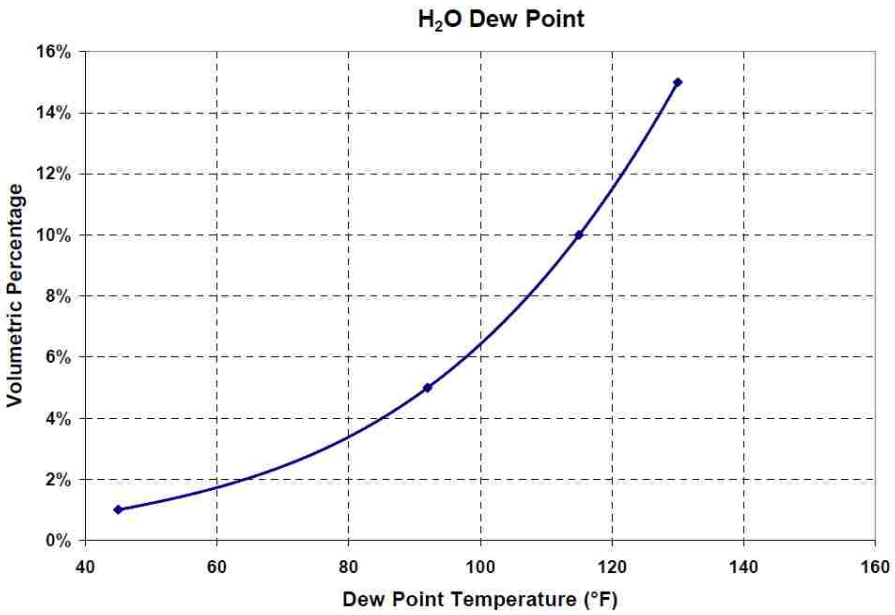

Figure 20 (15) – Water dewpoint

Studies were carried out by the Lehigh University Materials Science and Engineering Department to determine the best materials to use in the two distinct acid regimes explained above: (1) high temperature with high concentrations of sulfuric acid and (2) low temperature with a mixture of sulfuric and water condensation. The materials were selected based on their ability to provide corrosion resistance from acid attack.

Tube materials that were considered were Teflon (PTFE), stainless steel, high nickel alloy steels and Teflon coated steel. Based on a 20 year heat exchanger life and a minimum tube wall thickness of 5mm, the maximum allowable rate of corrosion is 0.25mm/year. For the low corrosion region tubes, the materials that would pass are Stainless Steel 304, 316 and 2205, Teflon and the high nickel alloy steels. In the high acid region, the materials that would work according to the allowable corrosion rate were Teflon and high nickel alloy steel Nickel Alloy 22.

The mechanical and thermal properties and the cost of the above materials were investigated. In the low temperature region Stainless Steel 304 proved to be the most attractive material. Stainless

Steel 304 offered about the same mechanical and thermal properties as the other grades of Stainless Steel, yet is cheaper than those grades and much cheaper than both PTFE and high nickel alloy steels. A quote from one manufacturer (Rolled Alloys) had Stainless Steel 304 at $8.60/linear foot for Schedule 40 OD 2.375" tubing.

On the high temperature end of the heat exchanger, Nickel Alloy 22 offered thermal conductivity in the same order as stainless steel (≈ 7 BTU/(ft*hr*F) @ 300^{o}F) (16). However, the price of Nickel Alloy 22 was quoted from $22/lb - $26/lb, or for 5mm thick tubing, $110 - $130 per foot of tubing. The other option for this region was Teflon (PTFE). While Teflon proved to be very resistant to sulfuric acid corrosion, the thermal conductivity is extremely low at 0.14 BTU/(ft*hr*F) (17). In addition to the low thermal conductivity of PTFE, the tensile strength is very low at 3.90 ksi, compared to a tensile strength of 120 ksi for Ni Alloy 22 (17) (18). An investigation of the cost of PTFE tubing led to an approximate cost of $32/lbm (Fluoro-Plastics). When considering the low density of PTFE, the price comes out to about $40.48/ft for PTFE compared to $110.71/ft for Ni Alloy 22 for the same wall thickness of 2.375" OD tube. To fully compare PTFE tubing to Ni Alloy 22, simulations were run with each material to account for the low thermal conductivity, low strength and relatively low cost PTFE against the high strength, relatively high conductivity and high cost Ni Alloy 22.

6.2 PTFE - Strength vs. Heat Transfer

Due to the extremely low thermal conductivity of PTFE, it was determined that a minimum tube wall thickness would give the lowest thermal resistance between the cooling water on the inside of the tube and the flue gas on the outside of the tube. However, the thickness of the tube wall would be constrained because of the poor strength properties of PTFE. For this reason, basic strength and stress calculations to determine a minimal thickness were done first and secondly, heat transfer calculations were completed and then compared to Ni Alloy 22 tubing. It should be noted that due to the poor

strength properties of PTFE, extra tube supports and special tube bundle arrangements would be needed for Teflon tubes. Despite this, the following comparisons of Ni Alloy 22 and PTFE heat exchangers assume the same tube bundle arrangement and no use of extra tube supports for the PTFE bundles.

6.2.1 Deflection

PTFE is a very elastic material in comparison to most metals. PTFE can elongate up to 400% of the original length before finally breaking (17). The elastic bending of PTFE tubes in the heat exchanger would greatly affect the tube spacing and therefore the heat transfer, pressure drop and overall performance of the heat exchanger. With a 40' x 40' duct cross section, the total length of each tube would be 40'. Calculations were first done to determine where supports would be needed so that the maximum deflection would not be too great to affect tube spacing. Vertical PTFE tubes were determined to be needed because the tubes would only need to support a distributed force from the flue gas induced drag, instead of the distributed load of the fluid drag and tube weight that would take place with horizontal tubes. The assumption was made that the tube would be fixed at both ends. For this set up, the maximum deflection occurs at the middle point and is equal to:

$$\Delta_{max} = \frac{wl^4}{384EI}$$

where w is the distributed load, *l* is the length between supports, E is the elastic modulus and I is the moment of inertia. The distributed load in this study would be the drag caused by the flue gas. The value of flue gas free stream velocity with a mass flow rate of 6.0E6 lb/hr and a 40' X 40' cross section is about 18 ft/sec. With this velocity and tube OD of 2.375", the Reynolds number would be 21,347. Using a conservative coefficient of drag value of 1, the following equation gives the distributed drag force:

$$Drag/_{length} = C_D \, 1/_2 \, \rho d_o$$

where C_D is the coefficient of drag, ρ is flue gas density, V is free stream velocity and d_o is the outer diameter of tube. With this equation, the distributed load on the tube is 0.0542 lbf/ft. Using this value in the maximum deflection equation above with a tube thickness of 0.20" the relationship shown in Figure 21 is obtained.

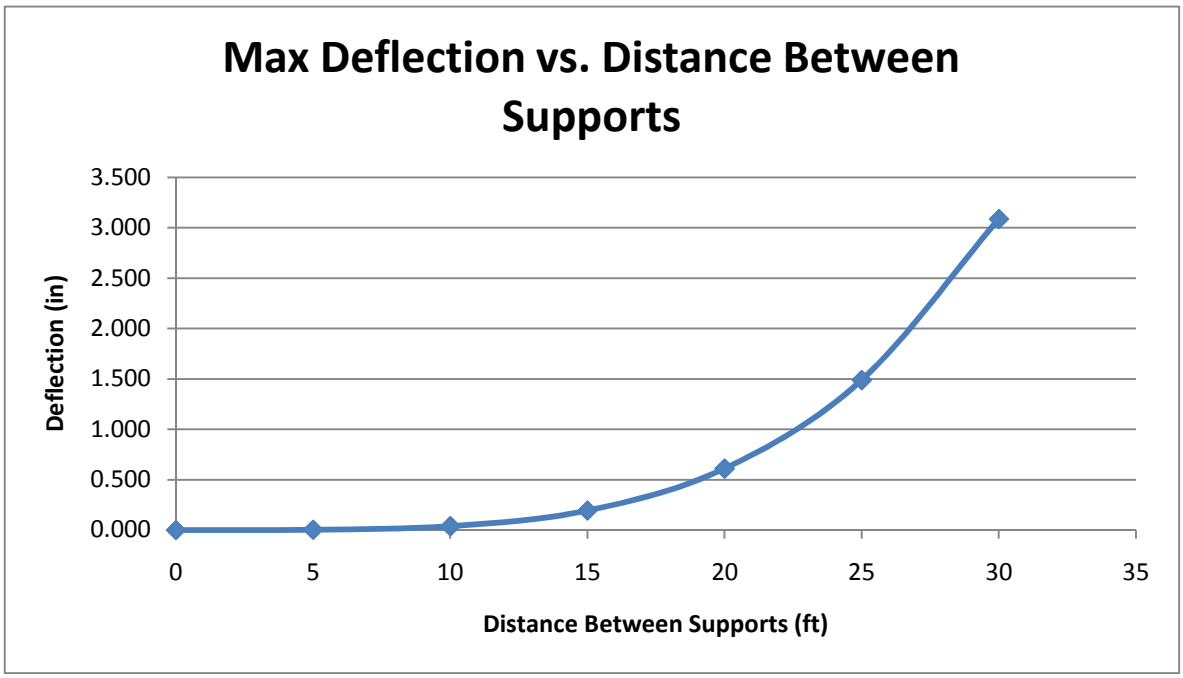

Figure 21 – Tube deflection

Center to center tube spacings that were used in the simulations varied from 1.25*OD to 2.60*OD, where OD is the outer diameter of the tube being used. The heat transfer and pressure drop calculations are sensitive to the spacing in both the longitudinal and transverse directions. Simulations and power requirement calculations done with varying tube spacing showed that a change in spacing of 0.10" will change the fan power required for the flue gas by 10.1%. Tube deflection will affect flue gas pressure drop and heat transfer and for this reason a maximum allowable deflection of 0.10" is assumed. This limit would also assist in extra stresses that would contribute to creep, which will be discussed shortly. From this graph and the data it was made from, if deflection between tubes needs to

be less than 0.10”, then the maximum distance between tube supports should be no greater than 10’. This result does not change much with increasing the thickness of tube as it is heavily dependent on distance between supports. Knowing that the tube must be supported every 10’ enables better calculation of stresses at different points down the tube to ensure yield stress is not exceeded. Vertical PTFE tubes supported every 10’ may not be practical. Nevertheless, this arrangement was used in this study to enable comparison between the performance of a hypothetical PTFE heat exchanger vs. a Nickel Alloy 22 heat exchanger.

6.2.2 Stress

When subjected to elevated temperatures, the yield stress of PTFE tends to decrease substantially. Available data shows that the yield stress at temperatures near 250^{o} F is close to 500 psi (19) (17). Taking a factor of safety of 2.5 this affords a maximum magnitude of stress at any point in the tubing to be 200 psi. The stresses that needed to be accounted for were: (1) Tensile axial stress due to material weight, (2) Bending stress from flow induced drag and (3) Stresses from the internal pressure. Stresses were calculated at three different locations, A, B and C, as shown in Figure 22.

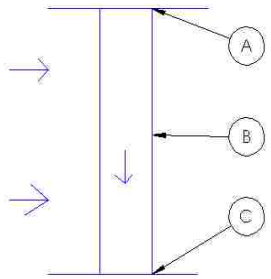

Figure 22 – Tube stress locations

The axial stress is calculated using the weight of the PTFE material within 10’ of tube with the following equation:

$$\sigma = \frac{F}{A}$$

Bending stresses due to drag are calculated from the bending moment imposed from the distributed drag force as explained earlier. The bending moment as a function of distance is calculated from the following equation for a beam fixed at both ends:

$$M = \frac{w}{12}(6lx_{tube} - l^2 - 6{x_{tube}}^2)$$

where w is the distributed drag force, l is the total beam length (10') and x_{tube} is the distance from one end. Using this equation, the maximum moment is at points A and C. The moment is input into the following bending stress equation:

$$\sigma = \frac{My}{I}$$

where M is the moment, y is the maximum distance from the center of gravity (in this case OD/2), and I is the moment of inertia.

The internal pressure of the cooling water causes stress on the thin walls of the tube. This stress is classified as hoop stress (20). An illustration showing the location of this stress is shown in Figure 23. It is calculated from the equation below.

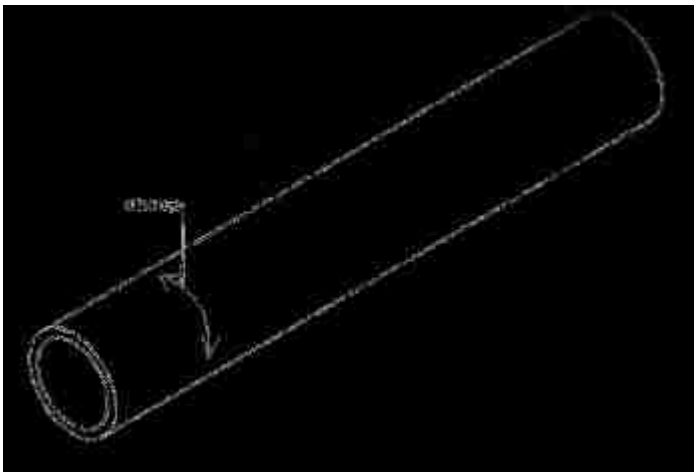

Figure 23 – Stress from internal pressure

$$\sigma_{hoop} = \frac{pr_1}{t}$$

where P is the internal pressure of the fluid, r_1 is the radius from the center to the inner tube wall surface and t is the thickness of the tube. Calculated pressure drops through the tubes varied from 50 psi to 300 psi depending on cooling water velocity and several other factors.

PTFE is influenced by creep when subjected to long term stress and this effect is amplified at high temperatures. A manufacturer of PTFE Schedule 80 pipe (2.375" OD, 0.218" wall thickness) recommended usage in only low pressure applications (21). This manufacturer gathered data on the effects of long term creep which created 5% deformation over 100,000 hours and published the graph shown in Figure 24. The company recommends an internal pressure of only 15 psi for 2" schedule 80 pipe at 300^{o}F (21). Pressure drop calculations shown elsewhere in this report show that axial pressure drops would be larger than 15 psi. Despite this, the following analysis assumes a maximum internal pressure of 15 psi.

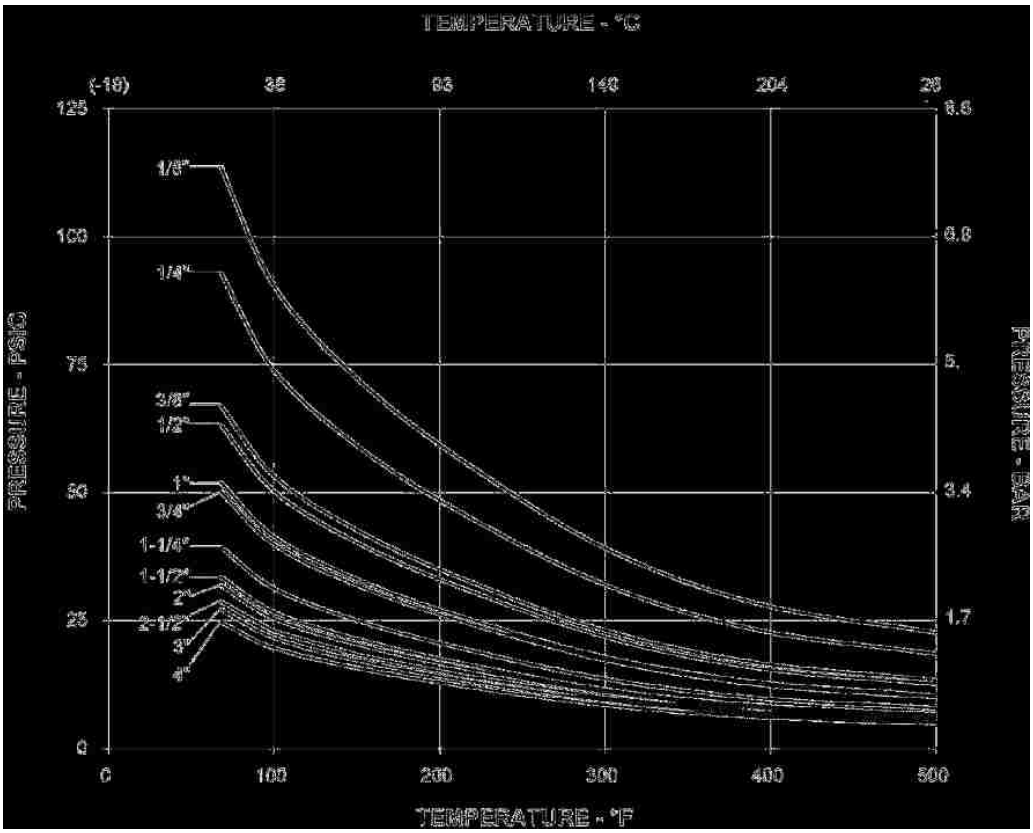

Figure 24 - Pressure Ratings for PTFE Schedule 80 Pipe (21)

With the loading shown in Figure 22 the maximum stress on the pipe would be at the location shown in Figure 25. At this point on the pipe, the bending stress, axial stress and stress from the internal pressure exert positive (tensile) forces. The principle of superposition and Saint-Venant's principle state that these stresses in the same direction can be added together if they do not exceed the proportional limit of the material, the deformations due to one of the loadings must not affect the stresses due to the others, and that the section used in the analysis must not be in the immediate vicinity of the points of application of the loads (20). Since these principles hold, stresses that are in the same direction are added together as seen in Table 15. The only stress in the lateral direction (see Figure 23) is contributed by the hoop stress. Shearing stresses were not accounted for because of their low magnitude. With stresses in two directions with no shearing, the maximum-distortion-energy criterion states that the maximum stress is equal to the following (20):

$$\sigma_m = \sqrt{\sigma_1^2 - \sigma_1\sigma_2 + \sigma_2^2}$$

Using the above equation, the maximum stress, σ_m, must not exceed the yield stress.

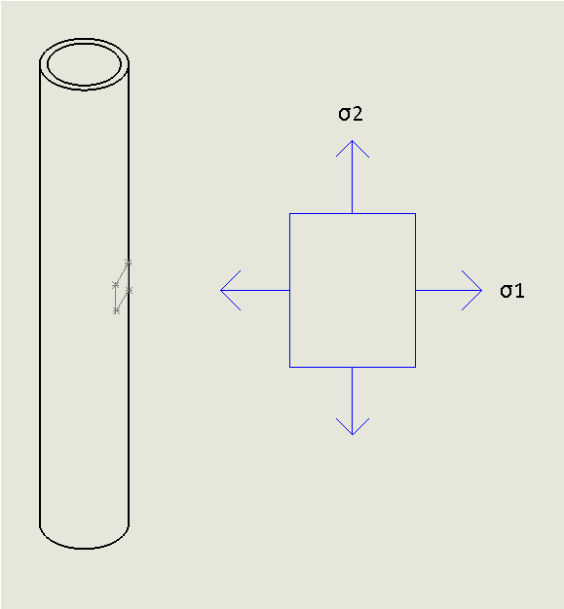

Figure 25 - Stress directions

Table 15 - Total Stress calculations with an internal fluid pressure of 40 psi

Longitudinal (Axial) Direction			
Location	Bending stress (psi)	Material Weight (psi)	Total (psi)
A	8.05	4.65	12.70
B	4.02	4.65	8.68
C	8.05	4.65	12.70

Lateral Direction	
Location	Hoop Stress (psi)
A	*203.59*
B	*203.59*
C	*203.59*

Maximum-Distortion-Energy Stress	
Location	Stress (psi)
A	***197.55***
B	***199.39***
C	***197.55***

For this particular static short-term analysis, the OD of tubing was 2.375”, tube thickness was 0.195”, tube length was 10’ and the internal pressure was varied. It can be seen from the results in Table 15 that the hoop stress in the lateral direction is the largest contributor to the maximum stress. Using the maximum-distortion-energy criteria it was found that the maximum internal pressure without the maximum stress exceeding the yield stress was 40 psi. This analysis was done for applied stress over a short period of time. However, the manufacturer of PTFE tubes recommended not exceeding an internal pressure of 15 psi for this size tubes because of the long term creep that would be caused at elevated temperatures. This indicates that using a higher internal pressure will require thicker tubes due to the creep issues. Figure 26 shows the relation between tube thickness and hoop stress. It shows that as tube wall thickness is increased the hoop stress decreases. This is important to the strength of the tubes since the hoop stress is the main contribution to the maximum stress. Although increasing the tube thickness gives better strength to the tubes, the thermal resistance and therefore the combined tube wall and heat transfer coefficient would decrease greatly as can be seen in Figure 27. A smaller heat transfer coefficient means less condensation and heat transfer. This graph uses the following equation to determine the equivalent heat transfer coefficient of the cooling water and tube wall.

$$U_o = \frac{1}{\frac{r_2}{r_1}\frac{1}{h_{cw}} + \frac{r_2}{k_{wall}}\ln\frac{r_2}{r_1}}$$

These calculations were made with the properties of PTFE and a cooling water heat transfer coefficient of 2000 BTU/(hr*ft^2*F). This was the average of the typical simulation values of heat transfer coefficient for the cooling water and has little effect on the total heat transfer coefficient due to the high order of magnitude.

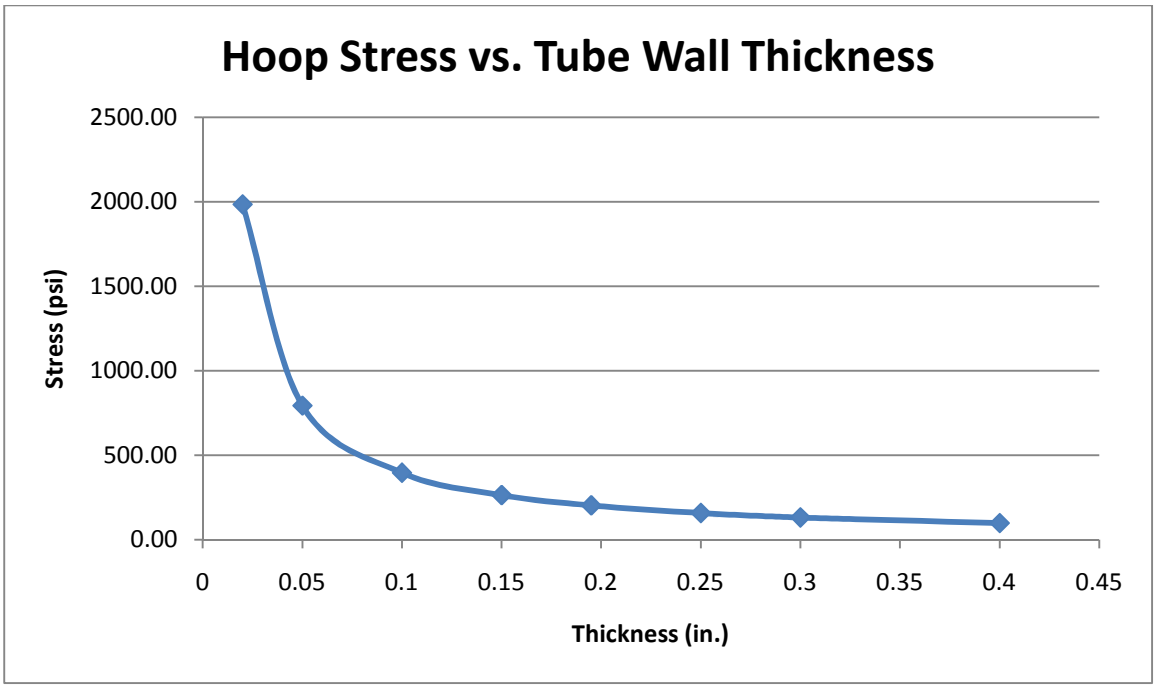

Figure 26 - Hoop stress as a function of tube wall thickness

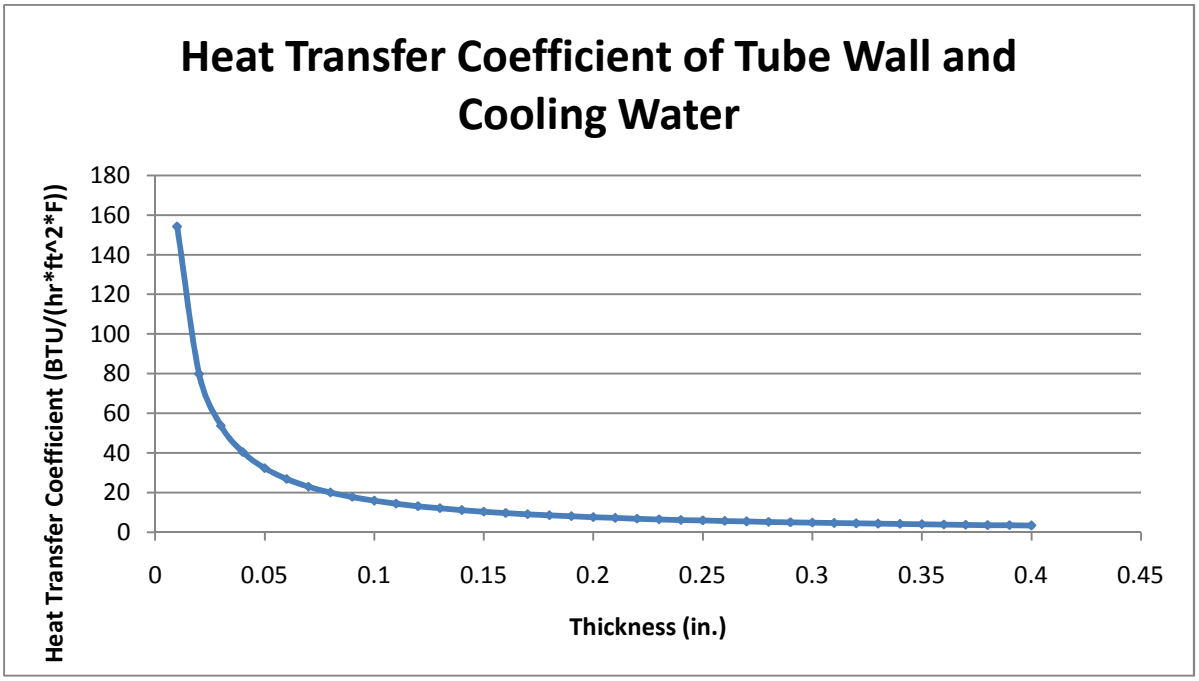

Figure 27 - Heat transfer coefficient between cooling water and outside tube surface

A cost and heat transfer comparison will be made in the next section between Ni Alloy 22 heat exchanger tubing and PTFE tubing with an OD of 2.375” and a tube wall thickness of 0.218”. This wall thickness has been determined to be the thinnest possible without compromising the tube strength over an extended period of time at elevated temperatures for an internal fluid pressure of 15 psi. While the short-term stress calculations done here show that a thinner wall or higher internal pressure may be possible, the tube wall thickness recommendations from the PTFE manufacturer will be used in the thermal analysis. In addition, the analysis above is for a heat exchanger with cooling water pressures in excess of 15 psi, which to avoid creep damage, would require significantly thicker tube walls. However, to facilitate direct comparison of Nickel Alloy 22 and PTFE heat exchangers, the same tube wall thicknesses are used in the analysis in the next section.

6.3 Heat Transfer and Cost Comparison between Nickel Alloy 22 and PTFE

For the following comparisons of the cost and heat transfer capabilities of PTFE to Nickel Alloy 22 tubes, the inlet conditions and heat exchanger geometries were the same. Tube spacings were kept the same and at the ranges that provided maximum heat transfer and condensation. Different duct lengths were simulated to provide information to compare values of heat transfer per cost for the PTFE tubes and the Ni Alloy 22 tubes. For both the Nickel Alloy 22 and PTFE heat exchangers, at the point in the heat exchanger where water condensation started ($T_{wall} < T_{H2O\ DP}$), 304 stainless steel tubes were used for the heat exchanger tubes downstream of the water vapor dew point. The inlet conditions and heat exchanger geometry are shown in Table 16.

Table 16 - Conditions and geometry for material cost comparison

Inlet Conditions				
Mfg (lbm/hr)	Mcw (lbm/hr)	Tcw (F)	yH2O (%)	Tfg (F)
6.00E+06	3.00E+06	100	0.12	300

HX Geometry (in-line arrangement)							
OD (in)	Tube wall thickness (in) (PTFE)	Tube wall thickness (in) (Ni & SS 304)	St (in)	Sl (in)	Duct Depth (ft)	Duct Height (ft)	Duct Length (ft)
2.375"	0.195	0.195	6.17	2.97	40	40	variable

The results show that the high thermal resistance of PTFE dramatically affects the condensation rate and total heat transfer when compared to the Ni Alloy 22 system. The temperature profiles shown in Figure 28 and Figure 29 for the same size heat exchangers clearly indicate this difference. With Ni Alloy 22 tubes, the tube wall temperature is close to the cooling water temperature, usually within 5^{o} F. This is because of the relatively high thermal conductivity of Ni alloy 22 tubes. With PTFE tubes, because of low thermal conductivity, the wall temperature is closer to the flue gas temperature than the cooling water temperature. The thermal resistance of the PTFE wall dominates the overall thermal resistance from flue gas to cooling water. With this particular case and with cases where the length of the PTFE heat exchanger increased up to 80', the tube wall temperature never became lower than the flue gas water dew point temperature of 121.3^{o}F. For this reason there was no condensation of water with the PTFE tube heat exchanger. Table 17 shows the performance of each material with different length heat exchangers.

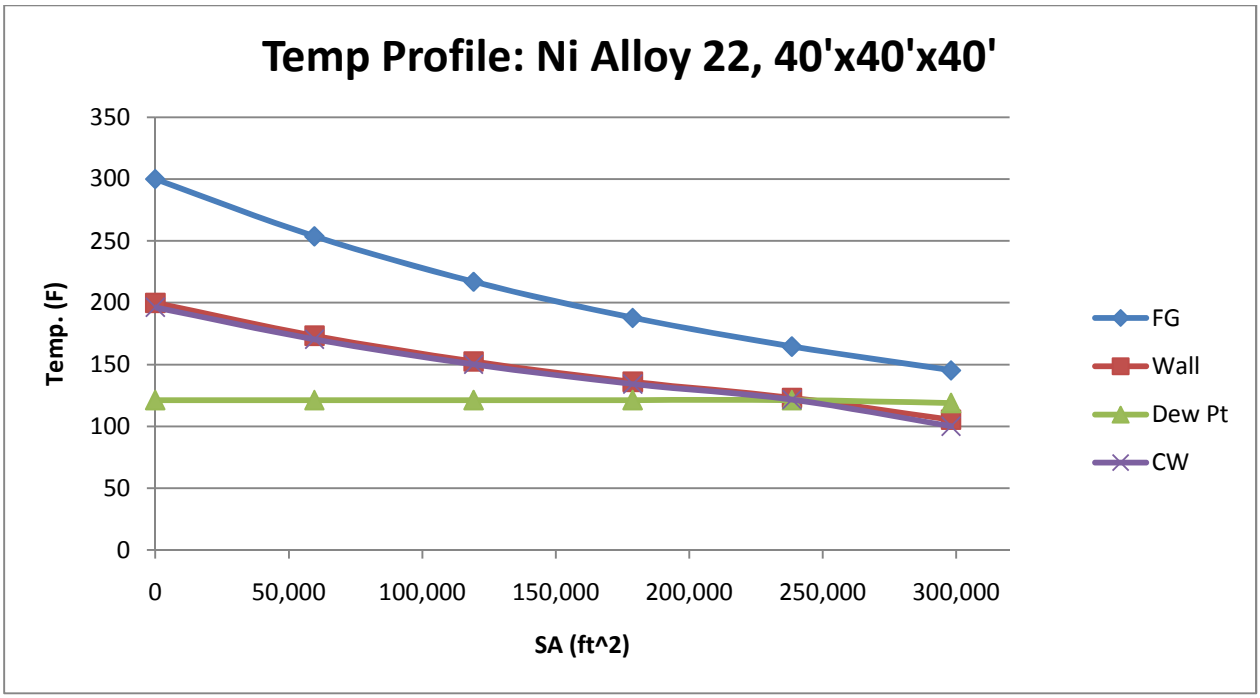

Figure 28 – Temperature profile with Ni Alloy 22 tubing

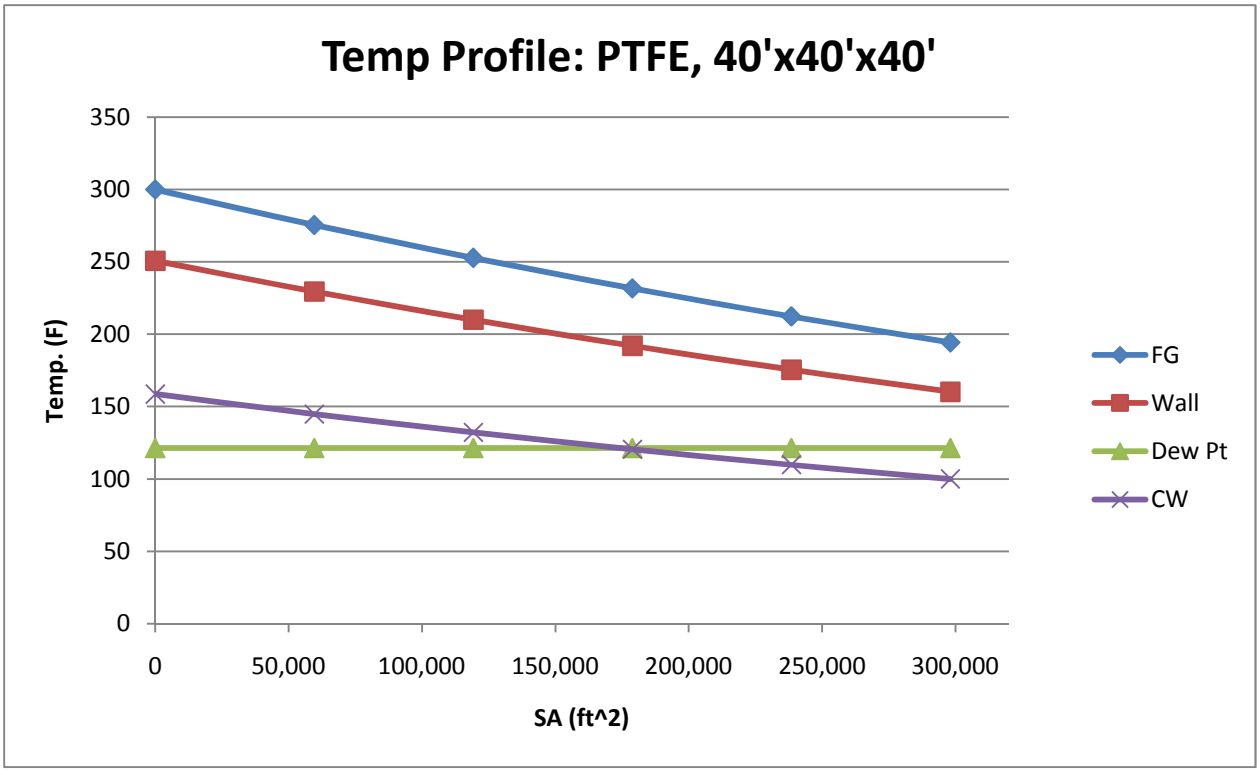

Figure 29 – Temperature profile with PTFE tubing

Table 17 - Performance of Ni Alloy 22 and PTFE tubes

Teflon (k = 0.14 BTU/(ft*hr*F))			
Duct Length (ft)	SA (ft^2)	Condensation Efficiency (%)	Total Heat Transfer (BTU/hr)
20	145343	0	1.10E+08
30	219872	0	1.46E+08
40	298127	0	1.76E+08
50	372656	0	1.98E+08
60	447184	0	2.16E+08
70	521713	0	2.31E+08
80	596242	0	2.44E+08

Ni Alloy 22 (k = 7 BTU/(ft*hr*F))			
Duct Length (ft)	SA (ft^2)	Condensation Efficiency (%)	Total Heat Transfer (BTU/hr)
20	145343	4.87	2.19E+08
30	219872	6.21	2.61E+08
40	298127	7.42	2.89E+08
50	372656	8.31	3.07E+08
60	447184	9.12	3.20E+08
70	521713	9.78	3.29E+08

Although the PTFE tubed heat exchanger did not allow condensation of water, sensible heat was transferred to the cooling water. Figure 30 and Figure 31 show the heat transfer rate vs. surface area and estimated 20 year total cost for PTFE and Ni Alloy 22 heat exchangers. Use of the Nickel Alloy 22 heat exchanger will give 2.19E8 BTU/hr of heat transfer for a heat exchanger with a total tube surface area of 145,000 ft^2. To get the same amount of heat transfer using the PTFE tubes, the heat exchanger surface area would have to be approximately 462,090 ft^2. While PTFE tubes are cheaper per pound, the total added cost between material and pumping power requirements that this would require are far more than would be the case for the Ni Alloy 22 heat exchanger. For example, the Nickel Alloy heat

exchanger that produces 2.19E8 BTU/hr of heat transfer will cost approximately $2,593,000 annually. A PTFE heat exchanger that produces the same amount of heat transfer will cost approximately $4,006,000 annually. This is because more surface area is required for the PTFE exchanger, increasing capital cost and operating cost. These results can be seen in Figure 31. The results consider the annual fixed cost and annual operating cost.

It should be noted that the calculations done in this section for the PTFE tubes were with a tube wall thickness of 0.218". As explained earlier, because of creep this wall thickness is not suitable for the more likely pressures anticipated that are in excess of 15 psi. Larger wall thicknesses would be needed for the structural integrity of the tubes and this would put a PTFE heat exchanger at an even further cost disadvantage when compared to the Alloy 22 heat exchanger.

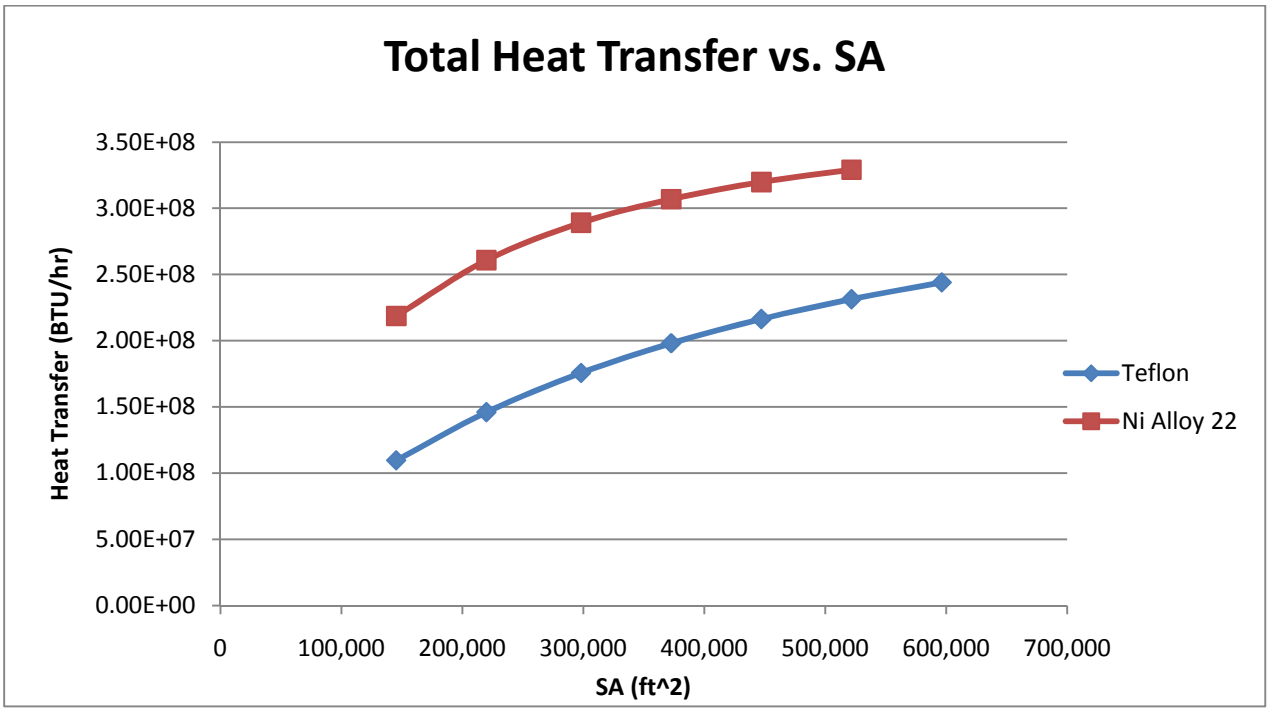

Figure 30 – Heat transfer for Ni Alloy 22 and PTFE tubing

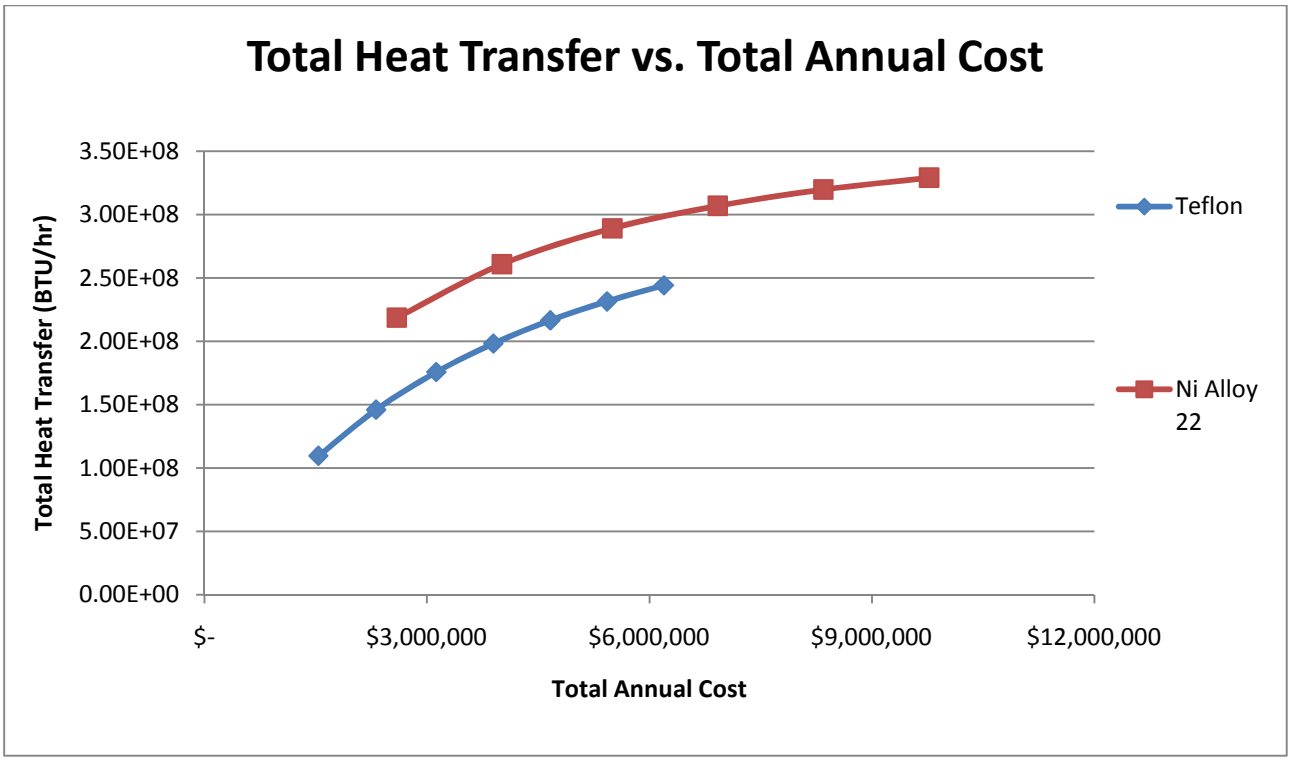

Figure 31 – Heat transfer and cost comparison for Ni Alloy 22 and PTFE tubing

Stainless Steel 304 provides the best tubing material option for locations in the heat exchanger where there is a mixture of sulfuric and water condensation because of its relatively low cost, thermal properties and resistance to corrosion in this region. The strength and heat transfer calculations were performed on Teflon (PTFE) and Ni Alloy 22 tube heat exchangers for the region where there is only sulfuric acid condensation. It was determined that for this particular region, Ni Alloy 22 tubes were the lower cost option because of their high corrosion resistance properties and relatively good heat conducting properties.

7. Effects of Operating Conditions

7.1 Case A - Flue Gas Entering at 300°F

7.1.1 Inlet Conditions and Heat Exchanger Geometry

The effects of inlet conditions of the cooling water were studied. The inlet conditions of the flue gas were based on a conventional coal-fired power plant producing 550 MW of net power with flue gas conditions evaluated downstream of the ESP. These conditions were flue gas coming into the heat exchanger at 6 million lb/hr with a bulk mean temperature of 300°F with a mole fraction of water vapor of 12%. The cooling water temperature and flow rate were varied and the effects of both were studied. The cooling water was assumed to enter at the temperature of the boiler feed water. This temperature can range from approximately 90°F to 105°F. Three increments of 90°, 100° and 105°F were looked at for effects. The flow rate ratio of boiler feed water to flue gas is typically around 0.5, leading to a cooling water flow rate of 3 million lb/hr. The effect of larger cw/fg flow rate ratios were also studied as these would provide higher heat transfer coefficients and create higher temperature differential between tube wall and flue gas. The following ratios were studied: 0.5, 1, 2, 3.

For the geometry of the heat exchanger, the optimized tube spacings of S_t = 6.17” and S_l = 2.97” were used. The tube material was Nickel Alloy 22 at locations in the heat exchanger upstream of the water vapor dew point and stainless steel 304 at locations downstream of the onset of water vapor condensation. Pipe size was kept constant at schedule 80 2” pipe. This corresponds to a tube wall thickness of 0.218”, which is slightly over 5 mm. The duct length and therefore surface area was varied also. A summary of conditions and geometry can be seen below in Table 18 and Table 19.

Table 18 – Tfg = 300F; Constant conditions and geometry for effects simulations

Constant Inlet Conditions		
Mfg (lbm/hr)	yH2O (%)	Tfg (F)
6.00E+06	12	300

Constant HX Geometry (in-line arrangement)					
OD (in)	Tube wall thickness (in)	St (in)	Sl(in)	Duct Depth (ft)	Duct Height (ft)
2.375	0.218	6.17	2.97	40	40

Note: Assumed tubing was Nickel Alloy 22 at locations upstream of the water vapor dew point and then 304 stainless steel downstream of the water vapor dew point.

Table 19 – Tfg = 300F; Variable conditions and geometry for effects simulations

Variable Conditions and Geometry			
Duct Length (ft)	**SA (ft^2)**	**Mcw/Mfg**	**Tcw (F)**
10	7.08E+04	0.5	90
15	1.08E+05	1	100
20	1.45E+05	2	105
30	2.20E+05	3	
40	2.98E+05		
50	3.73E+05		
60	4.47E+05		
80	5.96E+05		

7.1.2 Effect of Mass Flow Rate Ratio

The mass flow rate ratio between the cooling water and the flue gas was varied from 0.5 to 3. While water supply is usually limited and the case of Mcw/Mfg = 0.5 is more likely, there may be applications where there is an ample supply of water and higher water flow rates can be accommodated. The benefits of increasing the ratio while using an inlet cooling water temperature of 90^{o}F can be seen in Figure 32, Figure 33 and Figure 34. Higher mass flow rate ratios cause more heat transfer and therefore,

higher condensation efficiencies. Increasing the ratio from 0.5 to 1.0 usually increases the condensation efficiency by about 100%. For example, for a duct length of 20' and a cooling water temperature of 90°F, increasing the flowrate from 0.5 to 1.0 causes the condensation efficiency to rise from 8.67% to 16.66%. This same effect is seen for the cooling water temperature of 105°F, as the condensation efficiency rises from 3.13% to 6.44%. This effect is caused because the cooling water does not reach as high temperatures with the higher flow rate ratio and therefore the average tube wall temperature is lower. This enables more heat transfer per surface area and higher condensation rates. The same effect is seen with the other two inlet cooling water temperatures of 100° and 105°F. The graphs showing this are located in the Appendix (Figures A1 – A8).

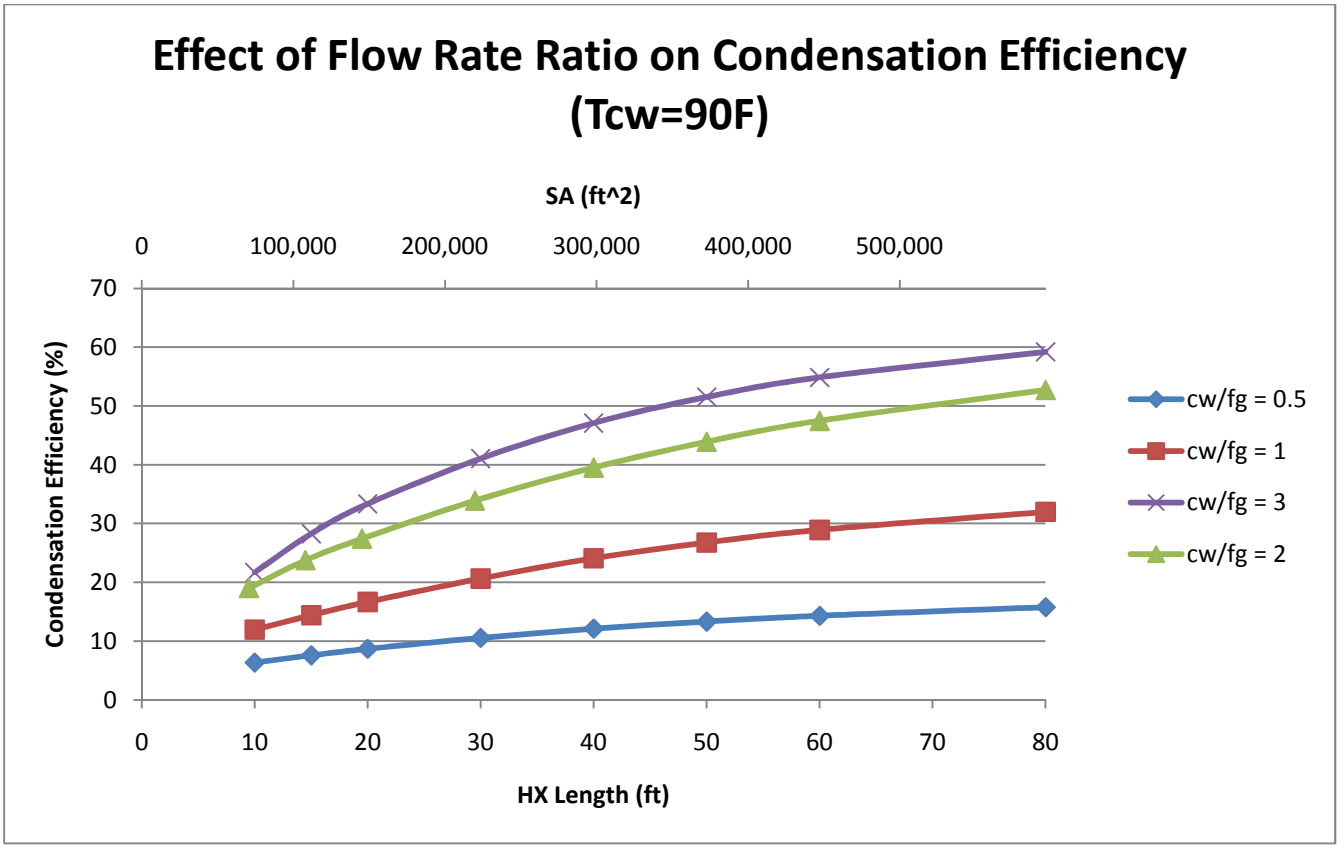

Figure 32 - Effect of flowrate on condensation efficiency

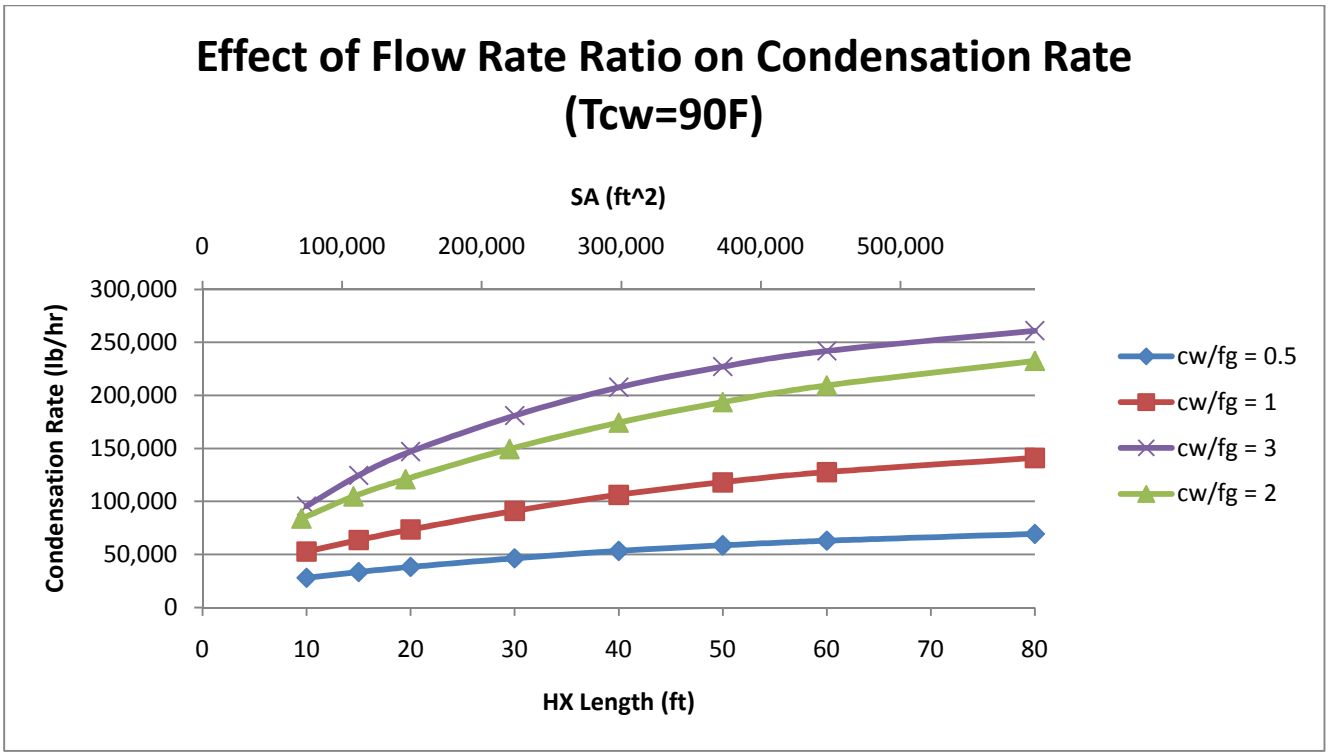

Figure 33 - Effect of flow rate on condensation rate

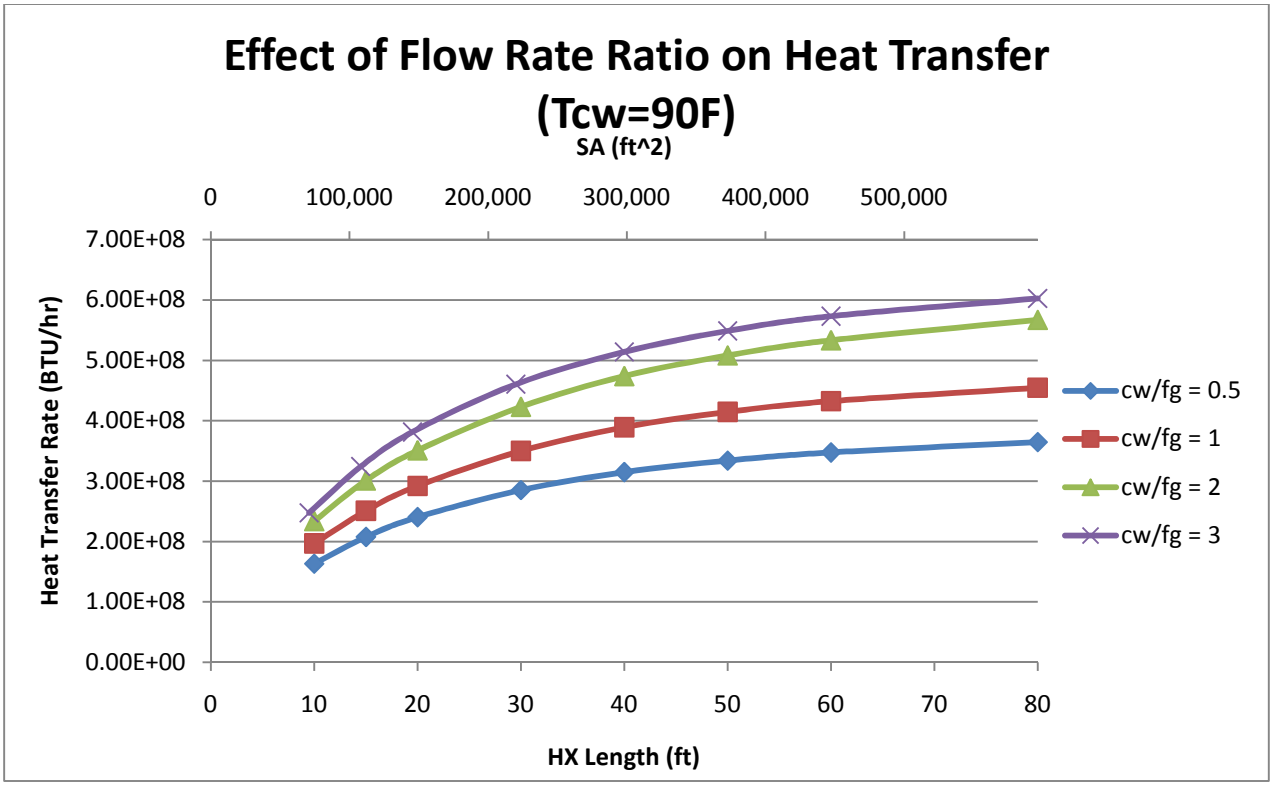

Figure 34 – Flow rate ratio effect on heat transfer

7.1.3 Effect of Inlet Cooling Water Temperature

The effects of varying inlet cooling water temperatures on condensation efficiencies can be seen in Figure 35, Figure 36 and Figure 37. In Figure 35, cooling water to flue gas mass flow rate ratio was kept constant at the base case of 0.5. The condensation efficiency was affected greatly by the cooling water inlet temperature. With a length of 40' (SA = 298,000 ft^2) , the condensation efficiency was 5.14% with a cooling water inlet temperature of 105^oF while the efficiency was 12.10% with a water inlet temperature of 90^oF. The lower inlet temperature of the cooling water drops the tube wall temperature below that of the flue gas dew point earlier in the heat exchanger and starts condensation earlier in the heat exchanger. The higher temperature differential between tube wall and flue gas caused by the lower cooling water inlet temperature also causes more convective heat transfer. It is also seen that a longer heat exchanger (more surface area) causes high condensation rates and heat transfer. Neither condensation nor heat transfer is directly proportional to the surface area and this effect eventually plateaus at higher lengths and larger surface areas due to the limiting exit temperature of the cooling water. The same effect of the cooling water temperature on increased condensation and heat transfer is seen with the other three mass flow rate ratios of 1, 2 and 3. These figures are in the Appendix (Figures A1– A8).

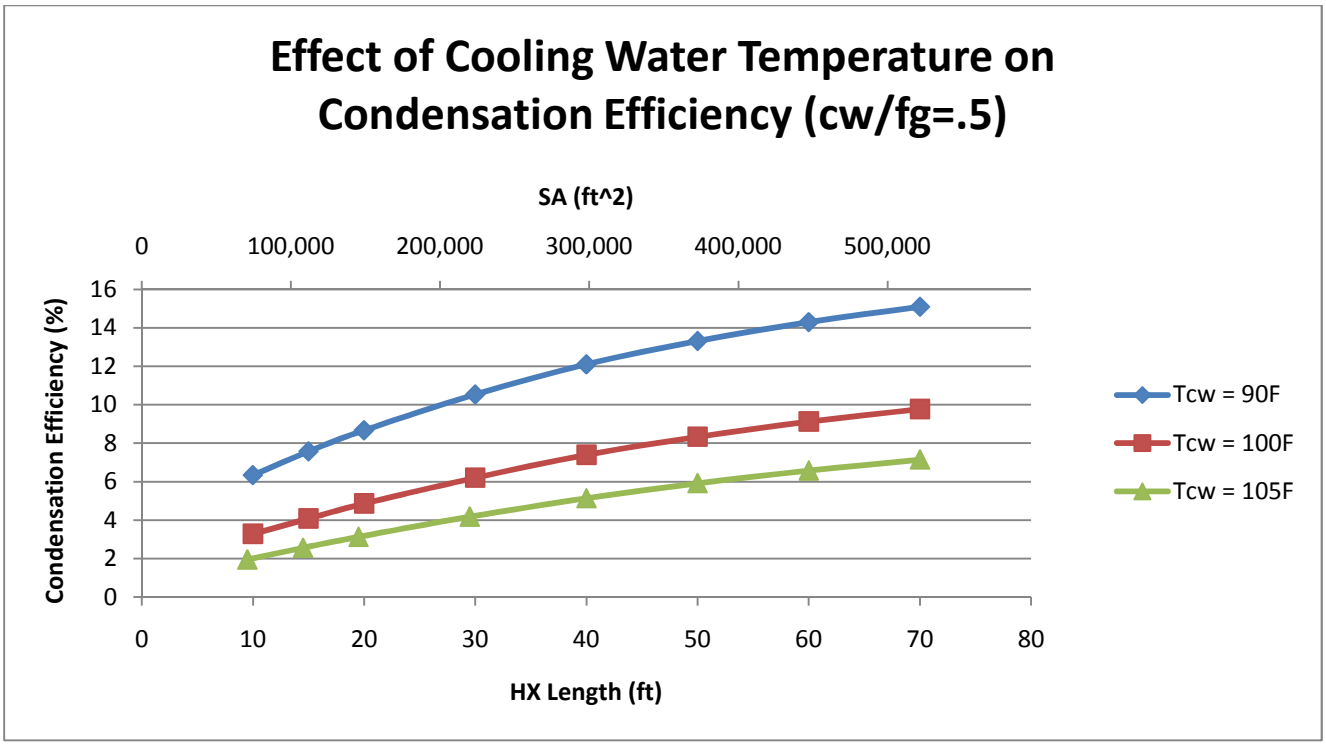

Figure 35 – Cooling water temperature effect on condensation efficiency

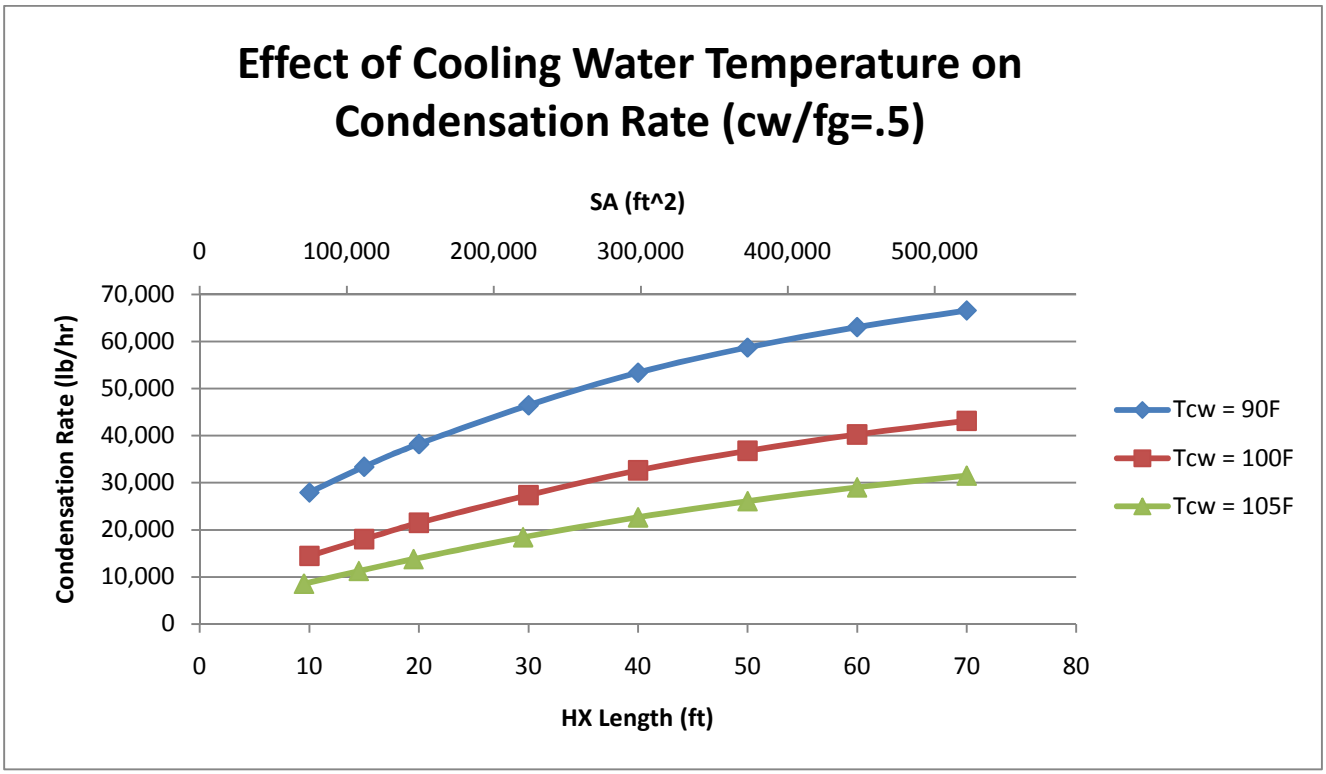

Figure 36 - Cooling water termperature effect on condensation rate

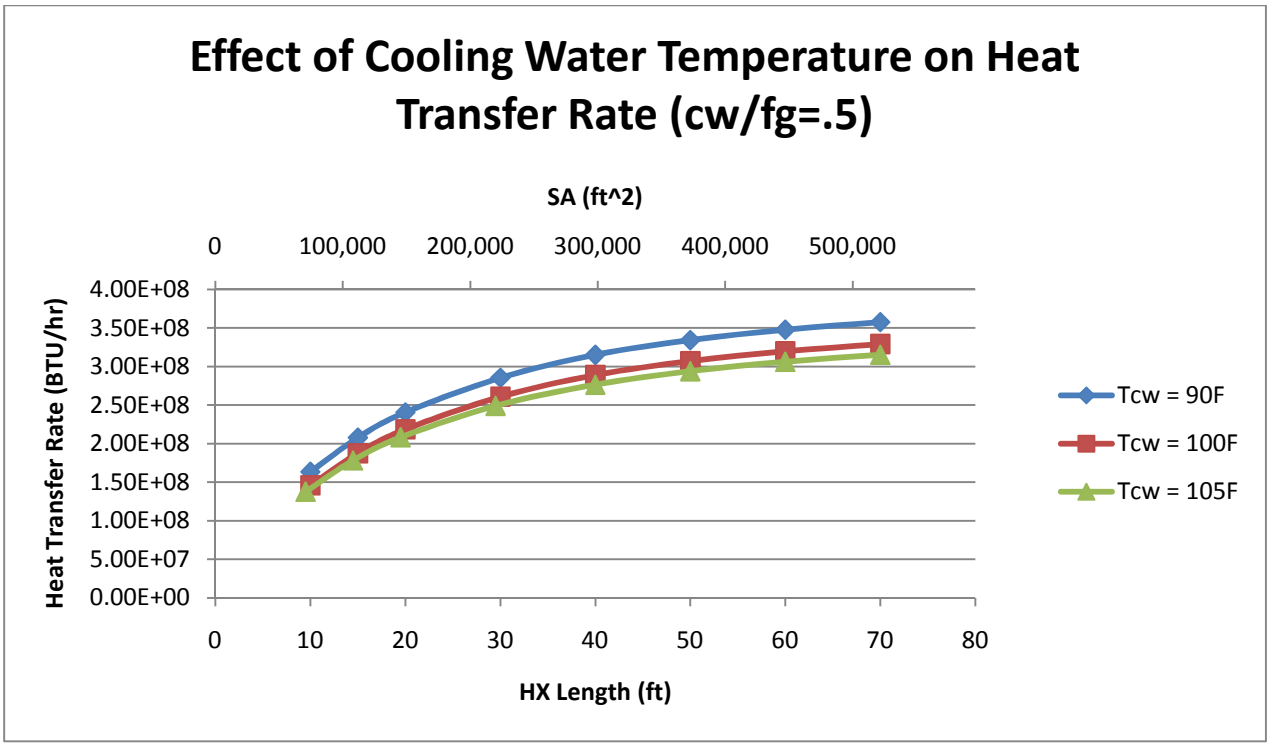

Figure 37 – Cooling water temperature effect on heat transfer

7.2 Case B - Flue Gas Entering Downstream of the FGD

An application of the full-scale condensing heat exchanger that has not been discussed so far in this report is usage downstream of a flue gas desulfurization unit (FGD). After leaving the FGD unit, flue gas is saturated at 135^{o}F with a mole fraction of water vapor of 17.2% and has an approximate temperature of 135^{o}F. Simulations with the full scale heat exchanger were run to determine the effectiveness of a heat exchanger in this location. In this situation recovering the water from the FGD is important as is heat recovery before leaving the stack. Conditions and geometry that were kept constant and were varied are shown in Table 20 and Table 21.

Table 20 – Tfg = 135F, saturated; Constant conditions and geometry for effects simulations

Constant Inlet Conditions		
Mfg (lbm/hr)	yH2O (%)	Tfg (F)
6.00E+06	17.2	135

Constant HX Geometry (in-line arrangement)					
OD (in)	Tube wall thickness (in)	St (in)	Sl(in)	Duct Depth (ft)	Duct Height (ft)
2.375	0.218	6.17	2.97	40	40

Note: Assumed first 5% of tubing surface area was Nickel Alloy 22 and the remaining 95% was 304 stainless steel.

Table 21 - Tfg = 135F, saturated; Variable conditions and geometry for effects simulations

Variable Conditions and Geometry			
Duct Length (ft)	**SA (ft^2)**	**Mcw/Mfg**	**Tcw (F)**
5	3.35E+04	0.5	90
10	7.08E+04	1	100
15	1.08E+05	2	105
20	1.45E+05	3	

Since the flue gas was coming into the heat exchanger at 135°F, there was less available heat to transfer to the cooling water than in the previous cases where flue gas was coming into the heat exchanger at 300°F. For this reason, shorter heat exchangers were used (5-20 ft) because less surface area was required.

7.2.1 Effect of Mass Flow Rate Ratio

Effects of different cooling water to flue gas ratios are shown in Figure 38, Figure 39 and Figure 40. The same effects occurred with flue gas conditions downstream of the FGD as with flue gas downstream of the ESP. Higher mass flow rate ratios cause a higher heat transfer coefficient and condensation begins earlier in the heat exchanger. With flow rate ratios of 0.5 and 1, the maximum condensation and heat transfer flatten out after heat exchanger lengths of 15'. This doesn't occur for

ratios of 2 and 3 as the cooling water does not reach the maximum temperature allowed by the flue gas. For the case where water is coming in at 100°F to a 20' length heat exchanger, condensation efficiency increases from 14.34% to 26.87%, due to increasing the flow rate ratio from 0.5 to 1. The same effects can be seen with increasing the ratios to 2 and 3 as is seen in Figure 38. Effects on heat transfer can be seen in Figure 40.

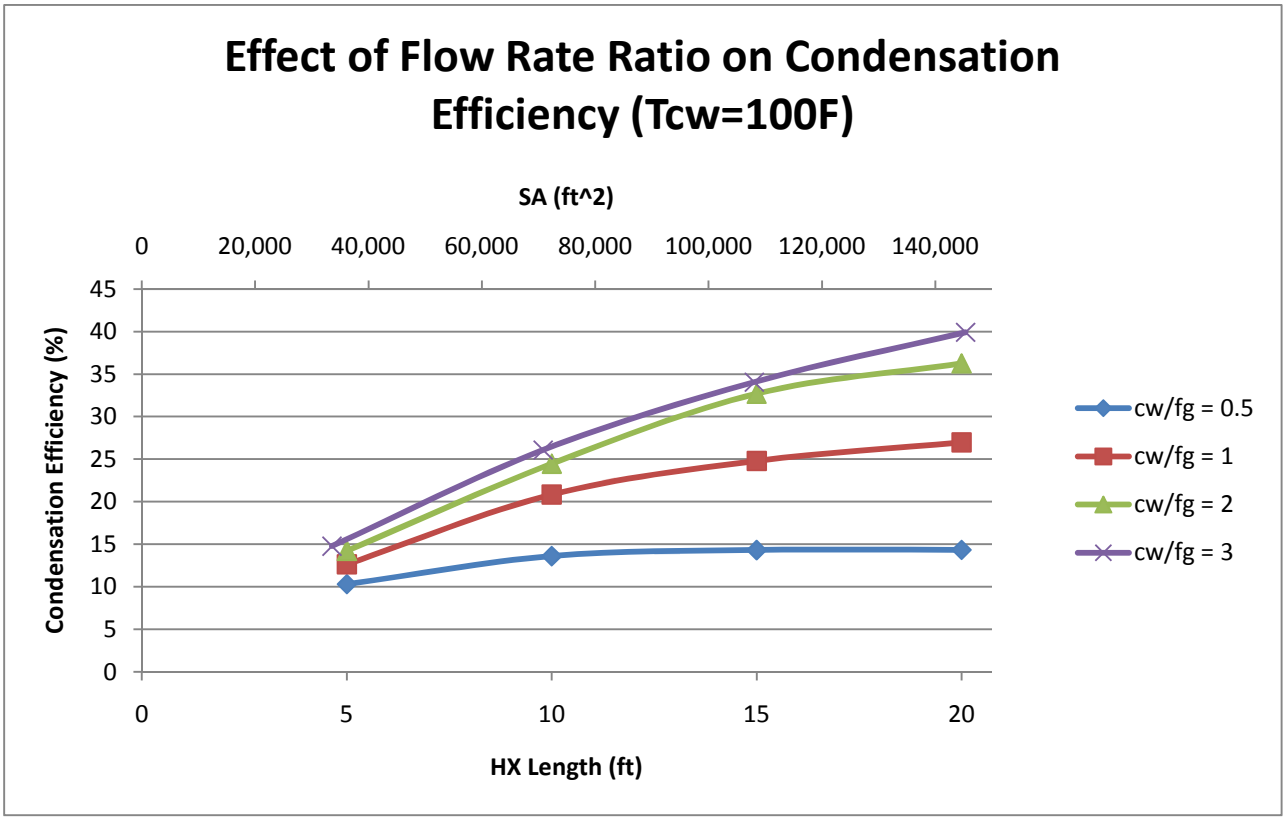

Figure 38 – Flow rate ratio effect on condensation efficiency

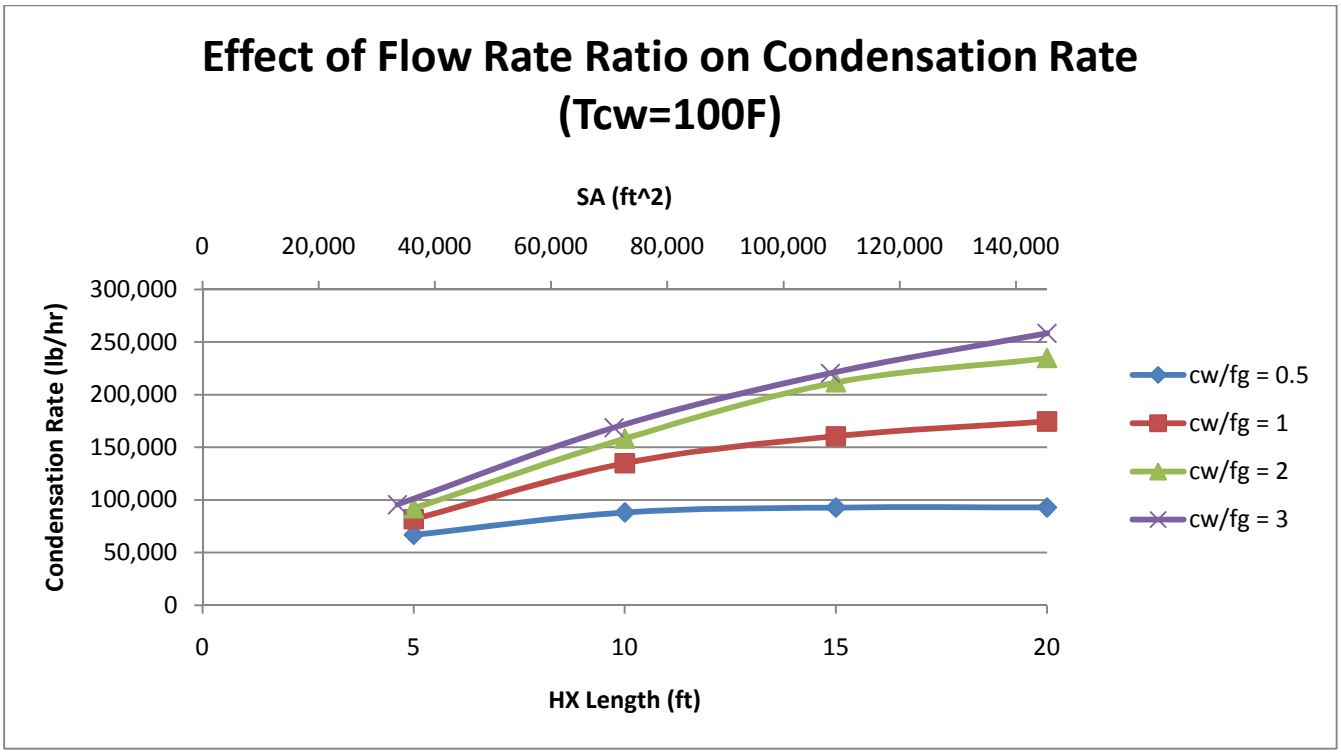

Figure 39 - Flow rate ratio effect on condensation rate

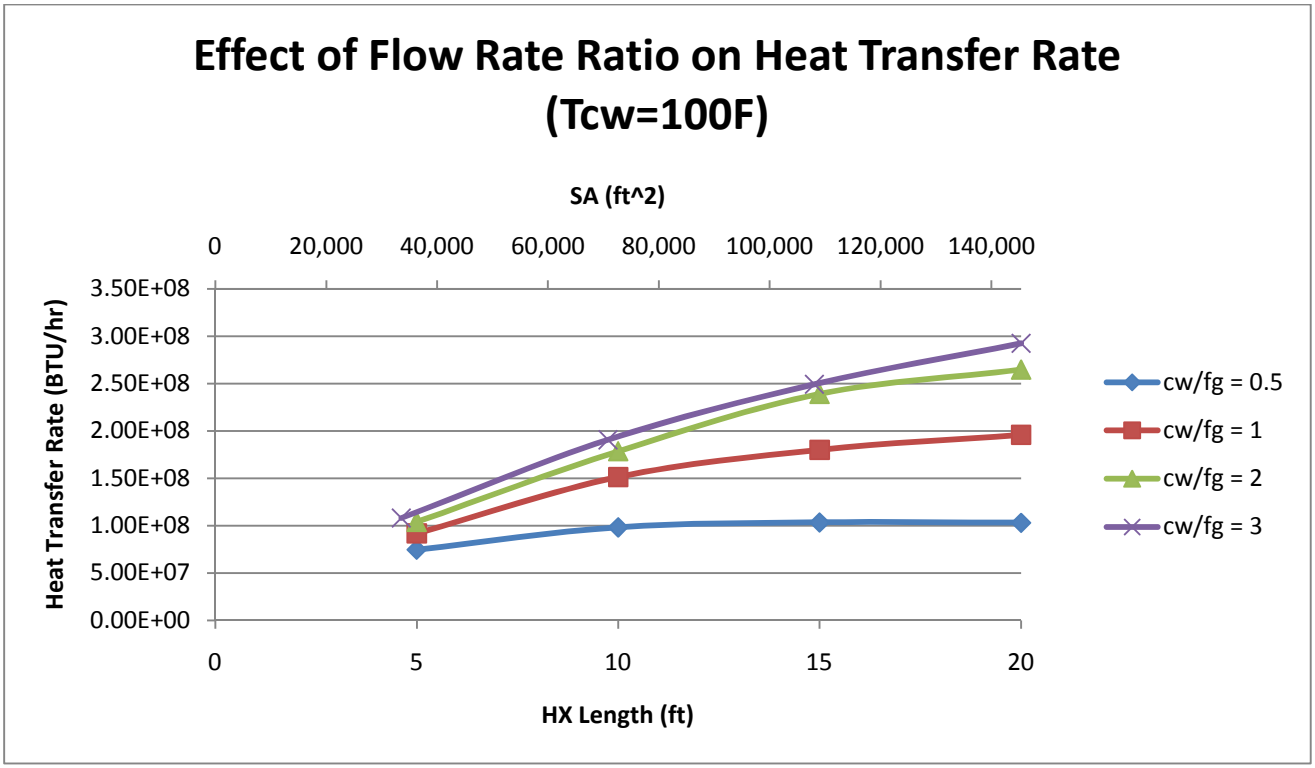

Figure 40 – Flow rate ratio effect on heat transfer

7.2.2 Effect of Inlet Cooling Water Temperature

Results for condensation efficiencies and heat transfer rate with a flow rate ratio of 0.5 are seen in Figure 41, Figure 42 and Figure 43. It is seen that lower cooling water inlet temperatures have the same effect as for previous cases, increasing condensation and heat transfer by causing a higher temperature differential between flue gas and cooling water. The graphs also show that a maximum condensation and heat transfer rate is reached between the lengths of 10' and 15'. This is because the cooling water achieves maximum heat intake and exits the heat exchanger near the inlet flue gas temperature of 135°F.

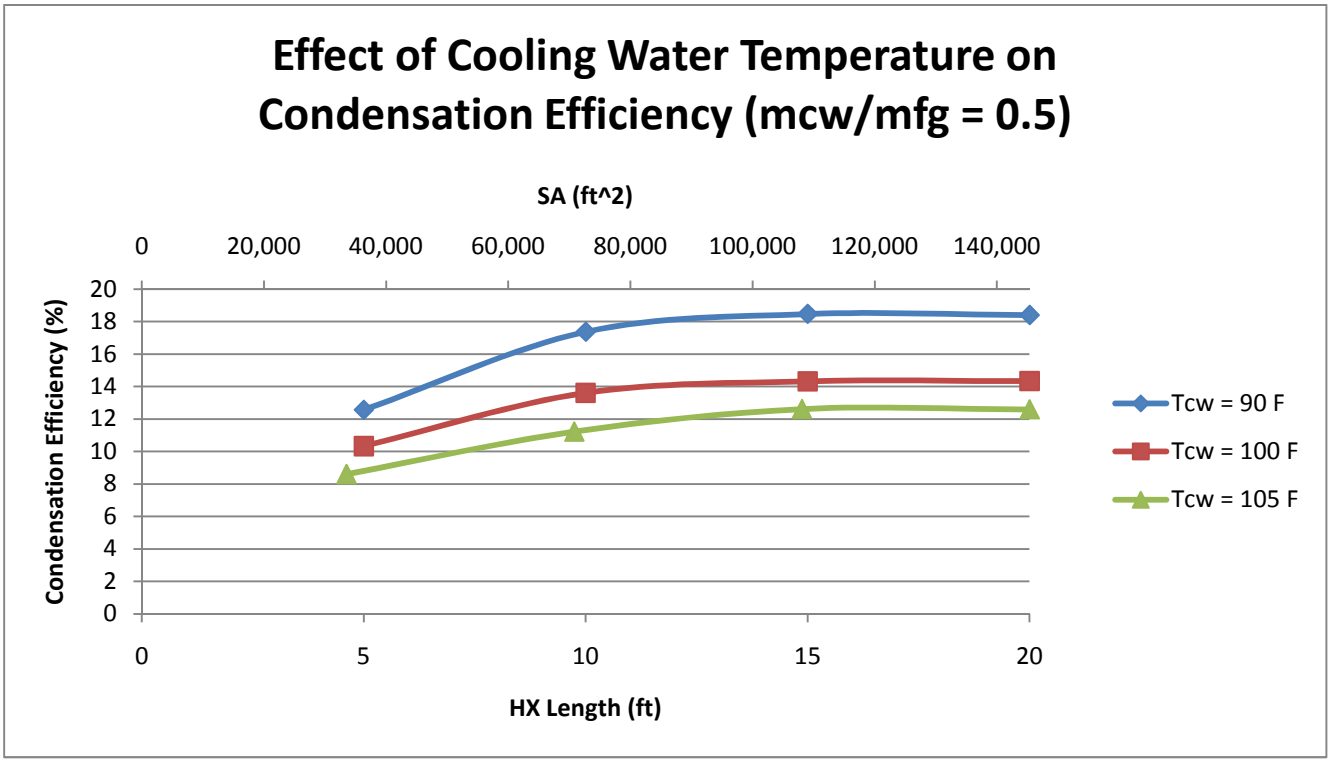

Figure 41 – Cooling water temperature effect on condensation efficiency

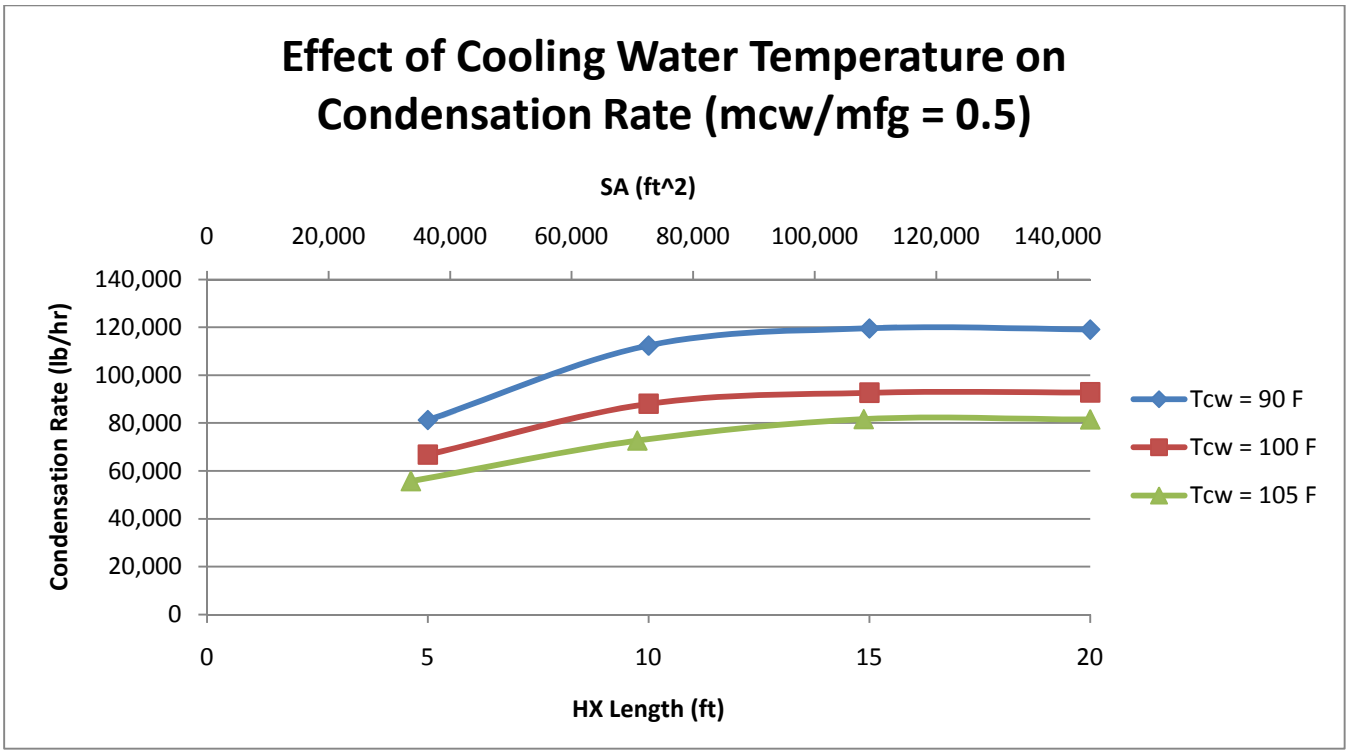

Figure 42 - Cooling water temperature effect on condensation rate

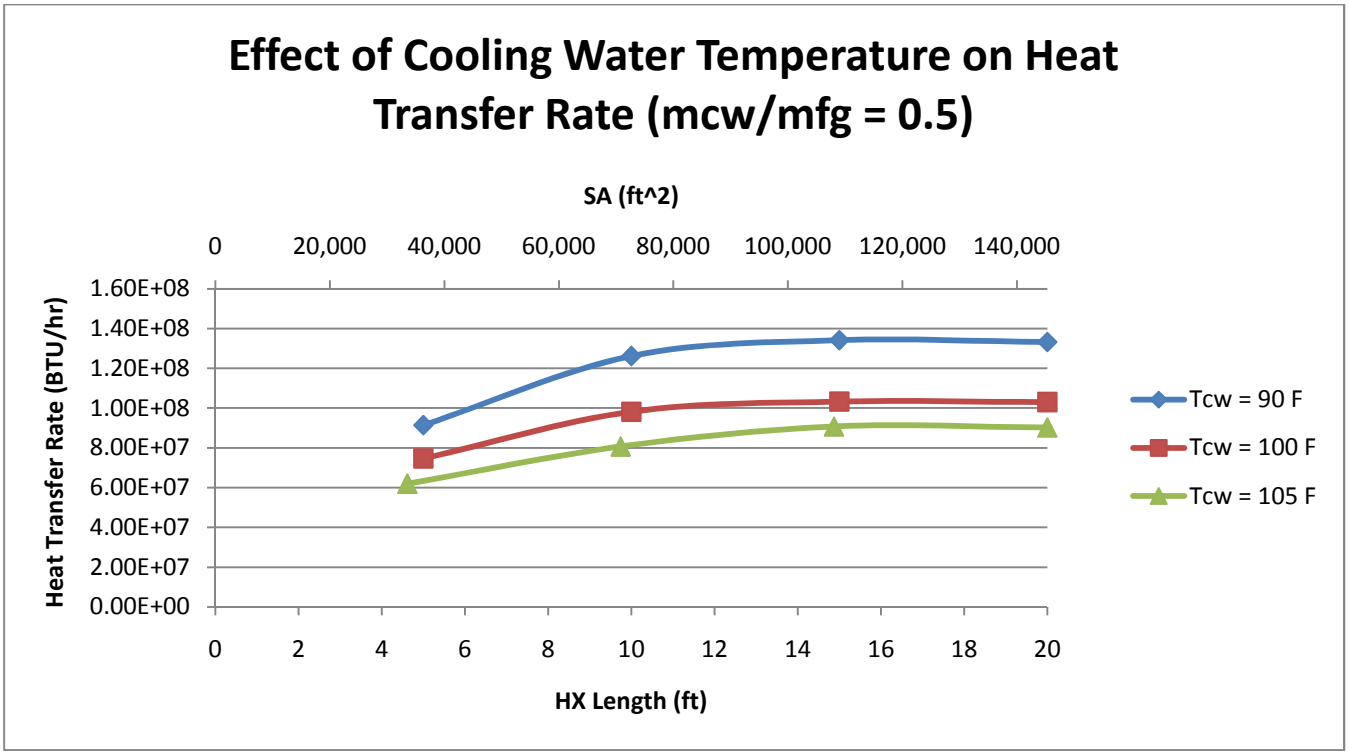

Figure 43 – Cooling water temperature effect on heat transfer

Figure 44 below shows the condensation rate performance using the different flue gas inlet conditions as represented by Case A and Case B. The cooling water to flue gas flow rate ratio is constant at 0.5 and the cooling water inlet temperature is constant at 100°F. The only difference is the temperature and water concentration of the flue gas. There is more water available for condensation in Case B. In addition, the temperature of the flue gas in Case B is already at the saturation temperature. For these reasons the condensation rate is much higher for Case B than for Case A. A cost comparison between the two cases is made in the next section.

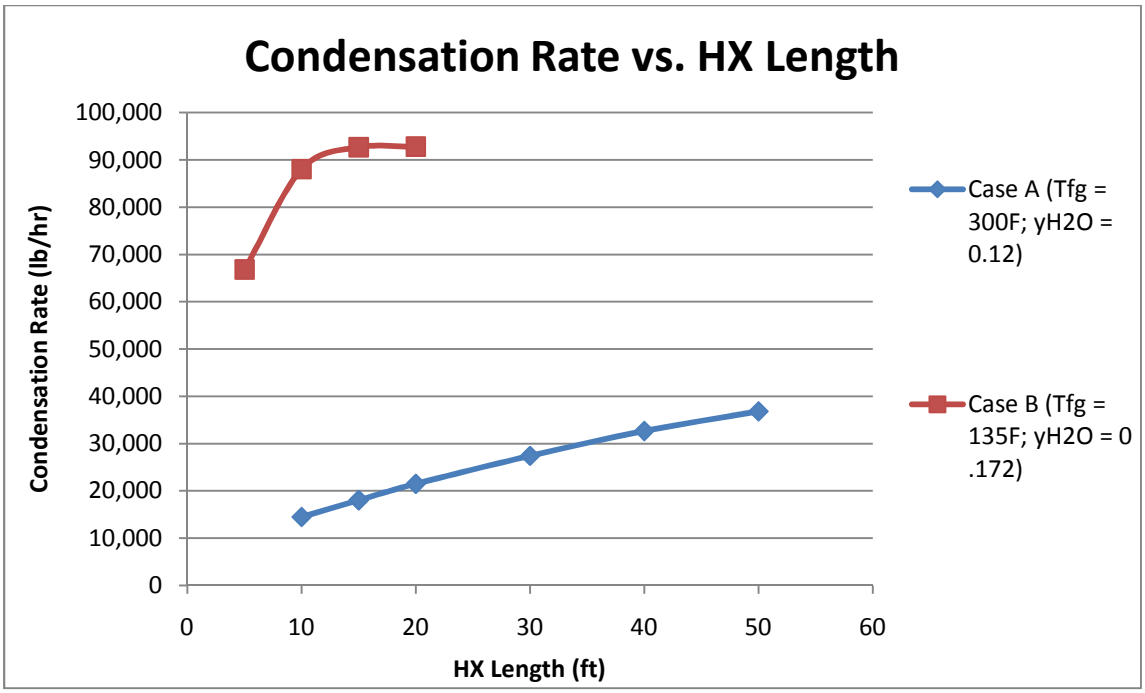

Figure 44 - Condensation rate for Case A and Case B

For both uses of the heat exchanger, when showing the effect of the flow rate ratio, flue gas flow rate was kept constant and the cooling water flow rate was changed. However, the same general effects would hold if cooling water flow rate was kept constant and flue gas flow rate was decreased in order to get higher flow rate ratios. It should also be mentioned that increasing the flow rate of the cooling water will increase the cooling water pressure drop of the heat exchanger. Split manifolds were

briefly investigated to decrease this effect. In such a case, if 6 million lb/hr of cooling was available, 3 million lb/hr would be introduced at the beginning of the heat exchanger and then exit halfway down the total length of the heat exchanger. The other 3 million lb/hr would then be introduced and exit after the second half of the heat exchanger.

7.3 Cost Comparisons – Case A vs. Case B

Section 6.1 (Case A) examined the effects of flue gas and cooling water inlet conditions on heat transfer and condensation with flue gas after the ESP at 300^{o}F. Section 6.2 (Case B) examined the same effects with flue gas downstream of the FGD unit, saturated at 135^{o}F. The following section compares the cost effectiveness of each scenario. To do this, common inlet conditions that might be encountered at either location were used. The cooling water temperature was kept constant at 100^{o}F and the cooling water to flue gas flow rate ratio was kept constant at 0.5. All heat exchanger geometry was kept constant except for the length of the heat exchanger which was adjusted to get a proper spectrum of results.

Table 22 below shows a comparison of flue gas and cooling water pressure drop with each flue gas inlet condition and the effect it has on the power costs. With the same duct length the cooling water pumping costs are the same regardless of the inlet flue gas condition. However, the flue gas fan power requirements for the same duct lengths change with the flue gas inlet conditions. Use of the heat exchanger downstream of the FGD causes lower flue gas exit temperatures and higher amounts of water being condensed when compared to use of the heat exchanger in case A. This change in temperature and mass flow rate cause the power requirement to drop despite the heat exchanger having the same surface area. For example, the flue gas power requirement for a heat exchanger in case A is 324 kW, compared to a power requirement of 253 kW for usage in case B.

Table 22 - Pressure drop and operating power requirements for Case A and Case B

Case A - Tfg = 300 F; yH2O = 0.12						
Duct Length	FG Pressure Drop	Cooling Water Pressure Drop	FG Fan Power	CW Pumping Power	FG Power Cost/Year	CW Pump Power Cost/year
ft	psi	psi	kW	kW	$/year	$/year
10	0.0235	82	174	268	$ 60,938.47	$ 93,689.84
15	0.0355	123	254	402	$ 88,819.36	$ 140,563.27
20	0.0465	164	324	535	$ 113,278.15	$ 187,379.68
30	0.0695	246	466	803	$ 163,202.46	$ 281,001.11
40	0.0925	333	606	1084	$ 211,954.78	$ 379,331.55
50	0.1135	415	732	1352	$ 256,091.50	$ 473,044.19

Case B - Tfg = 135 F; yH2O = 0.172 (saturated)						
Duct Length	FG Pressure Drop	Cooling Water Pressure Drop	FG Fan Power	CW Pumping Power	FG Power Cost/Year	CW Pump Power Cost/year
ft	psi	psi	kW	kW	$/year	$/year
5	0.0090	41	57	133	$ 20,071.26	$ 46,690.99
10	0.0195	82	124	268	$ 43,239.45	$ 93,792.46
15	0.0295	123	187	402	$ 65,316.38	$ 140,791.31
20	0.0400	165	253	536	$ 88,538.44	$ 187,755.95

Note: Assumed $0.05/kWhr for electrical power

Table 23 - Cost Efficiency of Case A vs. Case B

Tfg = 300 F; yH2O = 0.12								
Duct Length	Cond. Rate	HT	Capital Cost	Annual Fixed Cost	Annual Operating Cost	Total Annual Cost	Cost/Mass Condensed	Cost/Rate of HT
ft	(lb/hr)	(BTU/hr)	$	$	$	$	$/lbm H20	$/(BTU/hr)
10	14494	1.46E+08	$10,858,100	$1,022,800	$154,600	$1,177,400	$0.012	$0.008
15	18038	1.88E+08	$17,603,700	$1,658,200	$229,400	$1,887,600	$0.015	$0.010
20	21500	2.19E+08	$24,339,700	$2,292,700	$300,700	$2,593,300	$0.017	$0.012
30	27403	2.61E+08	$37,861,500	$3,566,400	$444,200	$4,010,600	$0.021	$0.015
40	32658	2.89E+08	$52,114,700	$4,908,900	$591,300	$5,500,200	$0.024	$0.019
50	36796	3.07E+08	$65,727,500	$6,191,200	$729,100	$6,920,300	$0.027	$0.023
Tfg = 135 F; yH2O = 0.172 (saturated)								
Duct Length	Cond. Rate	HT	Capital Cost	Annual Fixed Cost	Annual Operating Cost	Total Annual Cost	Cost/Mass Condensed	Cost/Rate of HT
ft	(lb/hr)	(BTU/hr)	$	$	$	$	$/lbm H20	$/(BTU/hr)
5	66811	7.47E+07	$1,717,300	$161,800	$66,800	$228,500	$0.0005	$0.003
10	88062	9.82E+07	$3,626,700	$341,600	$137,000	$478,600	$0.0008	$0.005
15	92686	1.03E+08	$5,536,000	$521,500	$206,100	$727,600	$0.0011	$0.007
20	92803	1.03E+08	$7,163,900	$674,800	$276,300	$951,100	$0.0015	$0.009

It is seen from the last two columns in Table 23 that the case where the heat exchanger is used after the FGD unit is more cost effective. The annual cost per condensation is much lower for this case. For a heat exchanger downstream of an FGD, the flue gas has a higher concentration of water at 17.2% than with case A which only has a vapor concentration of 12%. The second reason the second system is more effective at condensing water is that the flue gas is entering the heat exchanger saturated with water vapor. Therefore, the cooling water doesn't first have to lower the flue gas temperature and instead, condensation can start at the beginning of the heat exchanger. This reason also explains why there is more heat transfer per unit cost. Most of the heat transfer for case B is latent heat transfer from water condensation.

Perhaps the biggest reason why the case B heat exchanger is more cost effective is because of the tubing material cost. A heat exchanger with flue gas coming in at 300^{o}F still has sulfuric acid vapor that has yet to condense. As explained in the materials section, this type of heat exchanger requires expensive Nickel Alloy 22 tubes. The heat exchanger in case B condenses water at the beginning of the heat exchanger and therefore can use less costly stainless steel 304 tubes in the majority of the heat exchanger. For safety, Nickel Alloy 22 tubes were still used in the first 5% of the case B heat exchanger to ensure water would start condensing before entering the stainless steel portion of the heat exchanger. The other 95% of the heat exchanger used stainless steel 304 tubes.

7.4 Use of Streamlined Tube Shapes

Most published heat transfer and pressure drop data on flow over tube banks has dealt with circular tubes. The use of streamlined tubes in tube bundles has been investigated in recent years. Different shapes have included elliptical tubes and parabolic shaped tubes (22). The benefit of using streamlined shapes is that there is less resistance to flow and therefore less drag created by the tube. This same principle holds for streamlined tubes in a tube bundle when compared to circular tubes in a bundle. If there is less drag in a bundle, the flue gas side pressure drop would decrease and so would the fan power requirements, resulting in lower operating costs.

As was mentioned, there have been very few investigations done to study the pros and cons of using streamlined tube shapes in the bank of a heat exchanger at the low sub-critical Reynolds numbers that are typically used ($1000<Re<50,000$). One study that was done compared the performance of in-line bundles of elliptical tubes with an axis ratio of two to bundles of circular tubes with the same circumference (23). Initial experimental and numerical studies were conducted with the same center to center elliptical tube spacings as were used with the circular tubes. They used a transverse spacing to

diameter ratio of 3.6 and a longitudinal spacing to diameter ratio of 2.1. This setup was used in order to have an equivalent surface area between each study.

It was found that the elliptical tube bundle caused lower turbulence levels and poorer mixing in comparison with the circular tubes. Using the same tube spacing and surface area, the heat transfer rate of the elliptical tube bank decreased to 85% that of the circular tube bank. However, the external pressure drop was lowered to 19% that of the circular tube bank (23) (22). The author of that study proposed decreasing the spacings of the elliptical tubes in an effort to increase the heat transfer area without increasing the external pressure drop too drastically. Decreasing the tube spacing ratio in the transverse direction to 1.8 created a total heat transfer rate that was 85% larger than the original circular tube banks with transverse and longitudinal spacing ratios of 3.6 and 2.1 respectively. Meanwhile, the total pressure drop was still only about 60% that of the original circular tube bank.

Results were generated in the present study using the circular tube heat exchanger cost and performance information of the current investigation coupled with the heat transfer and pressure drop factors of the elliptical tube study. This enabled a comparison between elliptical tube performance and circular tube performance. For example, a 40’ X 40’ X 15’ heat exchanger using circular tubes has a flue gas side power requirement of 186.6 kW and a cooling water side power requirement of 402.3 kW resulting in a total power requirement of 588.9 kW. This translates to an annual cost of roughly $206,100. The annual fixed cost of the heat exchanger due to capital cost is $521,500, resulting in a total annual cost of $727,600. This particular heat exchanger would generate a total heat transfer of $1.03X10^{8}$ BTU/hr. Using the elliptical tube bank factors above for 85% of the heat transfer and 19% of the flue gas operating power generates a 35.5 kW fan power requirement on the flue gas side and an annual operating cost of $153,200. Assuming capital cost remains constant, the total annual cost of the elliptical tube heat exchanger is then $674,700. However, using the factor of 0.85 for the heat transfer means a

total heat transfer rate of $9.56X10^7$ BTU/hr. The total heat exchanger cost is cut by only 7.2% while the heat transfer is cut by 15%. These results are seen in Table 24 and Figure 45. Similar calculations were done for the case where the transverse spacing was cut in half (surface area doubled) and the total heat transfer was increased by 85%.

Table 24 - Comparison of circular tube performance to estimated elliptical tube performance

	Duct Length	FG Power	CW Pump Power	Total Power	Annual Operating Cost	Annual Fixed Cost	Total Annual Cost	Total Rate of HT	Cost/Rate of HT
	ft	kW	kW	kW	$	$	$	(BTU/hr)	$/(BTU/hr)
Circular with St/d = 2.60	5	57.3	133.4	190.7	$ 66,800.00	$ 161,800.00	$ 228,500.00	7.47E+07	$ 0.0031
	10	123.5	268.0	391.5	$ 137,000.00	$ 341,600.00	$ 478,600.00	9.82E+07	$ 0.0049
	15	186.6	402.3	588.9	$ 206,100.00	$ 521,500.00	$ 727,600.00	1.03E+08	$ 0.0070
	20	253.0	536.4	789.4	$ 276,300.00	$ 674,800.00	$ 951,100.00	1.03E+08	$ 0.0092
Eilliptical with St/d = 1.80	5	17.2	133.4	150.6	$ 52,700.00	$ 161,800.00	$ 214,500.00	6.91E+07	$ 0.0031
	10	37.1	268.0	305.0	$ 106,800.00	$ 341,600.00	$ 448,400.00	9.08E+07	$ 0.0049
	15	56.0	402.3	458.3	$ 160,400.00	$ 521,500.00	$ 681,900.00	9.56E+07	$ 0.0071
	20	75.9	536.4	612.4	$ 214,300.00	$ 674,800.00	$ 889,100.00	9.53E+07	$ 0.0093
Elliptical with St/d = 2.60	5	10.9	133.4	144.3	$ 50,500.00	$ 161,800.00	$ 212,300.00	6.35E+07	$ 0.0033
	10	23.5	268.0	291.5	$ 102,000.00	$ 341,600.00	$ 443,600.00	8.35E+07	$ 0.0053
	15	35.5	402.3	437.7	$ 153,200.00	$ 521,500.00	$ 674,700.00	8.78E+07	$ 0.0077
	20	48.1	536.4	584.5	$ 204,600.00	$ 674,800.00	$ 879,400.00	8.76E+07	$ 0.0100

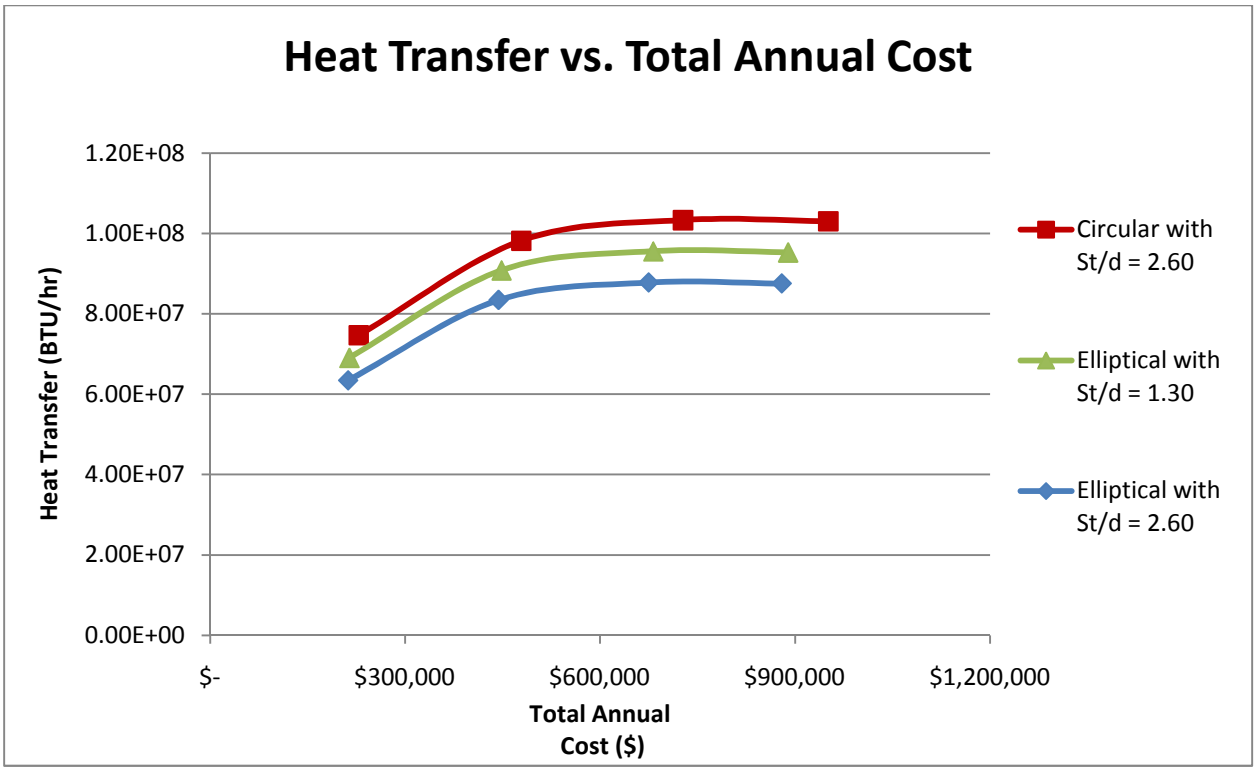

Figure 45 - Comparison of circular tube performance and elliptical tube performance

The positive effects of using streamlined tubes are clearly seen with increasing total heat transfer and decreasing the flue gas side pressure drop. However, as seen from Table 24, the main contribution to total cost is the capital cost of the heat exchanger, not the operating cost of the flue gas fan. Decreasing the flue gas fan power by 89% drops the overall cost by only 7.3%. This drop in overall cost is not enough to overcome the limitations of the elliptical tubes on heat transfer performance as seen in Figure 45.

Up to now, there have not been any studies to develop a Reynolds number vs. heat transfer correlation or a Reynolds number vs. pressure drop correlation for in-line banks of streamlined or elliptical tubes. More research needs to be done to generate results with different shapes of tubes at different Reynolds numbers before streamlined tubes can be eliminated as a possibility. Different

shapes and flow speeds may not alter the heat transfer significantly while still decreasing flue gas side pressure drop.

8. Conclusions

An improved computer code for simulating full scale heat exchangers was developed from previous versions of the code to better calculate heat transfer and to calculate pressure drop on the flue gas side and the cooling water side. After verifying the new full-scale code, cost estimates of the heat exchanger over a 20 year lifetime were calculated. It was determined that the largest contribution to the overall cost of the heat exchanger is the capital cost, outweighing operating cost. This is due to the high cost tubing material that must be used in the corrosive environment of condensing flue gas. Capital cost considered the tubing material, manufacturing and installation. Operating cost was calculated as a function of the power required to pump flue gas and cooling water through the heat exchanger.

Different materials were considered that would be acceptable in two distinct regions in the heat exchanger: upstream of water condensation and downstream of water condensation. Upstream of water condensation, where sulfuric acid condensation occurs, Teflon (PTFE) was considered as a possible material due to having low corrosion rates. However, a strength analysis and data from manufacturers of the tubing suggested that at elevated temperatures, creep would become a serious strength issue. After considering the strength, heat transfer and cost of the available materials, it was determined that Nickel Alloy 22 would be the best tubing material option at locations upstream of the onset of water vapor condensation and Stainless Steel 304 would be the most cost effective material downstream of the onset of water vapor condensation.

An optimization technique determined the most effective tube spacings in the heat exchanger. Larger spacings in the transverse direction and smaller spacings in the longitudinal direction were found to give the best performance versus total cost. For a tube diameter of 2.375”, a londitudinal spacing of

2.97” showed better performance when compared to larger spacings of 4.12” to 6.17” due to the loss in surface area, and therefore heat transfer, that occurs. Transverse spacings ranging from 4.12” to 6.17” showed better performance when compared to a transverse spacing of 3.09” due to the increased pressure drop that the smaller spacing induces.

The effect of cooling water temperature on heat transfer and condensation rate was substantial. Lowering the cooling water temperature by 15^{o}F from 105^{o}F to 90^{o}F increased the condensation rate by 100% in some cases. Decreasing the cooling water inlet temperature not only means a larger temperature differential between the hot fluid and cold fluid, but it also means that the onset of condensation of water in the flue gas will occur at an earlier location due to cooler tube wall temperatures.

The effect of the ratio of the cooling water mass flow rate to flue gas mass flow rate was also significant. Higher ratios caused higher heat transfer and condensation rates. Increasing the ratio from 0.5 to 1 typically increases condensation efficiency by a factor of two. Increasing the flow rate ratio allows the cooling water to stay at a lower temperature throughout the length of the heat exchanger. This, in turn, makes the average tube wall temperature much lower than with lower flow rate ratios and therefore increases heat transfer.

The condensing heat exchanger is much more cost effective if used downstream of a FGD unit. The flue gas at this location is saturated with water and at a relatively low temperature typically near 135^{o}F. The conditions at this location are much more favorable for condensation than at the location after an ESP where flue gas is typically at 300^{o}F. In addition, less heat exchanger surface area is needed to lower the temperature of the flue gas at the location downstream of the FGD, making for lower capital costs. Higher condensation rates occurred and lower cost per condensation rate and cost per heat transfer was encountered at this location.

Pressure drop and heat transfer ratios from a previous study were used to draw estimated comparisons between using circular tubes and elliptical tubes. With this specific set of elliptical tubes, the loss in heat transfer outweighed the lower operating cost and total cost. However, more research with streamlined tubes with different flow parameters needs to be done before the possibility of usage of these tubes can be eliminated.

References

1. **Jeong, Kwangkook.** *Condensation of Water Vapor and Sulfiric Acid in Boiler Flue Gas.* Ph.D. Dissertation, Lehigh University, 2008.

2. *Design of Cooler Condensers for Mixtures of Vapors with Noncondensing Gases.* **Colburn, A P and Hougen, O A.** 11, Industrial and Engineering Chemistry, 1934, Vol. 26.

3. *Thermodynamique - Tensions des vapeurs: nouvelle relation entre les tensions et les temperature.* **Antoine, Ch. M.** Comptes Rendus des Seances de l'Academie des Sciences, 1888, Vol. 107.

4. **Incropera, Frank P, et al.** *Fundamentals of Heat and Mass Transfer.* Hoboken : John Wiley & Sons, Inc., 2007.

5. **Zukauskas, A.** Heat Transfer from Tubes in Crossflow. *Advances in Heat Transfer.* New York : Academic Press, 1972.

6. **Idelchik, I.E.** *Handbook Of Hydraulic Resistance.* New York : Jaico Publishing House, 2003.

7. **Cengel, Yunus A and A, Boles Michael.** *Thermodynamics: An Engineering Approach.* Boston : McGraw Hill, 1998.

8. **The Babcock & Wilcox Company.** *Steam.* Barberton : The Babcock & Wilcox Company, 2005. 41.

9. **Fox, Robert W, McDonald, Alan T and J, Pritchard Philip.** *Introduction to Fluid Mechanics.* Hoboken : John Wiley & Sons, Inc., 2004.

10. **Lavigne, Michael.** *Numerical Simulations of Condensing Heat Exchangers with Oxyfuel Flue Gas.* Thesis, Lehigh University, 2010.

11. *Estimating Costs of Shell-and-Tube Heat Exchangers.* **Purohit, G. P.** Chemical Engineering, 1983, Vol. 90.

12. **Spalding, Brian D and J, Taborek.** *Heat Exchanger Design Handbook.* Washington : Hemisphere Publishing Corporation, 1983.

13. **Smith, Robin.** *Chemical Process Design and Integration.* Hoboken : Wiley, 2005.

14. **Peace, Glen Stuart.** *Taguchi Methods.* New York : Addison-Wesley Publishing Company, Inc., 1993.

15. **Levy, Edward K.** *Recovery of Water From Boiler Flue Gas - Final Technical Report.* Energy Research Center, 2008.

16. **ThyssenKrupp Stainless.** *Material Data Sheet No. 4021.* 2004.

17. **Bouquet, Frank L.** *Engineering Properties of Teflon.* Graham : Systems Company, 1989.

18. **Special Metals Corporation.** *Publication Number SMC-049.* Special Metals Corporation, 2006.

19. *The Properties of poly(tetrafluoroethylene) (PTFE) in Tension.* **Rae, P.J. and Brown, E.N.** Polymer, 2005, Vol. 46.

20. **Beer, Ferdinand P, Johnston, Russel E Jr. and DeWolf, John T.** *Mechanics of Materials.* New York : The McGraw-Hill Companies Inc., 2006.

21. **Micromold Products, Inc.** *Technical Bulletin 2.1-3b.* Yonkers : Micromold Products, Inc., 2009.

22. *Design of a novel, intensified heat exchanger for reduced fouling rates.* **Bouris, D, et al.** 18, International Journal of Heat and Mass Transfer, 2005, Vol. 48.

23. *An experimental and numerical study of the flow past elliptic cylinder arrays.* **Castiglia, D, et al.** 11, London : Proceedings of the Institution of Mechanical Engineers, Part C: Journal of Mechanical Engineering Science, 2001, Vol. 215.

Appendix A: Graphical Results for Full Scale Heat Exchanger

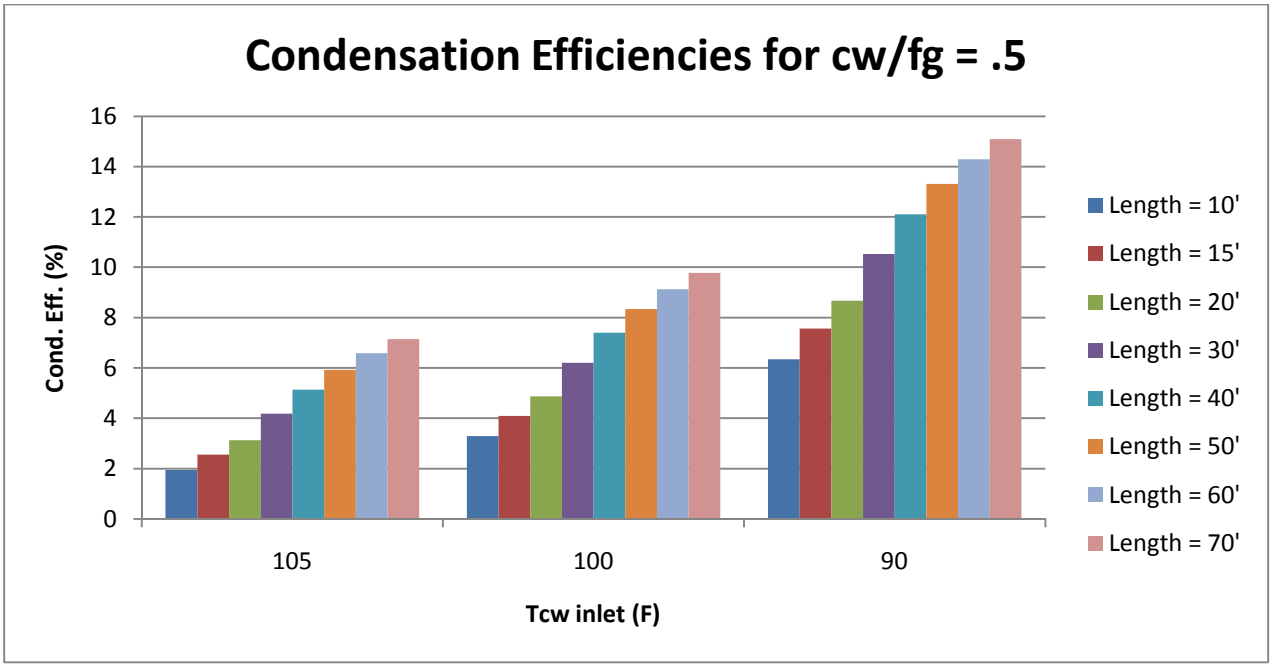

Figure A 1

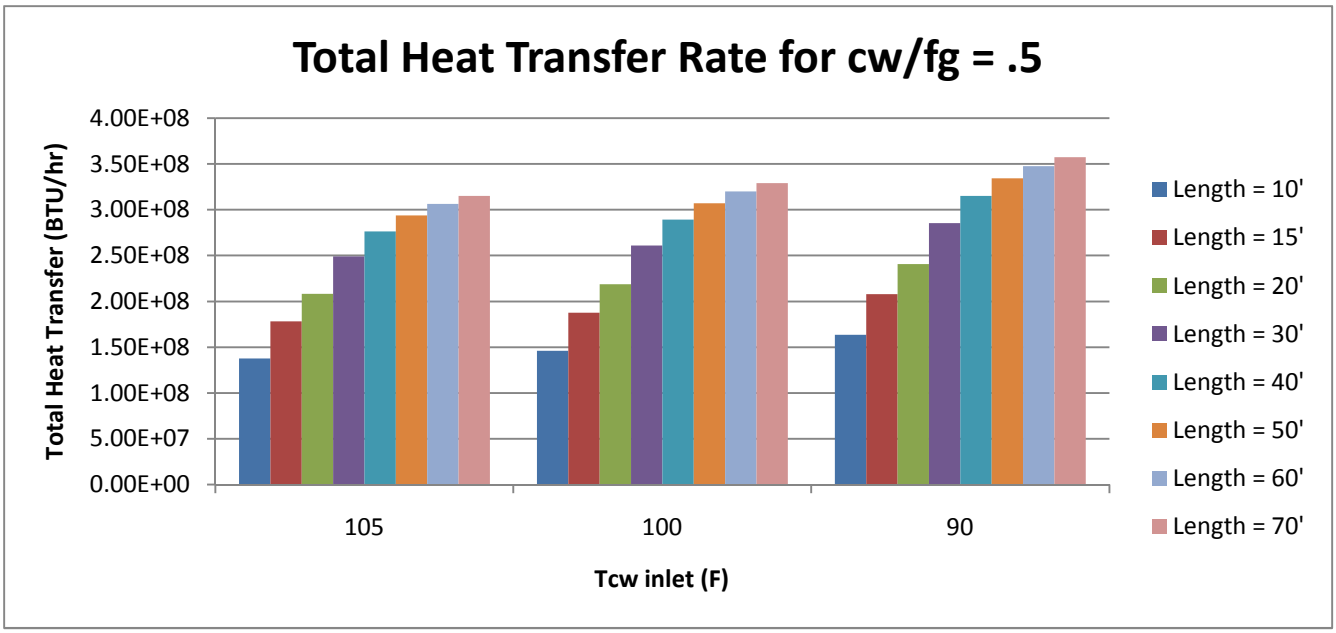

Figure A 2

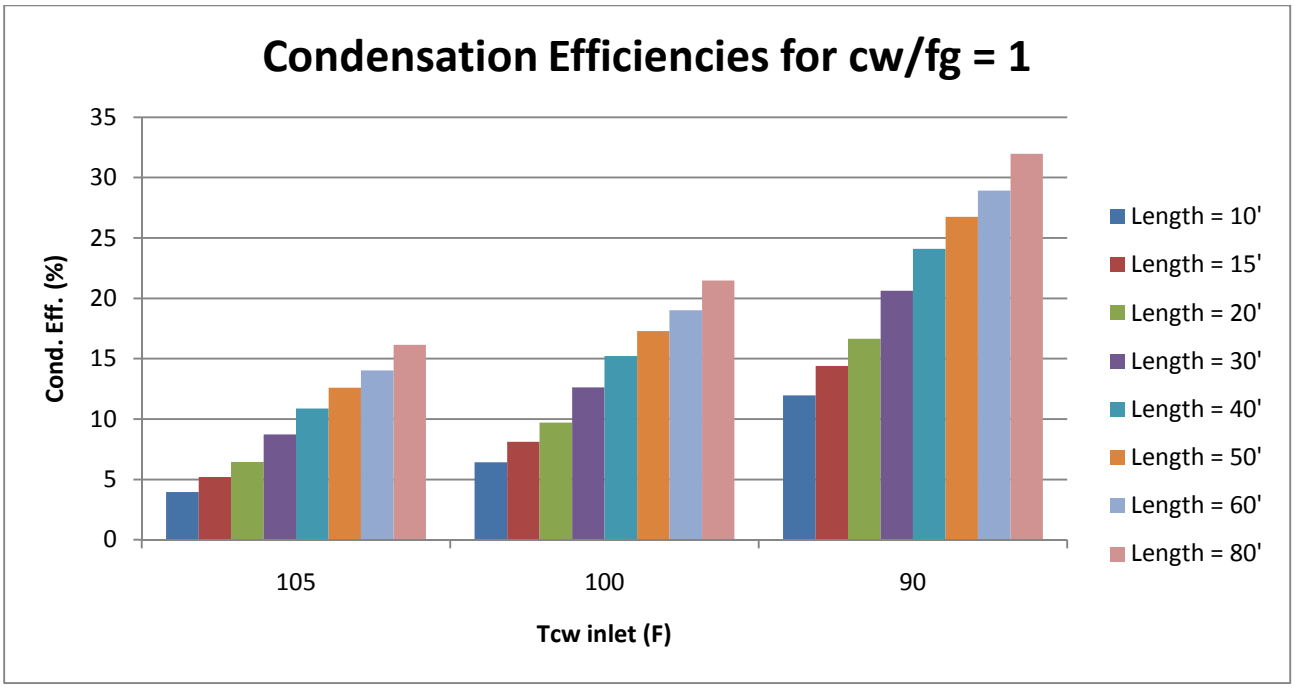

Figure A 3

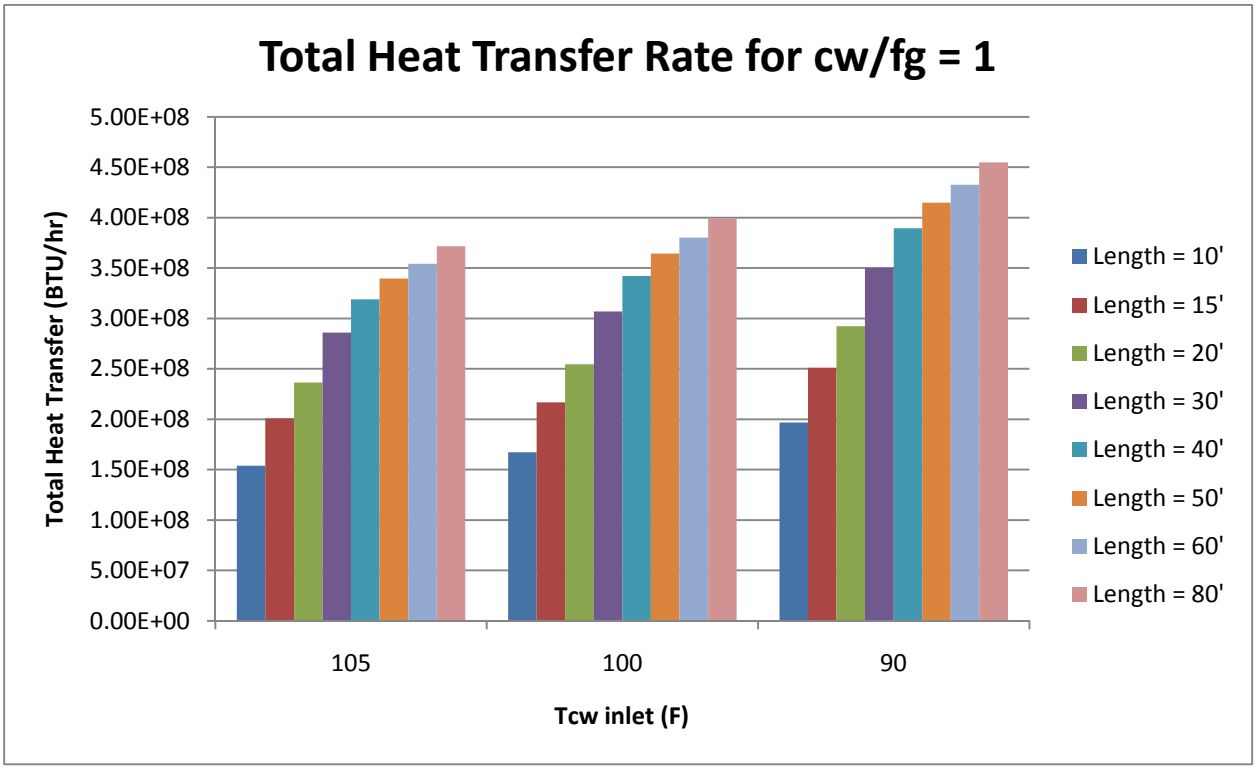

Figure A 4

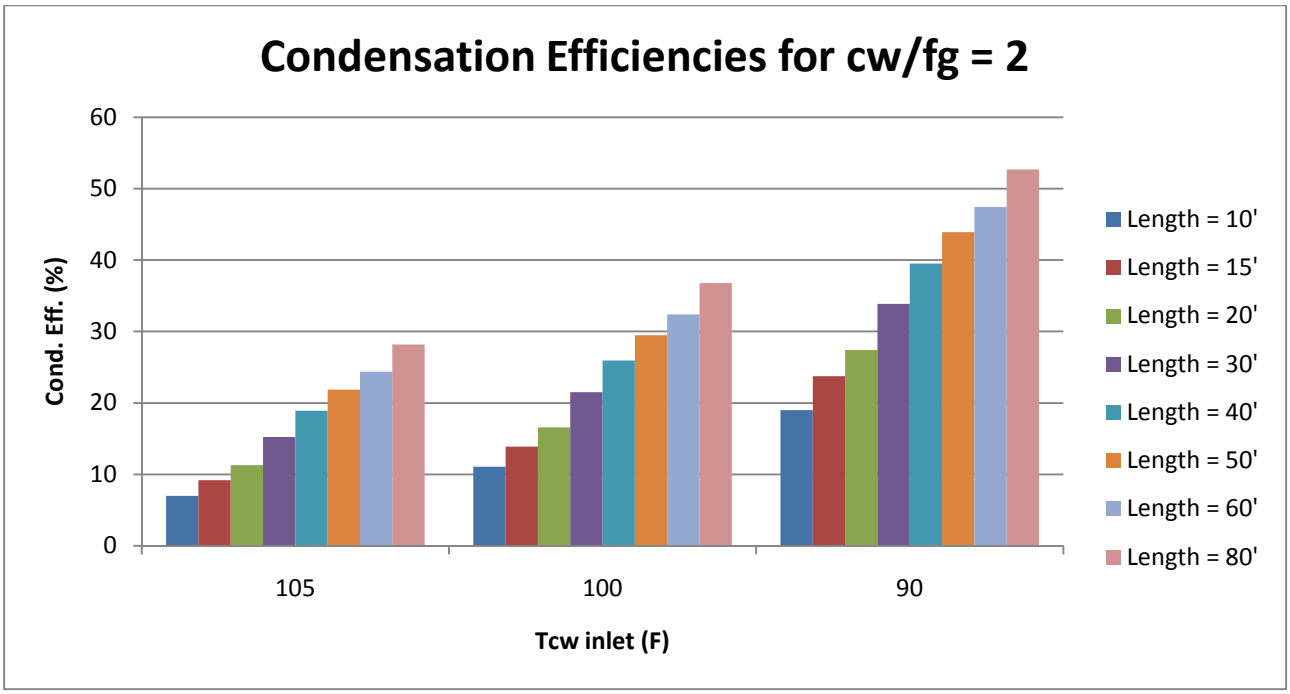

Figure A 5

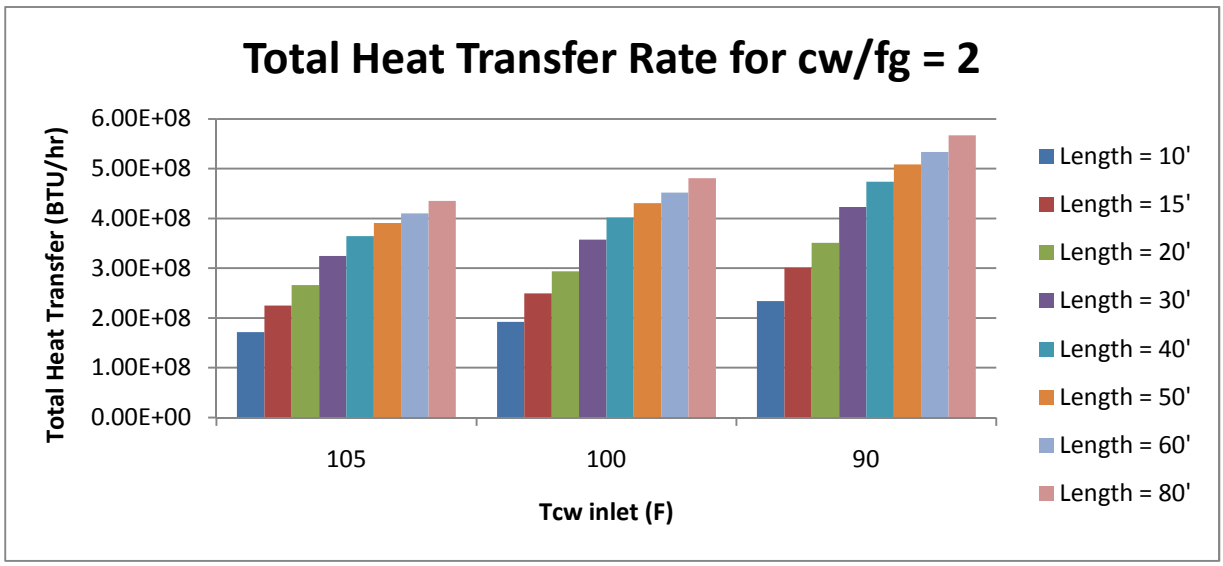

Figure A 6

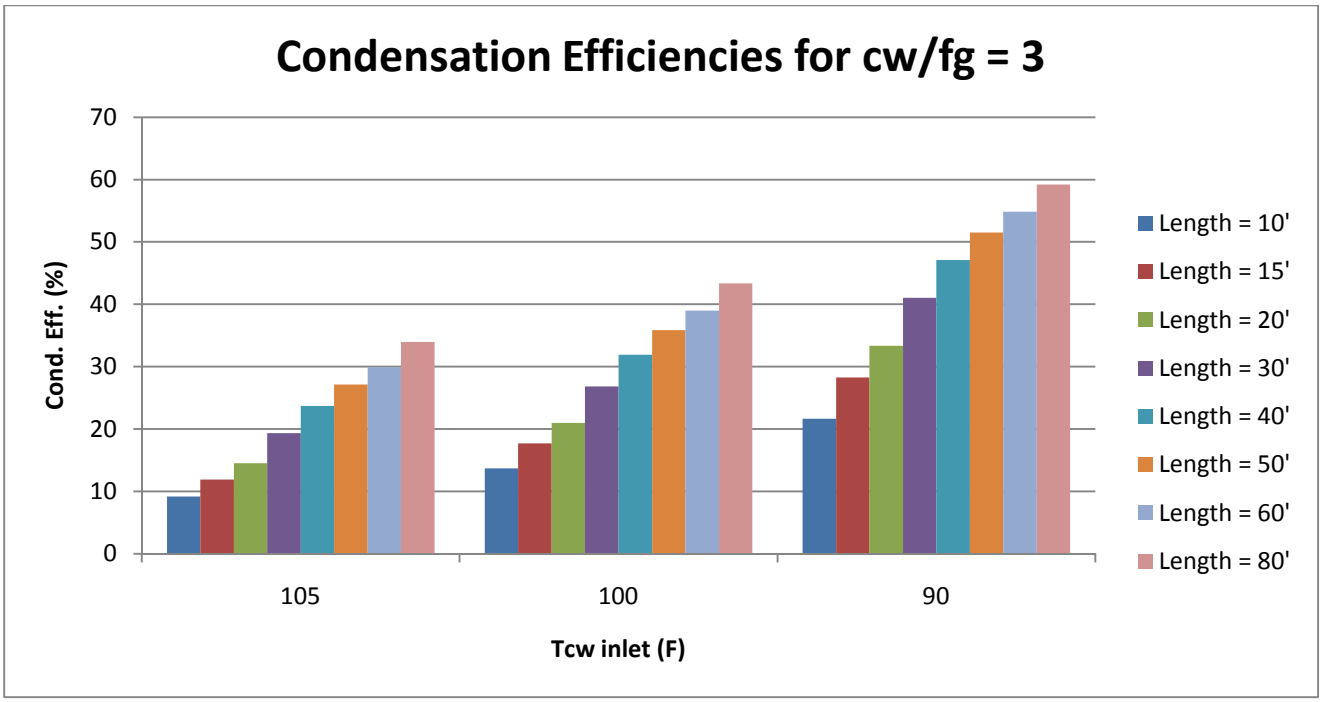

Figure A 7

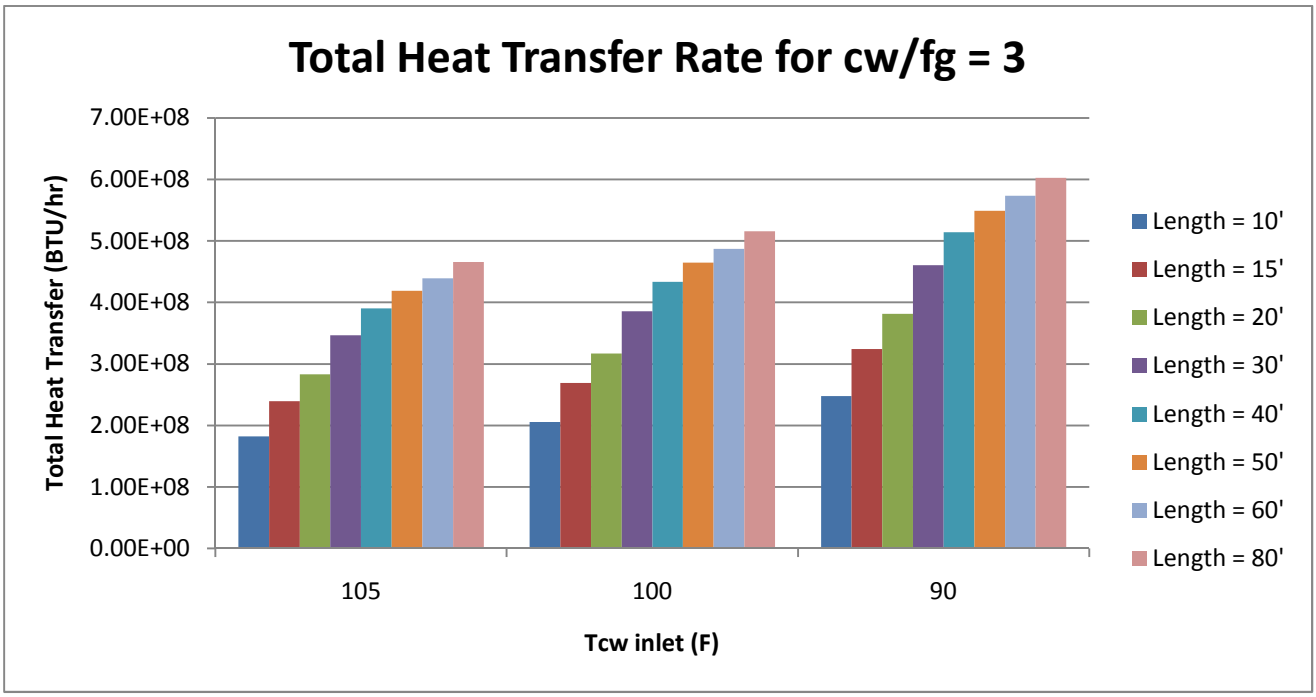

Figure A 8

Appendix: Additional Graphical Results for Heat Exchanger Downstream of the FGD

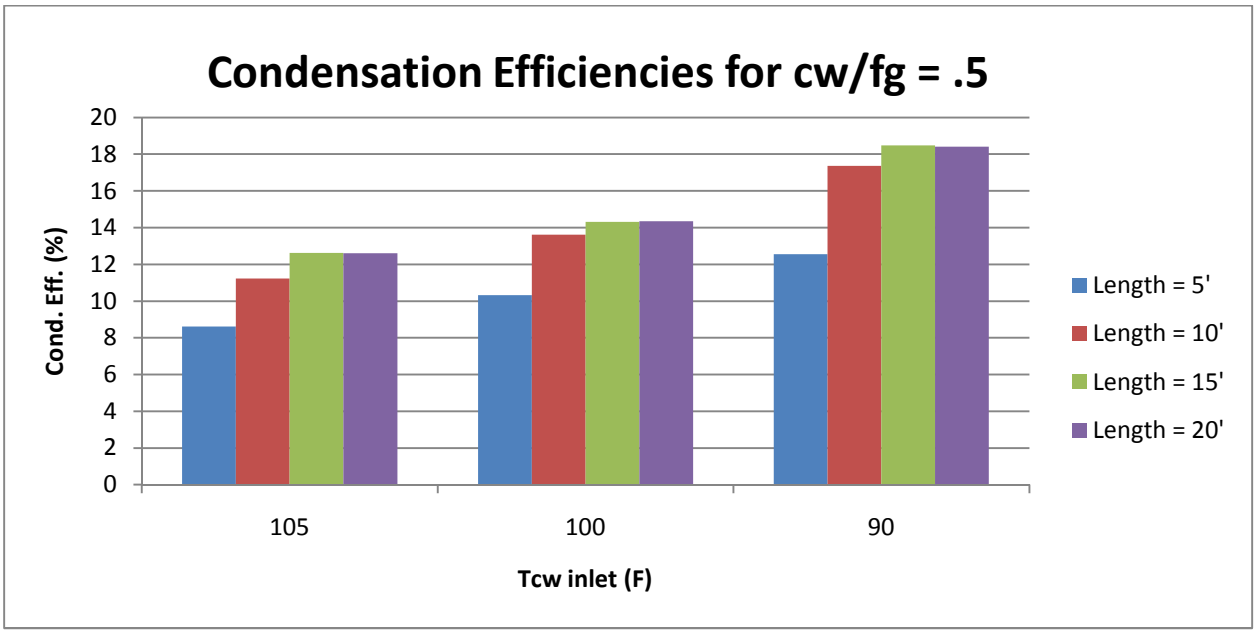

Figure A 9

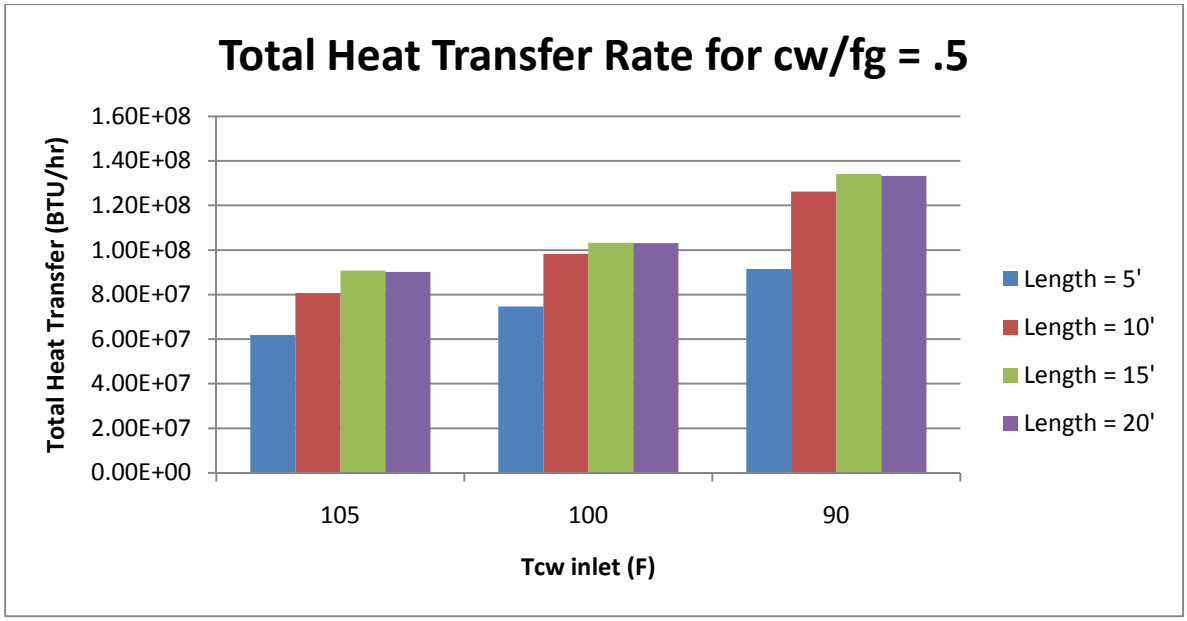

Figure A 10

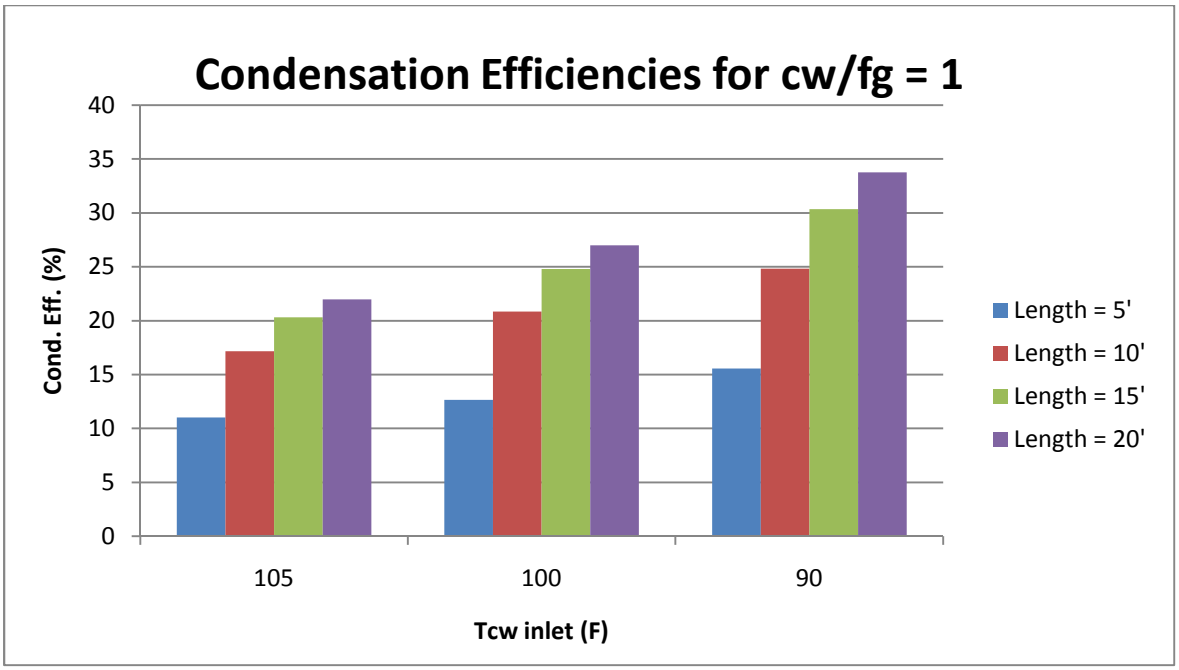

Figure A 11

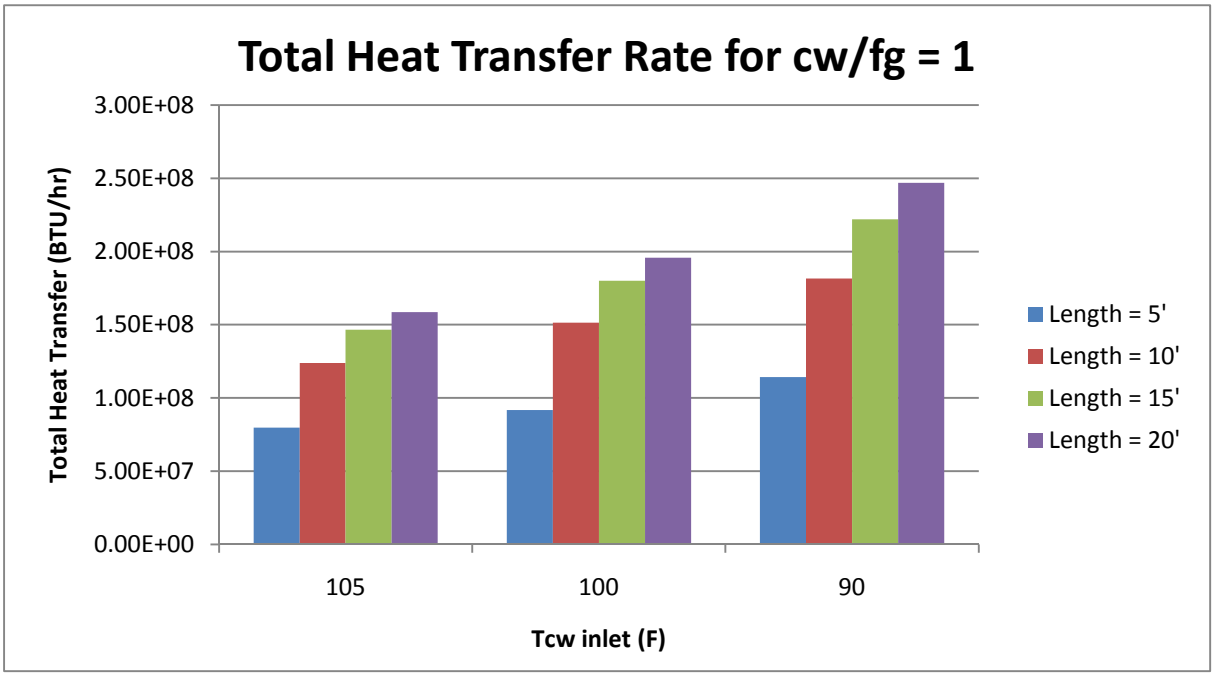

Figure A 12

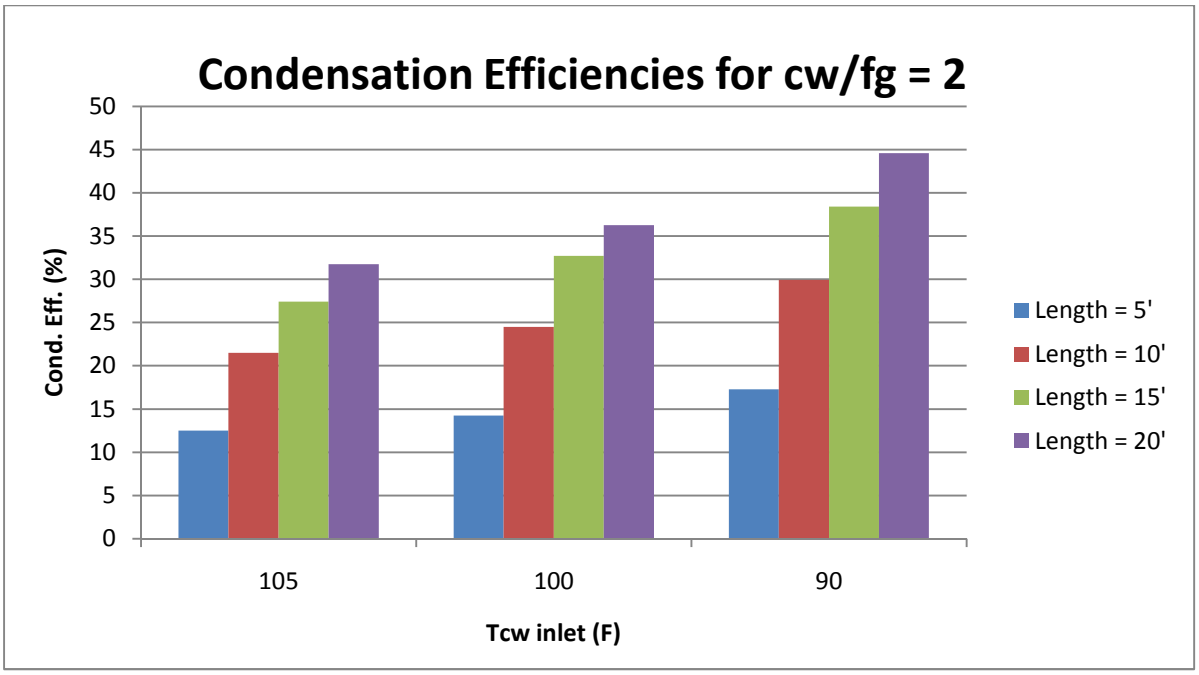

Figure A 13

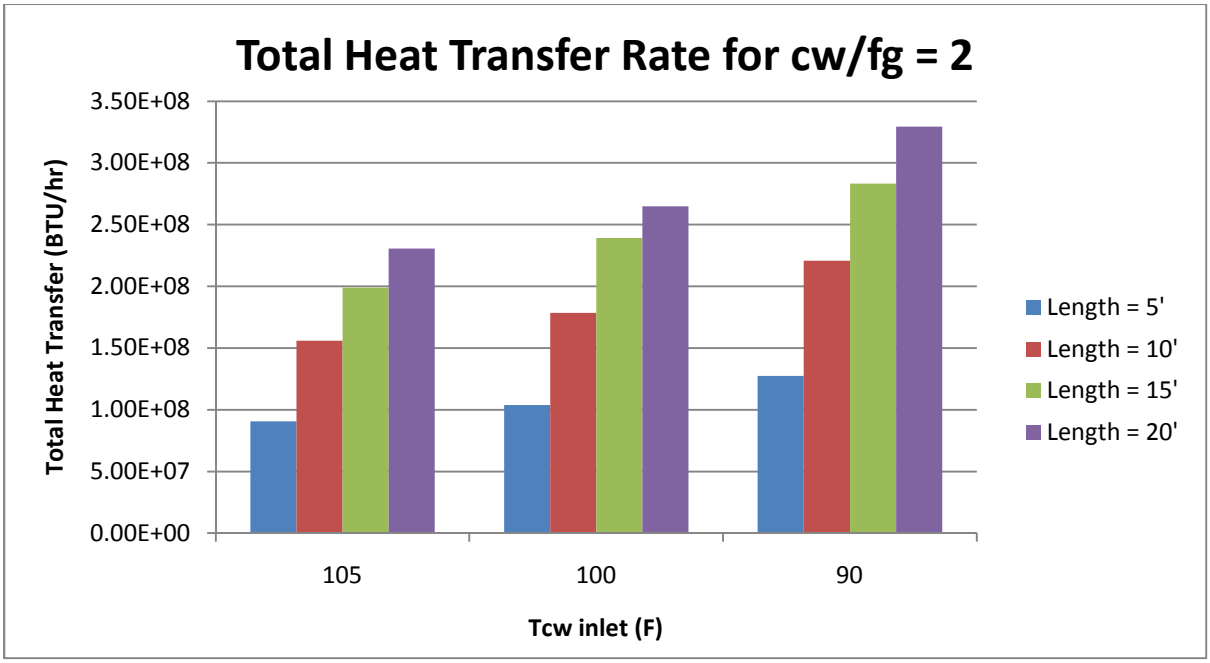

Figure A 14

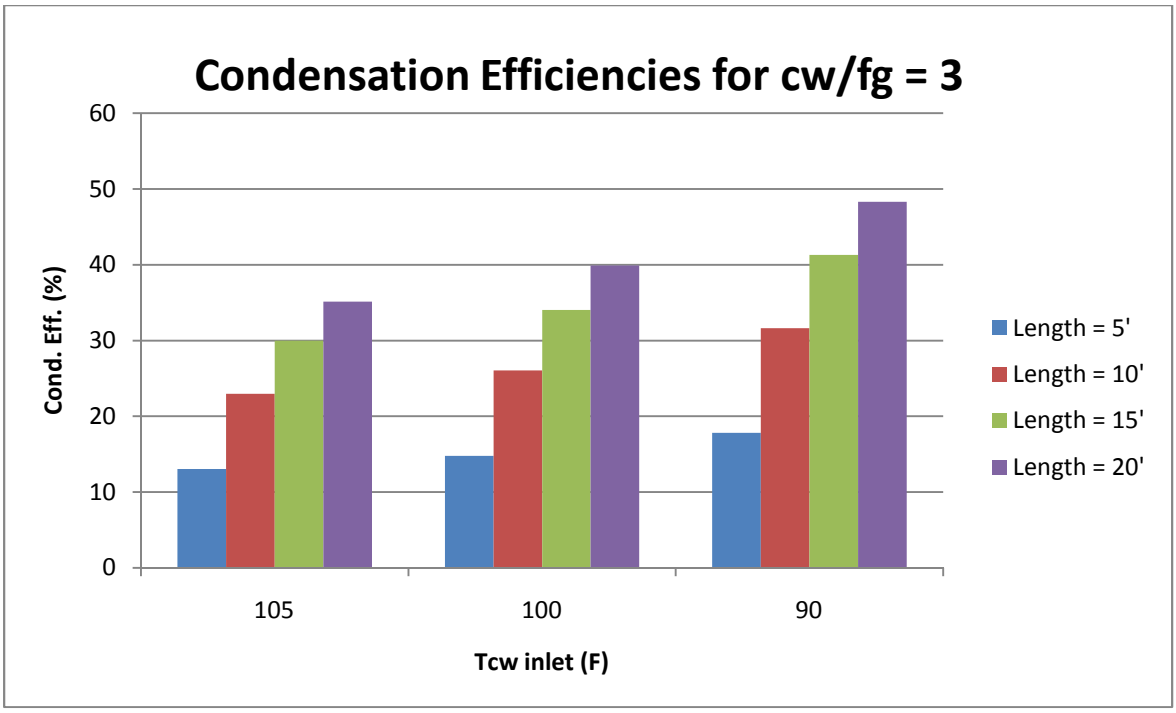

Figure A 15

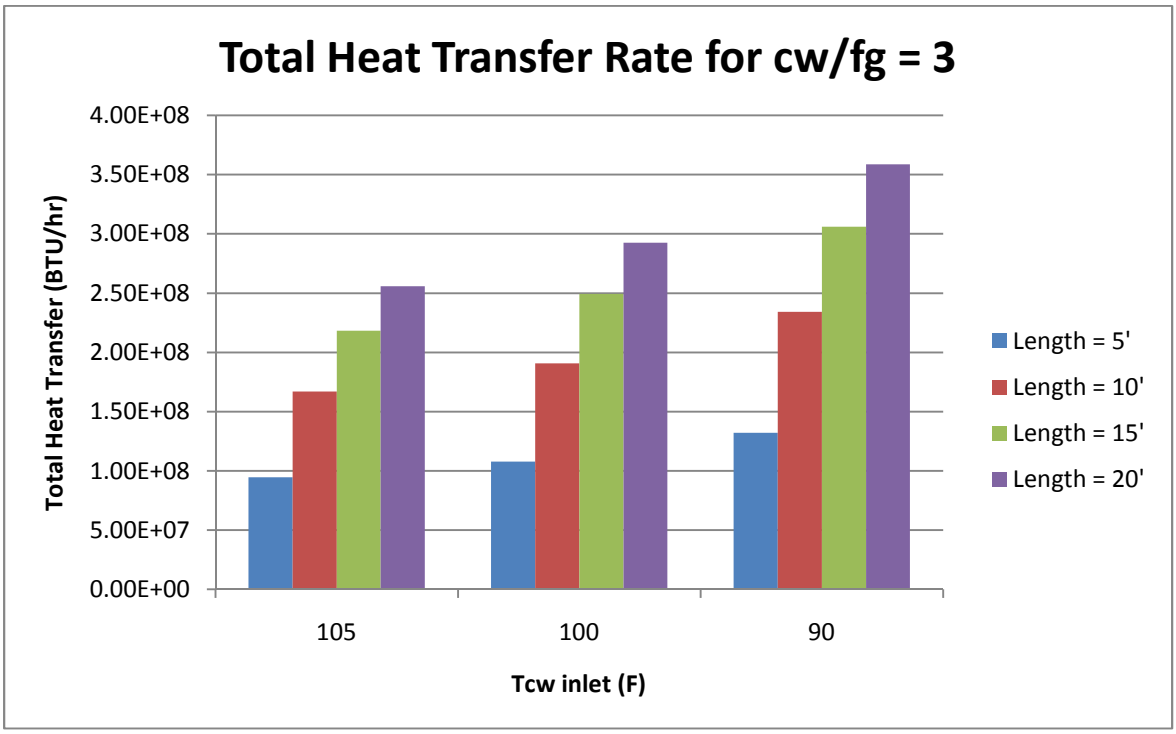

Figure A 16

Vita

Daniel D. Hazell was born in southern Maryland. After completing his work at Huntingtown High School, Huntingtown, MD, he attended Lehigh University. He received a Bachelor of Science in Mechanical Engineering from Lehigh in the Spring of 2009. In the Fall of 2009 he began a graduate program at Lehigh University.